Unione Europea

Ministero dell'Istruzione dell'Università e della Ricerca

Università degli Studi di Palermo

Tesi Di Dottorato

LIFETIMES AND STABILITY IN CLASSICAL AND QUANTUM SYSTEMS

TEMPI DI VITA E STABILITÀ IN SISTEMI CLASSICI E QUANTISTICI

Dottorando

Pasquale Caldara

Tutor

Prof. Bernardo SPAGNOLO

Coordinatore

Prof. Bernardo SPAGNOLO

SSD: *Fis03*

Università degli Studi di Palermo
Dipartimento di Fisica

Corso di DOTTORATO INTERNAZIONALE DI RICERCA

in FISICA APPLICATA (XXII CICLO) – 2011

To my parents without which...

Acknowledgements

I would like to thank, first of all, my tutor Prof. Bernardo Spagnolo who pushed me towards better and better results. I wish also to thank all the members of the Group of Interdisciplinary Physics guided by Prof. Spagnolo.

In particular, I wish to thank Alessandro Fiasconaro whose animated discussions greatly contributed to this work. I have to remember Davide Valenti whose help and friendship are undeniable. I want to recall my PhD course and laboratory mate Angelo La Cognata, with which a fruitful collaboration for both of us was found during our long years of the PhD course. Last but not least I need to remember my other laboratory mate Stefano Spezia for his vitality and my colleague and friend Nicola Pizzolato for his contagious calm.

Contents

List of Figures

Glossary

blip an off-diagonal state in DVR representation

FV Feynman-Vernon

gNICA generalized Non Interacting Cluster Approximation

IBCA Interacting Blip Chain Approximation

ME Master Equation

MET Mean Escape Time

MFPT Mean First Passage Time

NES Noise Enhanced Stability

NIBA Non Interacting Blip Approximation

NICA Non Interacting Cluster Approximation

PDF Probability Density Function

RWA Rotating Wave Approximation

SDE Stochastic Differential Equation

sojourn a diagonal state in DVR representation

SPA Static Path Approximation

SQUID Superconducting Quantum Interference Devices

STIRAP STImulated Raman Adiabatic Passage

1

Introduction

Metastability is a peculiarity of many complex systems, ranging from physics to biology and chemistry. Complex systems are usually open systems which strongly interact with a noisy environment. These systems can exchange with the environment energy and materials and this interaction can be modeled as noise.

Metastable states play a crucial role for example in protein folding dynamics, Ising spin glasses, complex dynamics of large molecules at surfaces, enhancement of cellular memory and in dynamics of cellular reactive oxygen species (1). The lifetime of a metastable state is the main interest in a variety of areas, including first-order phase transitions, field theory, chemical kinetics and Josephson junctions (2, 3, 4).

Scope of the present work is to discuss the behavior of systems which can be described by the evolution of the position of a fictitious particle subjected to a deterministic potential which has two stable positions at different energies (bistability) and is also interacting with a noisy environment.

The discussion will be carried out both for classical and quantum systems pointing out the differences between the two physical and, accordingly, mathematical frameworks and the different fields of applications.

It is straightforward that a classical description is the proper one in every case where the evolution of the system under study follows from an Newton-like equation of motion, as in Langevin equation. Otherwise when we are dealing

with elementary particles, whose undulatory nature cannot be neglected we have to use a quantum description with a Hamiltonian operator.

1.1 Classical systems

In this thesis we deal with a theoretical model for bistable classical physical systems in which the interaction with the environment is described by a multiplicative noise term, that is the noise amplitude depends on the state variable of the system considered. Many problems susceptible to be represented by this model abound not only in physics, but also in biology, ecology, economy and chemistry.

In statistical physics and in particular in phase transition phenomena an archetypal model is the Ising model. We will consider bistability and the role of the multiplicative noise in such a physical system.

1.1.1 Langevin Equation

In 1827, while examining pollen grains and the spores of Mosses and Equisetum suspended in water under a microscope, Robert Brown observed these minute particles executing a continuous jittery motion(5). He observed the same motion in particles of dust, enabling him to rule out the hypothesis that the effect was due to pollen being alive. However he wasn't able to explain the origin of the motion.

In his PhD thesis "The Theory of Speculation" published in 1900 (6), Louis Bachelier introduced the random walk as a way to model financial markets. Bachelier indeed anticipated the famous theoretical work published by Einstein in 1905 on the Brownian motion. Since then due to the seminal contributions of A. Einstein (7), M. Smoluchowski (8) and P. Langevin (9) the usage of the stochastic process has seen a large number of applications and generated the theory of stochastic processes (10).

The first example of the stochastic differential equation (**SDE**) was introduced by Langevin in 1908 to explain the Brownian motion (11), which is observed when

a classical particle is free to move in a fluid like air or water (10). Langevin introducing the concept of the equation of motion of a random variable, in this case the position of a Brownian particle, initiated a new train of thought culminating in a truly dynamical theory of Brownian motion (12).

The interaction with the environment (the molecules of the fluid) is given by the collisions of the particle with the molecules of the fluid ($m_{pollenparticle} \gg m_{fluidparticle}$). Each collision is deterministic and subjected to the ordinary classical equation of motion but the global effect can be described with a differential equation with a randomly fluctuating contribute. This means that when we study the evolution of the system at the mesoscopic level we take into account all the microscopic collisions of the particle with the environment by considering in the dynamical equation of our system a stochastic term which we call noise.

This interaction with the environment, usually has the effect to disorder the system. However, often such interaction can give rise to counterintuitive phenomena and several examples are found in nature in which the noise has a constructive role.

One of these is the stochastic resonance, which consists of an enhancement of sensitivity of a nonlinear system to external periodic forcing due to random fluctuations (13, 14, 14, 15, 16, 17, 18).

Another effect manifesting the constructive role of noise in physical systems is the resonant activation (19, 20, 21, 22). In this phenomenon a cooperative interplay beetween the barrier fluctuations and the thermal noise-induced barrier crossing events occurs. The crossing barrier process is strongly correlated with potential fluctuations and the average escape time exhibits a minimum at a resonant fluctiation rate (23).

Furthermore it can be found that the noise can have a stabilization effect on the metastable system, this is the noise enhanced stability (**NES**) phenomenon (24, 25, 26). The lifetime of the metastable state has a non monotonic behavior as a function of the noise intensity.

1.1.2 Multiplicative noise

The noise added into the system because of the interaction with the environment may be dependent or independent by the state variable of the system. When we are dealing with noise whose intensity is independent on the state of the system we call it *additive* noise. A typical case of additive noise is the thermal noise or the thermal fluctuations always present in natural systems.

Otherwise, when the coupling with the environment is such that the noise intensity depends on the state variable of the system we have a *multiplicative* noise. Typical examples of stochastic differential equations with multiplicative noise are those governing the population dynamics.

As well as the additive noise, also the multiplicative noise is involved in many scientific areas, not only in physics. Examples are in population dynamics, where the noise can break the symmetry of two or more interacting species (27) creating ordered patterns, or in phase transition phenomena, in the study of the decaying of false vacuum states (28) as well as in condensed matter (29).

Many studies have been performed with the goal of investigating the mathematical features related with the multiplicative noise and its relationship with phase transition (30, 31).

In the last decade the role of the multiplicative noise has been investigated in nonequilibrium phase transition phenomena (30, 32, 33, 34).

The functional form of the noise factor $g(x)$ (where x is the order parameter) depends on the physical system under investigation.

In many cases the pure multiplicative contribution has been used in the form $g(x) = x$. In a birth-dead process the functional form is given by $g(x) = \sqrt{1+x}$; in the Hongler's model (35) $g(x) = 1+x^2+o(x^2)$, in noise-induced nonequilibrium phase transitions $g(x) = 1+x^2$ Ref.(32, 33). Distinct contribution of two separate noise sources, pure additive and pure multiplicative, have been also investigated (36).

It has been noted (29, 37) that the qualitative behavior of a system of the Ising spin model can be well represented by a undimensional Langevin equation driven by a multiplicative noise intensity represented by the square root of a

polynomial, $g(x) = \sqrt{D + \mu x^2}$, where D represent the thermal contribution and μ is an environmental coupling factor.

1.1.3 Mean First Passage Time

In the study of a system whose dynamics is subjected to stochastic driving forces it might be of interest to know how long the system remains in a certain region of values of the state phase, with peculiar boundary conditions.

The usual boundary conditions used are: absorbing and reflecting barriers(10). We have the case of an absorbing barrier when, if the particle reaches the frontier, it is not more considered, i.e. it goes out of the subpace of interest.

We have absorbing barrier at some values of the order parameter when the particle is removed from the system when it reaches these boundaries.

Otherwise, when the particle reaches the boundary, and it is thrown back into the region under observation we have the case of a reflecting barrier. In term of a probability density function $P(x,t)$ we can say that for an absorbing barrier we have $P(x,t) = 0$ while for a reflecting boundary condition we have $\frac{\partial P(x,t)}{\partial x} = 0$.

A very important physical example occurs when the evolution of the system can be described by a bistable potential. In this case the particle starts its motion at a point a, near one of the two wells of the potential, and we are interested in how much time is needed in order to reach a point b near the second well of the potential. This is the case, for example, of a chemical reaction $A \rightarrow B$ where A and B are two chemical species. In fact we can model this kind of reaction by the chemical concentration parametero of one of the two chemical species (say B). The reaction starts when is present only the species A (point a in the state space) and diffuses towards the presence of only the chemical species B (point b).

The mean reaction time is well described by the well known formula for the mean first passage time (**MFPT**)

$$T(a \rightarrow b) = \frac{2\pi}{\sqrt{|U''(a)U''(b)|}} e^{\frac{2(U(a)-U(b))}{D}} \tag{1.1}$$

obtained by Kramers and published in 1940 (38). In the Eq.1.1 $U(x)$ is the function describing the potential profile of the system and $\Delta U = U(a) - U(b)$ is the height of the potential barrier that the Brownian particle has to cross.

The Eq.1.1 is a particular case of the more general formula for the **MFPT**

$$T(x) = \frac{2}{D}\int_x^b dx' \exp\left[\frac{2U(x')}{D}\right]\int_a^{x'} dx'' \exp\left[-\frac{2U(x'')}{D}\right] \tag{1.2}$$

where D is the noise intensity. For $\Delta U >> D$ and by retaining in the double integral of the Eq.1.2 only the main contributions of both integrals (which are around the a and b) and using the parabolic approximation (10, 38) we get Eq.1.2 from Eq.1.1.

It is worthy to note that this linearization procedure neglects all the possible effects due to the full potential profile which is viceversa considered in the general formula of the Eq.1.2.

1.2 Open Quantum systems

In classical mechanics a particle is described by the equation of motion given by the second principle of dynamics which at each time gives one and only one position in space. Because of this reason the particle has a completely determined trajectory.

In quantum mechanics the motion of a particle is described by a partial linear differential equation whose variable is a wave function. The square modulus of this wavefuntion gives for each volume of space the probability for the particle to be found there. This means that the particle loses the possibility to follow a trajectory being not zero the probability to be detected not only in a monodimensional curve (the classical trajectory) but in each point of a certain volume.

However, quantum mechanics contains the classical mechanics as limiting case ($h \longrightarrow 0$) but needs to interact with a classical system to make experimental forecasts.

This interaction causes the collapsing of the state of the system to an eigenstate of that observable. A measurement of that observable will give us the eigenvalue corresponding to that eigenstate. The classical system which acts this way is commonly called "observer" and this process is the measurement in quantum world.

The loss of the possibility for the particle to follow a trajectory means that if the particle is found at a time $t_{\mathbf{A}}$ in a point in the space $\mathbf{A}$ in a later time $t_{\mathbf{B}}$ might be detected in a point $\mathbf{B}$ without the possibility for the observer to say what (if any) points are reached by the particle for times t such as $t_{\mathbf{A}} < t < t_{\mathbf{B}}$. We see that the particle reached the point $\mathbf{B}$ starting from the point $\mathbf{A}$ without following any trajectory.

This is a feature which makes a strong difference between the behavior of a quantum system with respect to a classical one, when a particle should cross a finite potential barrier (quantum tunnel effect).

This effect often occurs in condensed matter physics, such as Josephson junctions and hetero-nanostructures (39, 40). In a dissipative quantum system interacting with a thermal bath, the quantum tunneling can play an important role on the relaxation time from a metastable state (41). During the last decades the effects of environment on quantum tunnelling phenomenon have been intensively studied (41, 42, 43, 44, 45).

In this context, symmetric and asymmetric quantum bistable systems are good enough to analyze superconducting quantum bits and decoherence phenomena (46, 47). Obtaining longer coherence times in such systems, when they interact with noisy environment, is one of the major requirements in devising and manufacturing devices capable of storing quantum bits.

In this respect, a main topic is to know the properties of a particle subject to an external potential, in the presence of random fluctuations. It can be also useful to study the changes occurring in the dynamics of a quantum particle affected by noisy perturbations, when different shapes of the potential profile are used. Potentials which model the interaction with laser beams have many interesting implications for quantum systems such as the coherent destruction of tunneling (48), the effect of quantum stochastic resonance (49), and the control and reduction of decoherence in open quantum systems (50).

1.2.1 Caldeira-Leggett model

Commonly an environment in quantum world is modelled as a number $\mathcal{N}$ (usually $\mathcal{N} \to \infty$) of harmonic oscillators considered at thermal equilibrium, i.e. a thermal

bath, interacting with the quantum system through a bilinear coupling (51, 52, 53, 54, 55).

In the chapter 3, in order to analyze the evolution of a quantum particle subject to time-independent asymmetric bistable potential and affected by environmental noise, the Caldeira-Leggett model (42) is used, which allows to derive a quantum mechanical analogue of the generalized Langevin equation through the modelization of the noisy environment as an ensemble of harmonic oscillators.

The total Hamiltonian contains information about all the degrees of freedom of the system and the environment.

1.2.2 The Feynman-Vernon approach

A key approach to modelize the noise in quantum systems is the Feynmann-Vernon analysis. In the framework of Feynman's space-time formulation of the non-relativistic quantum mechanics, the behavior of a system, which is coupled to other external quantum systems, can be calculated in terms of its own variables only.

If the behavior of a quantum system is to be investigated when it is coupled to one or more measuring instruments or, more general, to a system which can be defined as the universe (environment) the behavior of the environment in itself is not of primary interest and, in addition, if the environment is a measuring instrument is not possible to describe it as a quantum system at all beacuse of the formulation of quantum machanics. However its effects are capable of perturbing the characteristics of the evolution of the system being observed.

A more concrete example is the case of an atom in an excited state which interacts with the electromagnetic field in a lossy cavity resonator. Because of the coupling, there will be energy exchange between the field and the atom until equilibrium is reached, letting the atom go to a state which is in general different from the state in which the atom would go if it is not coupled to any external disturbances (i.e. its original excited state). The cavity field, although not of central interest, thus influences the behavior of the atom and it is necessary to be taken in account.

With the method developed by Feynman and Vernon in (56) is possible to include all the effect of the degrees of freedom of the environment in a functional, called "*phase influence functional*", and to express the system evolution as an integral which is function only of the system coordinates.

The difficulty is then to solve this integral which, in general, is not solvable. By a method called Discrete Variable Representation (**DVR**) (41, 57) it is possible to reduce the integration to a sum of infinite terms and calculate the evolution with the approximation needed by the problem.

In chapter 3 this approach is applied to a bistable asymmetric potential which resembles the kind of potential studied classically in chapter 2 in order to point out the differences and the similarities of this two cases.

This kind of potential is found in quantum system in several cases as reported in (41). In a macroscopic sample of molecular magnets consisting of a large number of chemically identical magnetic clusters of same magnetic size (regularly arranged on a crystal lattice) the evolution of magnetization can be affected by this kind of potential. These molecules have usually a large spin quantum number, typically $S \simeq 10$ and experiments indicate a strong uniaxial magnetocrystalline anisotropy which let the spin doubly degenerate along the c-axis of the crystal (the projection may span from $-S$ to $+S$) and generates an energy barrier for the reversal of the magnetization. This configuration can be described by a set of two-fold degenerate excited states corresponding to the spin projection $-(S-1) \leq m_s \leq S-1$ in a double well potential (41, 58, 59). Within the appropriate conditions the spin can tunnel through the anisotropy barrier.

A such material is known as Mn_{12}-acetate and possess a tunneling barrier of $\frac{\Delta U}{k_B} \leq 62K^o$. Its tunneling of magnetization is studied in (60, 61, 62) being revealed as quantum steps in hysteresis loop for specific values of an external magnetic field. Another such material studied (63, 64, 65, 66) is known as Fe_8 which has the anisotropy barrier ($\frac{\Delta U}{k_B} \leq 22K^o$) three times smaller than the Mn_{12}-acetate enhancing the tunneling effect by several order of magnitude.

Another class of physical situations where a double well potential configuration affects the evolution of the systems is when we deal with the magnetic flux in superconducting quantum interference devices (**SQUID**) (67, 68, 69, 70, 71, 72, 73, 74, 75). The equation of motion for the flux dynamics is similar to that of

a particle moving in a double well potential with dissipation which its lowest well corresponding to one of the two fluxoid states. For suitable conditions the transition between the states may occur via a tunnel effect through the potential barrier.

In (67) an incoherent tunneling in a macroscopic two-state system has been recognized while in (68) the experimental results have been explained as a resonant tunneling between two quasi degenerate states localized in different fluxoid wells.

1.2.3 Noise in solid state physics

Another important case when we have to deal with noise in quantum system is in solid state physics when we can't modelize the noisy environment with a bath composed by a series of harmonic oscillators. This is the case if low-energy excitations determine memory effects (76). In solid state physics this is a typical situation where in general additional statistical information is required in order to characterize the effect of the environment on the system dynamics.

In solid state devices we have to deal with broadband and structured noise which means that the noise spectrum extends non-monotonically to several decades with, sometimes, few resonances. Low-frequency noise is the most important source of decoherence in many of the solid state implementations of quantum bits (76, 77, 78).

The observation of coherent dynamics in nanodevices is an important achievement towards quantum control in solid state devices. In the last decade superconducting nanocircuits exhibiting the dynamics of single 'artificial atoms' (39, 79, 80), two coupled artificial atoms (81, 82) and artificial atoms coupled to electromagnetic resonators (83, 84) have been demonstrated.

This development opens new perspectives to study quantum phenomena in solid-state devices that traditionally have been part of quantum optics (85) as the phenomenon of the coherent population trapping (86) which is a key feature to obtain a stimulated coherent emission of electromagnetic radiation by an atom.

So far most of the research in this field has focused on the two lowest level of artificial atoms. In the last few years, it has been proposed that multilevel

quantum coherent effects (85, 87, 88) could be observed in superconducting nanodevices: various schemes have been proposed to observe electromagnetically induced transparency (89), and selective population transfer by adiabatic passage (90, 91, 92, 93, 94, 95).

Very recently, few experiments have demonstrated features of multilevel coherence in such devices, as the Autler-Townes effect (96, 97), coherent population trapping (98) electromagnetically induced transparency (99), preparation and measurement of three-state superpositions (100).

In studying quantum optical effects in solid state devices, several differences are encountered with respect to the atomic realm: coupling between subsystems is larger, but also noise is larger, and often extends over several decades, low-frequency noise being the most important source of decoherence in many of the solid state implementations of quantum bits (76, 77, 78).

On the other hand solid state devices offer several design solutions, and the possibility of tuning by external control the spectral properties of the artificial atom (101). All these elements come into play in multilevel structures (102), together with new features, as for example selection rules. Differences between specific designs may become crucial for the successful implementation of specific protocols.

A protocol which is largely used in this field is the so called **STIRAP** protocol which is described in section 4.2. In chapter 4 the effect of broadband noise on the sensitive parameters of this protocol used for coherent population transfer is discussed.

2

Classical systems

2.1 Brownian motion

Albert Einstein in 1905 published in **Annalen der Physik** (7) a paper where he, for the first time, described correctly this motion and used it in order to demonstrate indirectly the existence of elementar particles which constitute the matter (atoms and molecules).

Einstein in this paper was the first to connect the mathematical description of Brownian motion to physical quantities. In his work, in order to describe the motion of little particles in a fluid, he restricted himself to one dimension for the principle of the indipendence of the coordinate.

He supposed that in a time interval τ, which is chosen in such a way that evolution in the interval $[t-\tau, t]$ is indipendent from the trajectory in the interval $[t, t+\tau]$, the fraction $d\mathcal{N}$ of the $\mathcal{N}$ particles suspended in the fluid that have a variation of position (in one dimension) within Δ and $\Delta + d\Delta$ is given by the equation

$$d\mathcal{N} = \mathcal{N}\varphi(\Delta)d\Delta \tag{2.1}$$

and $\varphi(\Delta)$ is the distribution of probability for a particle of being subjected to such a collision that the particle a displacement Δ. This distribution is supposed to be symmetric around zero which means that the probability for the particle to go forward is the same probability to go backward.

For the definition of $\varphi(\Delta)$ and the particular choice of τ we can argue that the number of particles which are in the interval $[x, x+dx]$ at time $t+\tau$ is given by the number of particles which were at time t in position x and had a displacement Δ. Being $\nu = f(x,t)$ the number of particle per volume unity we can write for the number of particles in the x-dimension

$$f(x, t+\tau)dx = dx \int_{\Delta=-\infty}^{\Delta=\infty} f(x+\Delta)\varphi(\Delta)d\Delta \tag{2.2}$$

If we expand in power series both sides of the equation 2.2 we obtain

$$f(x, t+\tau) = f(x,t) + \tau\frac{\partial f(x,t)}{\partial t} + \frac{\tau^2}{2!}\frac{\partial^2 f(x,t)}{\partial t^2} + \cdots \tag{2.3}$$

for the left side and

$$f(x+\Delta, t) = f(x,t) + \Delta\frac{\partial f(x,t)}{\partial x} + \frac{\Delta^2}{2!}\frac{\partial^2 f(x,t)}{\partial x^2} + \cdots \tag{2.4}$$

for the right side. We put this expansion in Eq.2.2 retaining only the first order for the derivative in t and the second order for the derivative in x, which are the terms that deliver the first non zero terms of the expansions we put in the equation. Remembering the normalization condition

$$\int_{-\infty}^{+\infty} \varphi(\Delta)d\Delta = 1 \tag{2.5}$$

and the condition $\varphi(x) = \varphi(-x)$ and letting

$$D = \frac{1}{\tau}\int_{-\infty}^{+\infty} \frac{\Delta}{2!}d\Delta \tag{2.6}$$

we have

$$\frac{\partial f(x,t)}{\partial t} = D\frac{\partial^2 f(x,t)}{\partial x^2} \tag{2.7}$$

which is the equation of the diffusion and D is the coeffient of the diffusion. In order to fully indentify the form of the function we have to choose the boundary conditions that comes from the physical situation and namely

$$f(x,t) = 0 \int_{-\infty}^{+\infty} f(x,t)dx = \mathcal{N} \tag{2.8}$$

From Eq.2.7 and Eq.2.8 we obtain the functional form of the $f(x,t)$ which, for the unidimensionall motion, is given by

$$f(x,t) = \frac{\mathcal{N}}{\sqrt{4\pi Dt}} e^{-\frac{x^2}{4Dt}} \tag{2.9}$$

Extending the discussion to the 3-dimensional space we have

$$f(\vec{x},t) = \frac{\mathcal{N}}{(4\pi Dt)^{\frac{3}{2}}} e^{-\frac{x^2}{4Dt}} \tag{2.10}$$

and then

$$\langle \vec{x}(t) \rangle = 0 \tag{2.11}$$

$$\langle \vec{x}^2(t) \rangle = 6Dt \tag{2.12}$$

In his paper Einstein showed also that it is possible to write

$$D = 6\frac{k_B T}{\gamma} t \tag{2.13}$$

where γ is the friction coefficent of the fluid whereinto the particles are moving. The Eq.2.2 is a special form of the Chapman-Kolmogorov equation which rules all the stochastic processes.

Moreover it has to be noted that the Einstein's assumption that it is only necessary to know the initial position at time t and not its previous history in order to describe the motion is now well known as Markov postulate.

The theoretical approach by Paul Langevin in 1908 was much more direct, because he wrote the Newton equation of a particle in motion in a fluid with a friction coefficent α due to viscosity and a random fluctuating force term $\eta(t)$ as follows

$$m\frac{d\vec{x}(t)}{dt} = -\alpha\vec{x}(t) + \eta(t) \tag{2.14}$$

with

$$\langle \eta(t) \rangle = 0 \tag{2.15}$$

$$\langle \vec{x}(t)\eta(t) \rangle = 0. \tag{2.16}$$

Langevin observed that at the equilibrium we have

$$\langle \frac{1}{2} m v^2 \rangle = \frac{3}{2} k_B T \tag{2.17}$$

and then obtained indipendently the Eq.2.12. The Eq.2.14 is the first example of a stochastic differential equation.

2.2 Stochastic processes

A stochastic process is a time-dependent random variable ($\mathbf{X}(t)$), whose evolution has to be described probabilistically (10, 28)

The starting point for the analysis of stochastic processes is the assumption that a set of joint probabilities exists $p(\mathbf{x}_1, t_1; \mathbf{x}_2, t_2; \mathbf{x}_3, t_3; \mathbf{x}_4, t_4; \mathbf{x}_5, t_5; \mathbf{x}_6, t_6; \ldots)$ that describes completely the system. In terms of these joint probability density functions, we can define conditional probability densities

$$p(\mathbf{x}_1, t_1; \mathbf{x}_2, t_2; \ldots | \mathbf{y}_1, \tau_1; \mathbf{y}_2, \tau_2; \ldots) = \frac{p(\mathbf{x}_1, t_1; \mathbf{x}_2, t_2; \ldots; \mathbf{y}_1, \tau_1; \mathbf{x}_2, \tau_2; \ldots)}{p(\mathbf{y}_1, \tau_1; \mathbf{y}_2, \tau_2; \ldots)} \tag{2.18}$$

The knowledge of all the possible joint probabilities defines the so called *separable stochastic processes*. The simplest kinds of stochastic process is the case of Bernoulli trials for which the probability law is the same at all times or the case of the complete indipendence.

The next most important simple stochastic process is the Markov process in which the condition probability at time $t + \tau$ is completely determined by the knowledge of the condition at time t, i.e. we must require that the condition

$$p(\mathbf{x}_1, t_1; \mathbf{x}_2, t_2; \ldots | \mathbf{y}_1, \tau_1; \mathbf{y}_2, \tau_2; \ldots) = p(\mathbf{x}_1, t_1; \mathbf{x}_2, t_2; \ldots | \mathbf{y}_1, \tau_1) \tag{2.19}$$

(where $t_1 \geq t_2 \geq \ldots \geq \tau_1 \geq \tau_2 \geq \ldots$) is fulfilled. It is straightforward that if we know the probability $p(\mathbf{x}_1, t_1; \mathbf{x}_2, t_2)$ with $t_1 \geq t_2$ we know the conditional probability density at every time.

If we want to know the probability density for a stochastic process (the motion of a Brownian particle for instance) to have, at time t_1, for the stochastic variable

$\mathbf{X}$ the value $\mathbf{x}_1$ assuming that at the previous time t_2 the variable $\mathbf{X}$ had the value $\mathbf{x}_2$ we have to start from the law of the probability concepts.

If we have the probability for three probabilistic mutually exclusive events ($\mathbf{A}$,$\mathbf{B}$, $\mathbf{C}$) and we want to know the joint probability of only two ($\mathbf{A}$,$\mathbf{B}$) of these exclusive events we have to sum over all the possible realization of the event $\mathbf{C}$ i.e.

$$P(A \cap B) = \sum_C P(A \cap B \cap C) \tag{2.20}$$

In case of continous variables we have

$$\begin{aligned} p(\mathbf{x}_1, t_1; \mathbf{x}_3, t_3) &= \int d\mathbf{x}_2 p(\mathbf{x}_1, t_1; \mathbf{x}_2, t_2 | \mathbf{x}_3, t_3) \\ &= \int d\mathbf{x}_2 p(\mathbf{x}_1, t_1 | \mathbf{x}_2, t_2; \mathbf{x}_3, t_3) p(\mathbf{x}_2, t_2; \mathbf{x}_3, t_3) \end{aligned} \tag{2.21}$$

with $t_1 \neq t_2 \neq t_3$.

In the case of a Markov process in the last term of Eq.2.22 there is no dependence from t_3 in the $p(\mathbf{x}_1, t_1 | \mathbf{x}_2, t_2; \mathbf{x}_3, t_3)$ term.

Therefrom we can write

$$p(\mathbf{x}_1, t_1; \mathbf{x}_3, t_3) = \int d\mathbf{x}_2 p(\mathbf{x}_1, t_1 | \mathbf{x}_2, t_2) p(\mathbf{x}_2, t_2; \mathbf{x}_3, t_3) \tag{2.22}$$

which is the Chapman-Kolmogorov equation.

A typical Markovian process is the random walk, in fact the position a time $t + \tau$ depends only on the position at time t, i.e. $x(t + \tau) = x(t) \pm l$ where l is the discrete step of the walk and we take the minus sign if the walker goes to the left and plus if goes to the right. Because the probability to jump to the left is equal to the probability to jump to the right for the probility we can write

$$P(n, (N+1)\tau | n', N'\tau) = \frac{1}{2}[P(n+1, N\tau | n', N'\tau) + P(n-1, N\tau | n', N'\tau)]. \tag{2.23}$$

2.2.1 Overdamped motion

The classical equation of motion reads

$$\frac{d^2x}{dt^2} = \frac{1}{m}\sum_i F_{ext_i} \tag{2.24}$$

The external forces F_{ext_i} can be conservative, with a related potential function, or not conservative, which may be friction or viscous forces or, according to Langevin, random forces. By explicitly writing all these forces we have

$$m\frac{d^2x}{dt^2} = -\frac{dU}{dx} + \gamma\frac{dx}{dt} + \xi(t). \tag{2.25}$$

This is the so called underdamped Langevin equation which in the massless limit ($\frac{m}{\gamma<<1} << 1$) gives the overdamped Langevin equation

$$\frac{dx}{dt} = -\frac{dU}{dx} + \xi(t) \tag{2.26}$$

2.3 Functional approach

The Langevin equation of a general system driven by a noise is given by the following **SDE**

$$\frac{dx(t)}{dt} = f(x(t)) + g(x(t))\xi(t) \tag{2.27}$$

where $f(x(t))$ and $g(x(t))$ are arbitrary deterministic functions of the order parameter $x(t)$ and $\xi(t)$ is a random force. In this work $\xi(t)$ is a Gaussian white noise with the usual statistical properties

$$\langle \xi(t)\xi(t+\tau)\rangle = 2\mathcal{D}\delta(\tau) \tag{2.28}$$

and

$$\langle \xi(t)\rangle = 0 \tag{2.29}$$

Using the Eq. 2.27 and the relation

$$P(x,t) = \int_{-\infty}^{+\infty} dx(t)P(x(t))\delta(x - x(t)) = \langle \delta(x - x(t))\rangle \tag{2.30}$$

it is possible connect the probability density function with the mean value of the delta function calculated at a position x.

For the derivative of the probability density function then we can write

$$\begin{aligned}\frac{\partial P(x,t)}{\partial t} &= \frac{\partial}{\partial t}\langle\delta(x-x(t))\rangle \\ &= \frac{\partial}{\partial x}\langle\delta(x-x(t))[-\dot{x}(t)]\rangle \end{aligned} \tag{2.31}$$

and by using Eq.2.27, we have for the time derivative of the probability distribution function $P(x,t)$

$$\frac{\partial P(x,t)}{\partial t} = -\frac{\partial}{\partial x}f(x)\langle\delta(x-x(t))\rangle - \frac{\partial}{\partial x}g(x)\langle\delta(x-x(t))\xi(t)\rangle \tag{2.32}$$

To obtain a simpler and clearer equation we can use the methods of the functional analysis.

In this framework we use the Furutsu-Novikov formula (103) in order to split the correlation formula which is expressed by the last term of equation 2.32.

For an arbitrary functional $\mathcal{F}(t)$, this formula reads

$$\langle\mathcal{F}(t)\delta(x-x(t))\rangle = \mathcal{D}\left\langle\frac{\delta}{\delta\mathcal{F}(t)}\delta(x-x(t))\right\rangle \tag{2.33}$$

where $\frac{\delta}{\delta\mathcal{F}(t)}$ is the operator of the functional derivative with respect to the generic functional $\mathcal{F}(t)$. The functional chain rule gives

$$\frac{\delta}{\delta\mathcal{F}(t)}\delta(x-x(t)) = \frac{\partial\delta(x-x(t))}{\partial x(t)}\left[-\frac{\delta x(t)}{\delta\mathcal{F}(t')}\right] \tag{2.34}$$

In order to evaluate the last functional derivative we formally integrate the Eq.2.27

$$x(t) = \int_0^t \left[f(x(\tau)) + g(x(\tau))\xi(\tau))\right]d\tau \tag{2.35}$$

and then

$$\frac{\delta x(t)}{\delta\xi(t')} = \int_0^t d\tau\left[\frac{\delta f(x(\tau))}{\delta\xi(t')} + \frac{\delta}{\delta\xi(t')}\left(g(x(\tau))\xi(\tau)\right)\right] \tag{2.36}$$

Using the fact the functional derivative of a function is the usual derivative and for the functional chain rule we have

$$\frac{\delta x(t)}{\delta\xi(t')} = \int_0^t \left[\frac{\partial f(x)}{\partial x}\frac{\delta x(\tau)}{\delta\xi(t')} + \frac{\partial g(x)}{\partial x}\frac{\delta x(\tau)}{\delta\xi(t')}\xi(t) + g(x)\frac{\delta\xi(\tau)}{\delta\xi(t')}\right]d\tau \tag{2.37}$$

By considering that the future part of the trajectory can't affect the previous part, otherwise the causality principle would be violated, we have

$$\frac{\delta \mathcal{F}[\xi(t)]}{\delta(\xi(t'))} = 0 \tag{2.38}$$

with $t' > t$ and $\mathcal{F}[\xi(t)]$ any arbitrary functional which may be function the random function $\xi(t)$. In particular for Gaussian noise we have $\mathcal{F}[\xi(t)] = \xi(t)$.

The integration of the first and second term of Eq.2.37, because of Eq.2.38, gives zero as $t' \to t$.
If $0 < t' < t$ the third term gives

$$\int_0^t g(x(\tau))\frac{\delta\xi(\tau)}{\delta\xi(t')}d\tau = \int_0^t g(x(\tau))\delta(\tau - t')d\tau = g(x(t)). \tag{2.39}$$

With these results the Eq. 2.34 becomes

$$\langle \delta(x - x(t))\xi(t')\rangle = -\mathcal{D}\frac{\partial}{\partial x}\left[\langle \delta(x - x(t))\rangle\, g(x)\right] \tag{2.40}$$

The Eq.2.32 gives the general Fokker-Planck equation for arbitrary deterministic functions $f(x)$ and $g(x)$. In the case of a Gaussian white noise, the Fokker-Planck equation is

$$\frac{\partial P(x,t)}{\partial t} = -\frac{\partial}{\partial x}\left[f(x)P(x,t)\right] + \mathcal{D}\frac{\partial}{\partial x}\left[g(x)\frac{\partial}{\partial x}\left[g(x)P(x,t)\right]\right] \tag{2.41}$$

It can be interesting to point out that because we obtained this equation using the usual rules of calculus this is the **FP** equation according to Stratonovich (10, 104).

If we interpret the Langevin equation 2.27 in the Ito sense, that is according to the Ito calculus (105, 106), the Eq.2.41 has to be written

$$\frac{\partial P(x,t)}{\partial t} = -\frac{\partial}{\partial x}\left[f(x)P(x,t)\right] + \mathcal{D}\frac{\partial^2}{\partial x^2}[g^2(x)P(x,t)] \tag{2.42}$$

We can switch to the Ito (10) form by means of the following substitutions in Eq.2.27:

$$f_I(x) = f_S(x) + \frac{1}{2}g_S(x)\frac{\partial}{\partial x}g_S(x) \tag{2.43}$$

$$g_I(x) = g_S(x) \tag{2.44}$$

Comparing the Eq.2.41 and Eq.2.42 we can see that if $g(x)$ is a constant, the two forms coincide.

2.3.1 Asymptotic Probability Density Function

The Eq.2.41 has the form of a continuity equation where the current term has the form

$$J_P = f(x)P(x,t) + \mathcal{D}\left[g(x)\frac{\partial}{\partial x}\left[g(x)P(x,t)\right]\right] \tag{2.45}$$

which is the term of probability current.

In order to obtain the asymptotic distribution ($t \to \infty$) we set the equilibrium condition

$$\frac{\partial P_{st}(x,t)}{\partial t} = 0 \tag{2.46}$$

and so we have

$$\frac{\partial J_P}{\partial x} = \frac{\partial}{\partial x}\left[\left[f(x)P_{st}(x,t=\infty)\right] - \mathcal{D}\left[g(x)\frac{\partial}{\partial x}\left[g(x)P(x,t=\infty)\right]\right]\right] = 0 \tag{2.47}$$

which can be integrated once in the space of coordinate x becoming

$$f(x)P_{st}(x) - \mathcal{D}g(x)\frac{d}{dx}\left[g(x)P_{st}(x)\right] = J(x,t=\infty) = \mathcal{A} = 0 \tag{2.48}$$

where the partial derivation can be replaced by the total derivative as long as the $P(x)$ doesn't anymore depend on time.

The formal solution of this equation is then

$$\begin{aligned} P_{st}(x) &= \mathcal{N}\exp\left[\int_0^x \frac{f(x') - \mathcal{D}g(x)g'(x')}{\mathcal{D}g^2(x')}dx'\right] \\ &= \mathcal{N}\exp\left[\int_0^x \frac{f(x')}{\mathcal{D}g^2(x')}dx' - \int_0^x \frac{g'(x')}{g(x')}dx'\right] \end{aligned} \tag{2.49}$$

which gives

$$P_{st}(x) = \mathcal{N}\exp\left(\int \frac{\mathcal{A} - f(x')}{\mathcal{D}g^2(x')}dx - \ln(g(x))\right) \tag{2.50}$$

The costant $\mathcal{A}$ in Eq. 2.48 is the value of the probability current at $t = \infty$ which has to be zero because then the system is in equilibrium (it's in a stationary state), so, as a result, we have the asymptotic probability density (see Eq. 2.51)

$$P_{st}(x) = \frac{\mathcal{N}}{g(x)}\exp\left(-\int \frac{f(x')}{\mathcal{D}g^2(x')}dx'\right) \tag{2.51}$$

Where the value of $\mathcal{N}$ is given by the normalization condition

$$\int_{-\infty}^{+\infty} P_{st}(x)dx = 1 \tag{2.52}$$

and then

$$\mathcal{N} = \left(\int_{-\infty}^{+\infty} \frac{1}{g(x')} \exp\left(- \int \frac{f(x'')}{\mathcal{D} g^2(x'')} dx'' \right) dx' \right)^{-1} \tag{2.53}$$

2.3.2 The polynomial potential

Now we apply the latter results to a system governed by a potential described by a polynomial

$$U(x) = -\sum_{i=0}^{n} a_i x^i \tag{2.54}$$

then

$$f(x) = -\frac{du}{dx} = \sum_{i=0}^{n-1} (i+1) a_{i+1} x^i \tag{2.55}$$

If we take

$$g(x) = \sqrt{\sum_{j=0}^{m} b_j x^j} \tag{2.56}$$

the integral in Eq.2.51 becomes

$$\int \frac{f(x)}{g^2(x)} dx = \int \frac{\sum_{i=0}^{n-1} (i+1) a_{i+1} x^i}{\sum_{j=0}^{m} b_j x^j} dx \tag{2.57}$$

We can write (if $n \geq m$)

$$\frac{f(x)}{g^2(x)} = p_{n-m}(x) + \frac{R(x)}{g^2(x)} \tag{2.58}$$

where $p_{n-m}(x) = \sum_{i=0}^{n-m} \alpha_i x^i$ is the polynomial quotient (degree $n-m$) and $R(x) = \sum_{i=0}^{r} \beta_i x^i$ is polynomial rest ($r < m$). The Eq.2.57 becomes then

$$\begin{aligned} \int \frac{f(x)}{g^2(x)} dx &= \int p_{n-m}(x) dx + \int \frac{\sum_{i=0}^{r} \beta_i x^i}{\sum_{j=0}^{m} b_j x^j} dx \\ &= \int p_{n-m}(x) dx + \sum_{i=0}^{r} \beta_i \int \frac{x^i}{\sum_{j=0}^{m} b_j x^j} dx \end{aligned} \tag{2.59}$$

From this equation we see that the positions of the minima and of the maxima are depending on the functional form of $g(x)$. Only if $g(x)$ is a constant (case of additive noise) the minima and the maxima of the effective potential not change their position (28).

2.4 Physical models

It has been noted (29, 37) that the qualitative behavior of a system of the Ising spin model can be well represented by an overdamped Langevin equation driven by a multiplicative noise intensity represented by the square root of a polynomial, $g(x) = \sqrt{D + \mu x^2}$, where D represent the thermal contribution and the μ is an environmental coupling factor.

The aim of this section is to investigate the role played by the two parameters in both the stationary probability distribution functions (**PDF**) and the non equilibrium stability features of the Ising spin model.

The Fokker-Planck equation for a system affected by a multiplicative noise has been evaluated by functional analysis technique applied in the case of a delta-correlated Gaussian noise. Then the stationary **PDF** ($t \longmapsto \infty$) in the presence of a bistable asymmetric potential is obtained.

By considering an initial unstable state, the mean first passage time to reach a boundary close to the global minimum of a strongly asymmetric double well potential, is numerically evaluated. The system shows the presence of an increase of stability in both the parameters (pure multiplicative and pure additive noise and mixed), in a particular choice of their intervals. This confirms that a suitable presence of noise can always stabilize the system. In Refs.(107, 108, 109, 110) it is possible to find an analysis for a system in an unstable initial state of a cubic potential in the presence of additive Gaussian noise.

It is found that the presence of multiplicative noise increases the lifetime of a metastable state with a non monotonic behavior with maxima as a function of both D and μ noise intensity parameters.

In a bidimensional square spin lattice with periodic boundary conditions the spins of the atoms interact between themselves and with external field. This interaction may be represented by the Ising Hamiltonian

$$H = -\sum_{ij} s_i s_j - h \sum_i s_i \tag{2.60}$$

where the sum runs over all nearest-neighbors pairs and h is the external magnetic field. It has been noticed (29, 37) that the system can be described by an over-damped unidimensional Langevin equation with a multiplicative Gaussian white

noise because the fluctuations increase with the value of the order parameter. The noise intensity is then modelled by

$$g(x) = \sqrt{D + \mu x^2} \tag{2.61}$$

where D is the strength of thermal noise, μ is the non equilibrium parameter and x is the order parameter.

The potential has the polynomial form (see Fig.2.1)

$$U(x) = -\frac{\mathcal{A}}{4}x^4 - \frac{\mathcal{B}}{3}x^3 - \frac{\mathcal{C}}{2}x^2 - \mathcal{F}x - \mathcal{E}. \tag{2.62}$$

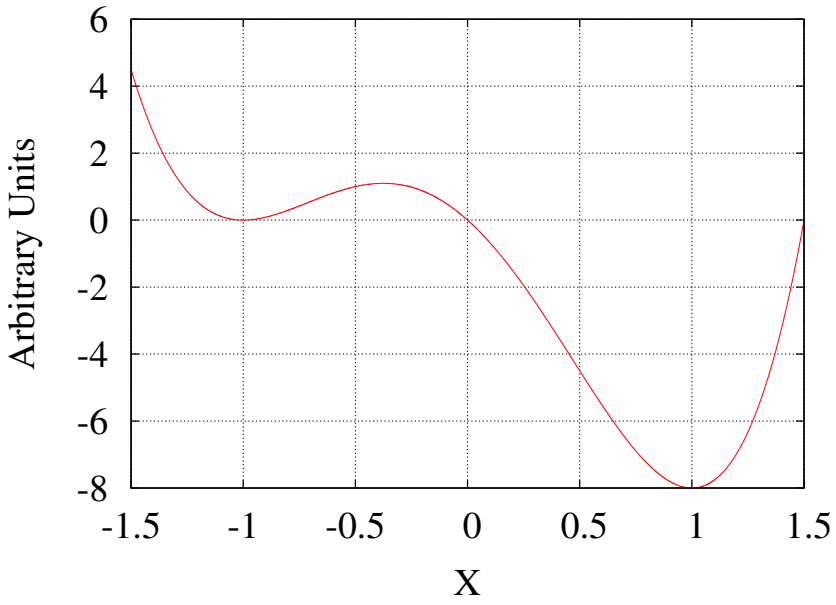

Figure 2.1: Deterministic potential $V(x)$

Because of the relation

$$f(x) = -\frac{dU(x)}{dx}, \tag{2.63}$$

the integral of the exponential function of Eq.2.51 becomes:

$$\begin{aligned} \int \frac{f(x)}{g^2(x)}dx &= \int (\alpha x + \beta)dx + \int \frac{\gamma x + \epsilon}{D + \mu x^2}dx \\ &= \frac{\alpha}{2}x^2 + \beta x + \frac{\gamma}{2\mu}\ln|D + \mu x^2| \\ &+ \frac{\epsilon}{\sqrt{D\mu}}\arctan\left(\sqrt{\frac{\mu}{D}}x\right) + C \end{aligned} \tag{2.64}$$

with

$$\alpha = \frac{\mathcal{A}}{\mu} \tag{2.65}$$

$$\beta = \frac{\mathcal{B}}{\mu} \tag{2.66}$$

$$\gamma = \mathcal{C} - \frac{\mathcal{A}D}{\mu} \tag{2.67}$$

$$\epsilon = \mathcal{F} - \frac{\mathcal{B}D}{\mu} \tag{2.68}$$

$$\mathcal{D} = 1 \tag{2.69}$$

A calculation of the integral for more general polynomials $f(x)$ and $g^2(x)$ is outlined in the previous section. The Eq.2.51 can be written in the same form obtained in the case of additive noise

$$P_{st}(x) = \mathcal{N} e^{-\frac{V_{eff}(x)}{D}}$$

where

$$\begin{aligned} V_{eff} &= \frac{\alpha}{2}x^2 + \beta x + \frac{\gamma}{2\mu}\ln\left(|D + \mu x^2|\right) + \\ &+ \frac{\epsilon}{\sqrt{D\mu}}\arctan\left(\sqrt{\frac{\mu}{D}}x\right) + D\ln(\sqrt{D + \mu x^2}) = \\ &= \frac{\alpha}{2}x^2 + \beta x + \left(D + \frac{\gamma}{2\mu}\right)\ln\left(\sqrt{D + \mu x^2}\right) + \\ &+ \frac{\epsilon}{\sqrt{D\mu}}\arctan\left(\sqrt{\frac{\mu}{D}}x\right) \end{aligned} \tag{2.70}$$

is the probabilistic potential describing the stationary behavior of the system. The new states that eventually appear in this probabilistic potential give rise to the noise-induced phase transition (28).

In the simplified Ising spin dynamics here studied (see Ref.(29)) the system is driven by the following asymmetric bimodal (quartic) potential

$$V(x) = 4x^4 + 2x^3 - 8x^2 - 6x \tag{2.71}$$

i.e. the potential of Eq.2.62 with the choice of the parameters $\mathcal{A} = -16$, $\mathcal{B} = -6$, $\mathcal{C} = 16$, $\mathcal{F} = 6$. The graph is plotted in Fig.2.2. The potential presents two

minima: the lowest (stable) located at $x = 1$, the highest at $x = -1$, and the maximum at $x = -3/8$.

Examples of the potential V_{eff} with these parameters are also shown in Fig.2.2 for $D = 0.32$ and $\mu = 5$. We note a shift in the position in the extrema of the **PDF** and the potential profile. This is a general feature of the potential $V_{eff}(x)$ in the case of multiplicative noise.

The shift of the position of the extrema is due to the term $\ln(g(x))$ as shown in Eq.2.70.

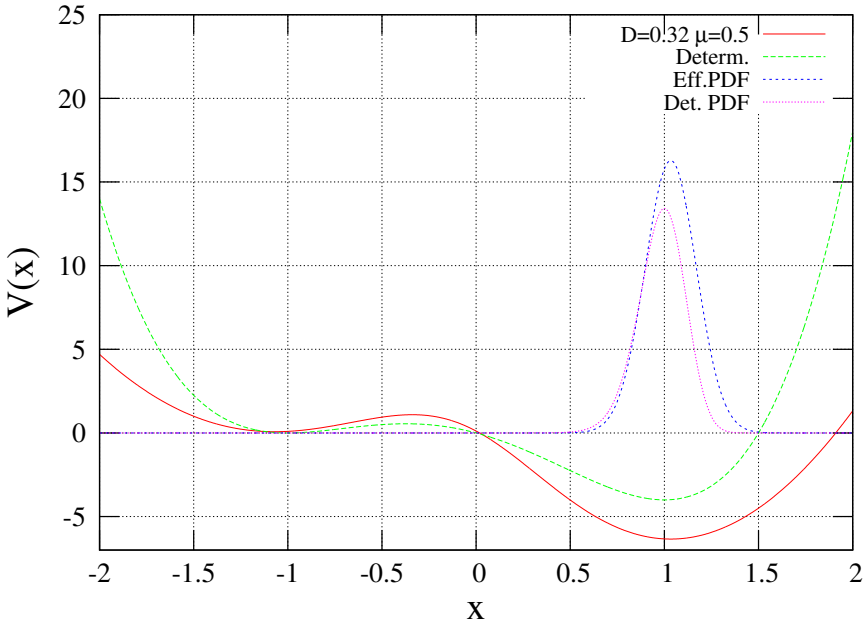

Figure 2.2: Deterministic potential $V(x)$ and comparison with the effective potential $V_{eff}(x)$ for $D = 0.32$ and $\mu = 0.5$. The role played by the μ parameter is to change the concavity of the potential. Also wee can see that the position of the maximum of the "multiplicative" **PDF** has a little shift with the respect to the "deterministic" **PDF** corresponding to $V(x)$

If $g(x)$ is a constant, the positions of the extrema of $\int \frac{f(x)}{g^2(x)}dx$ are the same of the $V_{eff}(x)$ and the positions of the maxima of the **PDF** are coincident with the minima of the deterministic potential $V(x)$. From the Eq.2.70 is clear that the maxima of the **PDF** match with the minima of V_{eff} making clear the usefulness of this definition.

In Fig.2.3 are reported the stationary **PDF**s calculated using Eq. 2.70 for $\mu = 1$ and various thermal noise intensities. We see that the increase of the parameter D doesn't change the position of the maxima and that the distributions tend to enlarge. Moreover the right maximum of **PDF** decreases while the left maximum increases, according to the trend of the dimensionless effective potential (see the inset) which become flatter and flatter by increasing D.

Something analogous appears in Fig.2.4, where $P_{st}(x)$ for $D = 1$ and increasing values of μ are plotted. As in the case of the increase of the D parameter, also in this case the effective potential becomes flatter and flatter and the stationary distributions tend to loose the left minimum by increasing the μ. In this case we observe also a shift in the position which depends on the contribution of the "$g(x)$" factor within V_{eff}.

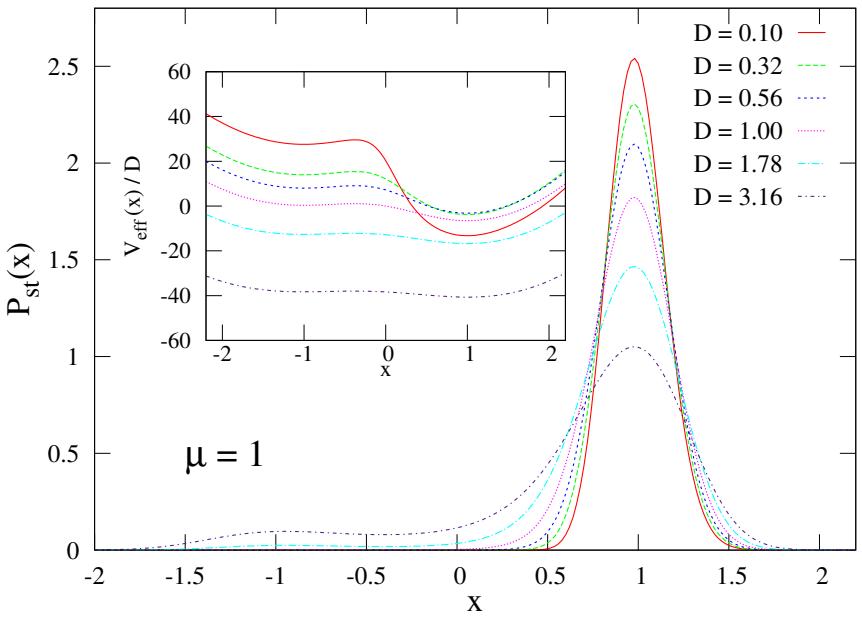

Figure 2.3: Effective potential $V_{eff}(x)$ with $D = 0.5$ and (from left to right) $\mu = 0.5$, $\mu = 10$ and $\mu = 50$

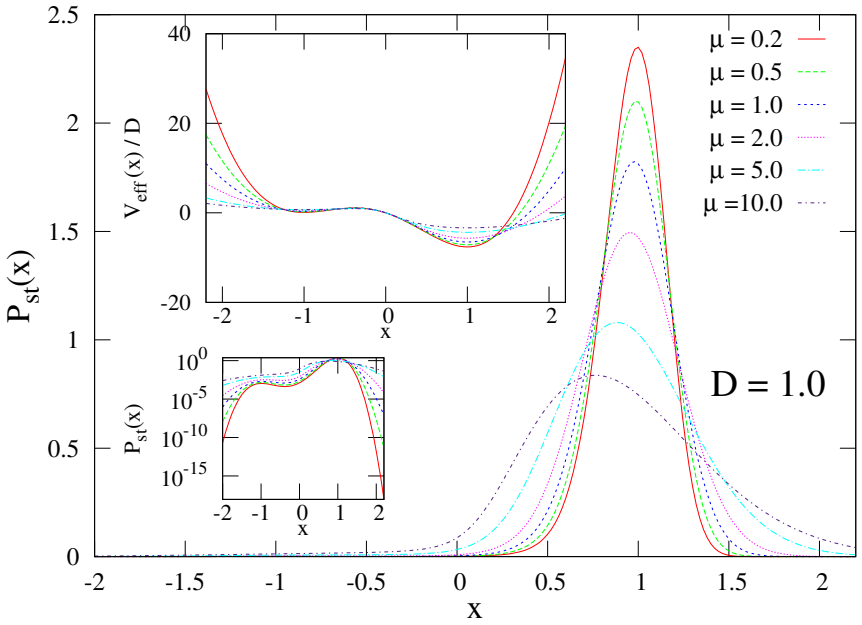

Figure 2.4: Effective potential $V_{eff}(x)$ with $D = 0.5$ and the **PDF** calculated (from left to right) for $\mu = 0.5$, $\mu = 10$ and $\mu = 50$

2.5 Mean First Passage Time in unstable state

In order to explore the features of D and μ parameters we performed a series of simulations that show a non monotonic behavior for the mean escape time of a stochastic system subjected to a bistable asymmetric potential. This potential has two minima which corresponds to two state where the system can reside (see Fig.2.2).

We start our simulations by choosing for the system the initial unstable condition at $x = -0.25$, just on the right of the maximum. We put an absorbing barrier at $x = 0.99$.

We investigate the mean first passage time (**MFPT**) seen as a function the two parameters D and μ. In these simulations the **MFPT** can be seen as equal to the mean escape time (**MET**) because we choose to stop them at the first moment the fictitous particle reaches the 97% of the depth of the deeper well. This can be considered as the mean lifetime of the metastable state, that is the left minimum of the potential profile.

As time of observation it is used 750000 arbitrary units and the number of realizations is chosen 500000.

The results show that there is a nonmonotonicity of the **MET** in both the parameters D and μ. In Fig.2.5 it is shown the behavior of the **MET** as a function of the parameter D for five different values of the parameter μ chosen in order to better show another feature of this particular system. We observe that for every value of μ we have the same nonmonotonic trend with a maximum. It is clear from Fig.2.5 that the maximum for each curve is in a different position, i.e. it comes for a different value of D.

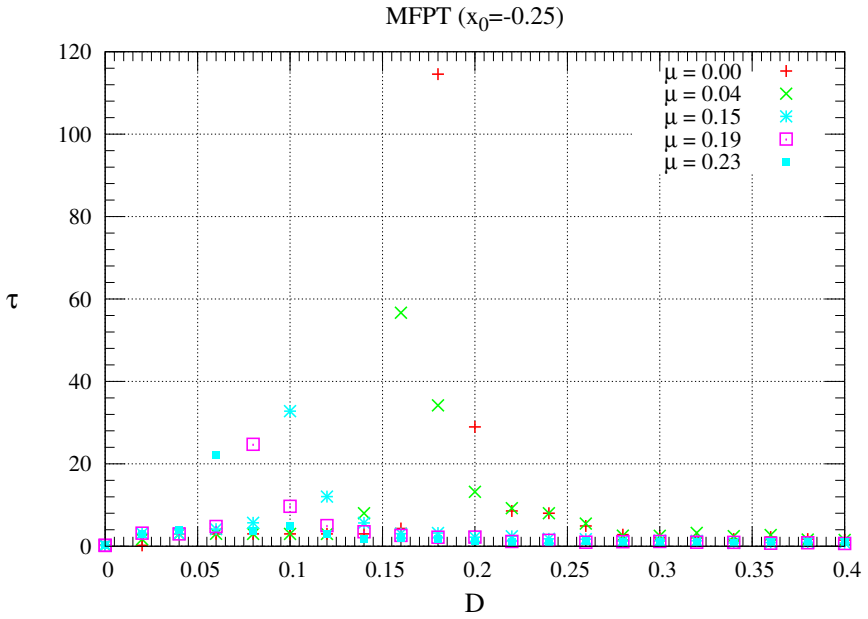

Figure 2.5: Plot of the behavior of the **MFPT** as function of D for several values of the parameter μ as shown in the legend

In particular we can see that for incresing μ the value of the parameter D which gives the maximum for the mean lifetime of the metastable state tends to zero and, at the same time, the value of the **MET** at the maximum becomes lower and lower.

In Fig.2.6 the behavior of lifetime τ is shown as a function of μ for several values of the parameter D. In this plot it is possible to see that the lifetime τ

shows a nonmonotonic behavior also as a function of the parameter μ, with fixed parameter D. This means that we can observe a sort of islands defined by certain set of the parameters D and μ where the lifetime of the metastable state increases with the respect to the deterministic lifetime.

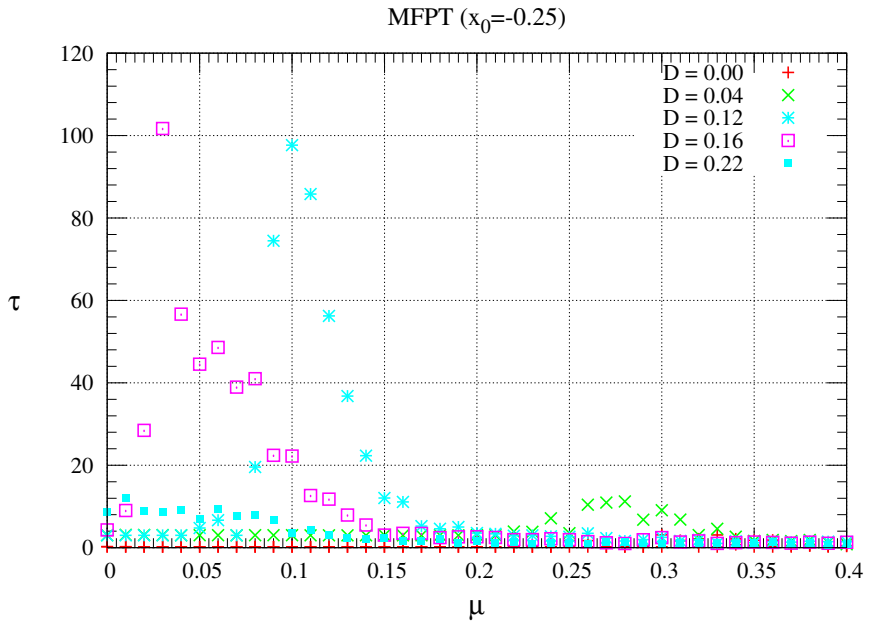

Figure 2.6: Plot of the behavior of the **MFPT** as function of μ for several values of the parameter D as shown in the legend

In Fig. 2.7 a 3D plot of the mean lifetime is shown, where is also visible the nonmonotonicity of the lifetime vs. the two parameters.

In Fig. 2.8 it is shown a color map of the **MFPT** where we can see clearly this behavior.

In Fig.2.9 the positions of the maxima are plotted. We can see clearly this feature and that the position of the maxima for increasing μ decreases and for $\mu > 0.18$ we observe no more maxima, that is the lifetime decreases reaching very small values and the nonmonotonicity of the behavior vanishes.

It is possible to conclude that the nonmonotonicity of the the mean lifetime of the metastable state vs. the parameters D and μ gives rise to islands of enhancement of the stability of the metastable state (**NES** islands). In these

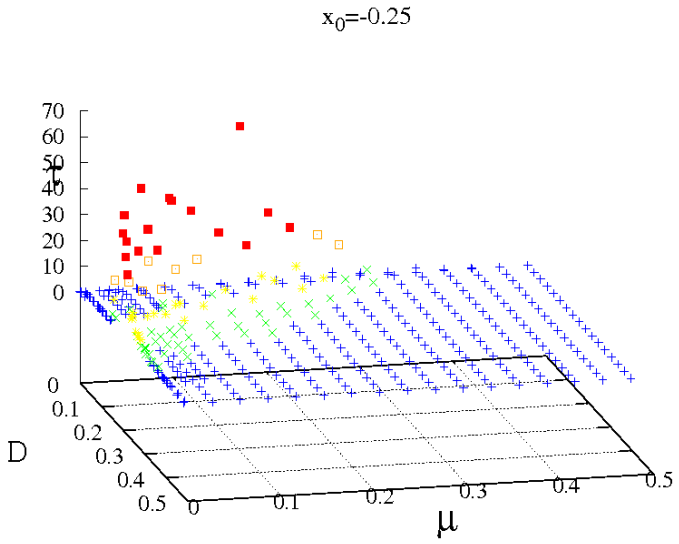

Figure 2.7: 3D plot of mean lifetime for both D and μ from 0 to 0.5

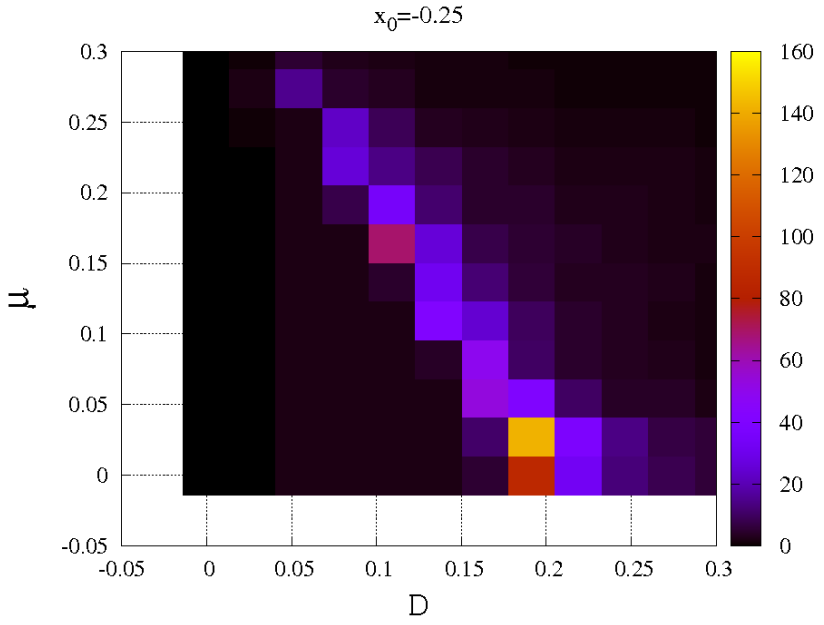

Figure 2.8: Map of mean lifetime for both D and μ range from 0 to 0.3

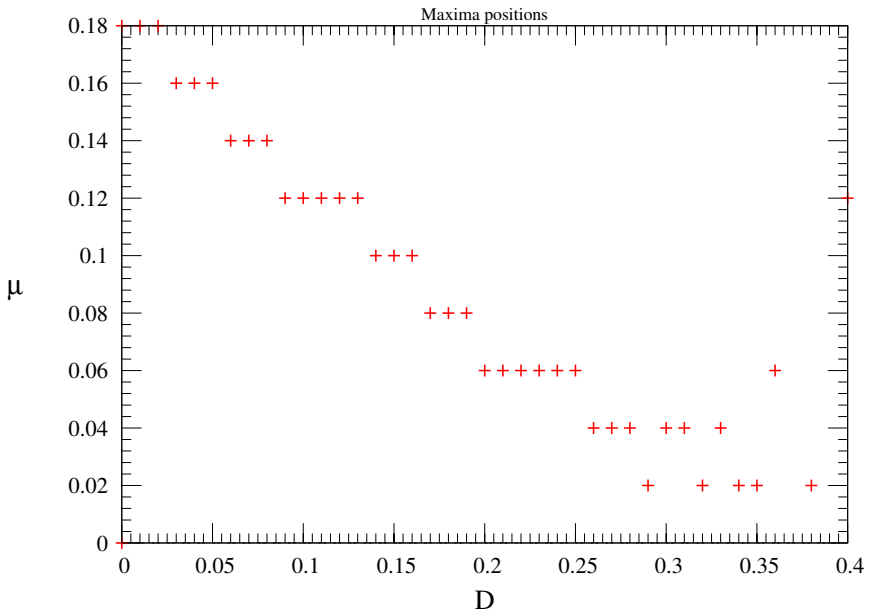

Figure 2.9: Plot of the position of the maxima in the plane (D, μ) found for fixed D. For $D > 0.3$ we are out of the islands of enhancement of stability and the mean lifetime of the metastable state is of the same order of magnitude of the fluctuations.

islands the MET is greater than deterministic deacy time of the system from unstable initial position.

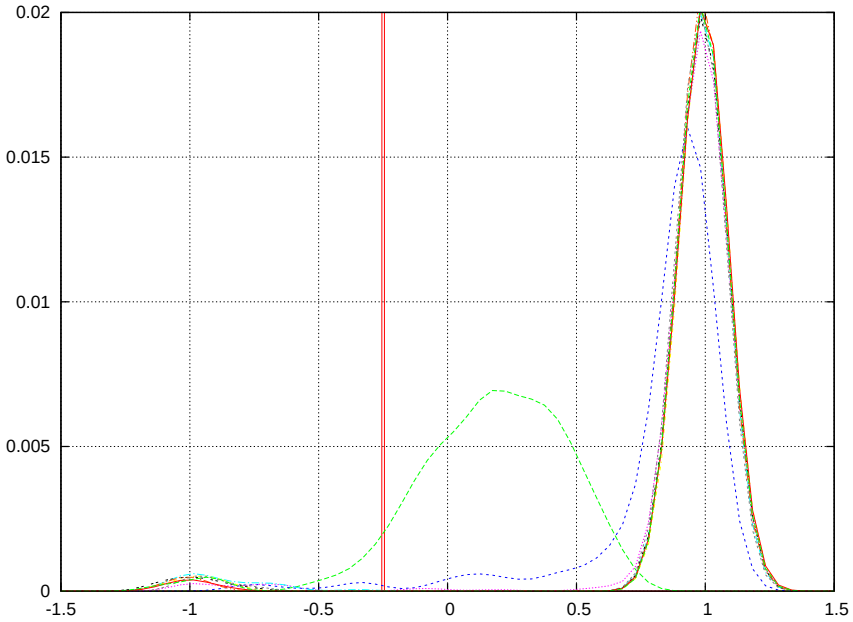

Figure 2.10: The Probability Density Function calculated for $D = 0.225$ and $\mu = 0.1$ for different values of time ranging from $t = 0$ to $t = 20$. The red line is the delta function which is the pdf at $t = 0$, in the following temporal step the pdf widens (green line) and then it goes towards its stationary shape with the its principal maximum at $x = 1$ (the lower energy state) and its secondary maximum at $x = -1$ (the higher energy state)

In Fig.2.10 is shown the time behavior of the probability density function $P(x(t))$, calculated through numerical simulations, for $D = 0.225$, $\mu = 0.1$ and different values of time ranging from $t = 0$ to $t = 20$. This (**PDF**) moves from the initial condition, which is obviously a delta function because all the particles are in the same positions, towards the stationary **PDF**, which exhibits two maxima.

The calculation of the mean lifetime of the metastable state obtained through the use of numerical simulations has two main problems:

- the number of the realizations cannot be infinite

- for each realization the observation time cannot be infinite

This means that each numerical evaluation is affected by these systematic errors. The first error affects the evaluation of the lifetime, which is dependent on the number of realizations. This error can be minimized by increasing of the number of realizations, until then lifetime doesn't depends anymore from this number.

The second error has the effect to lower the value of the average lifetime of the metastable state, understimating the **MET**. This error can be minimized by increasing the observation time until the number of trapped particles, that is the number of particles that at the end of the observation time are still in the metastable state, is a very low number compared to the number of realizations.

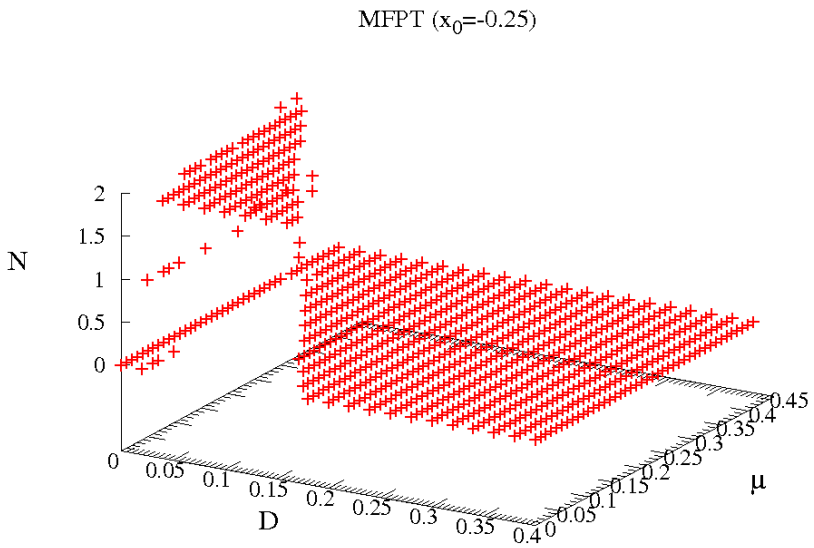

Figure 2.11: 3D graph of the number of the trapped particles at the end of the simulation time as function of D and μ for 750000 realizations.

In Fig. 2.11 the number of trapped particles as function of the two parameters is shown. It is possible to note that we find trapped particles for the same range of parameters where we find the monotonicity. The highest number of trapped particles is 2 giving a percentage of trapped particles which is 0,0004 % .

Moreover it is possible to note that the behavior of the number of the trapped particles as a function of the two parameters is nonmonotonic too and we can conclude that the nonmonotonicity of the lifetime is not an artefact coming out from the numerical evaluation.

2.5.1 Other initial conditions

In the previous paragraph it waas shown the nonmonotonic behavior of **MET** for the initial condition $x_0 = -0.25$. Here we present the results of simulations performed for other initial conditions, namely $x_0 = -0.1$ and $x_0 = -0.225$.

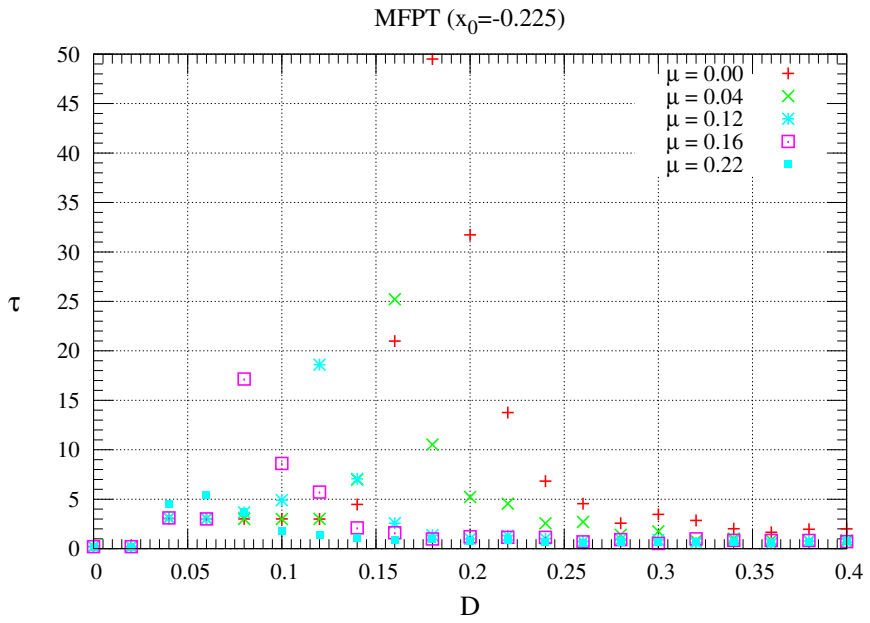

Figure 2.12: Plot of the behavior of the **MET** as function of D for several values of the parameter μ as shown in the legend. The initial condition is $x_0 = -0.225$

In Fig. 2.12 the plot of the lifetime as function of D and for several values of μ (the same set of values of Fig.2.5) and for the initial condition $x_0 = -0.225$ is shown. It's possibile to note that the nonmonotonicity is still present.

In Fig. 2.13 the plot of the lifetime as function of μ, for several values of D (the same set of values of Fig.2.5) and for the initial condition $x_0 = -0.225$ is

shown. It's possibile to note that also in this case the nonmonotonic behavior is still present.

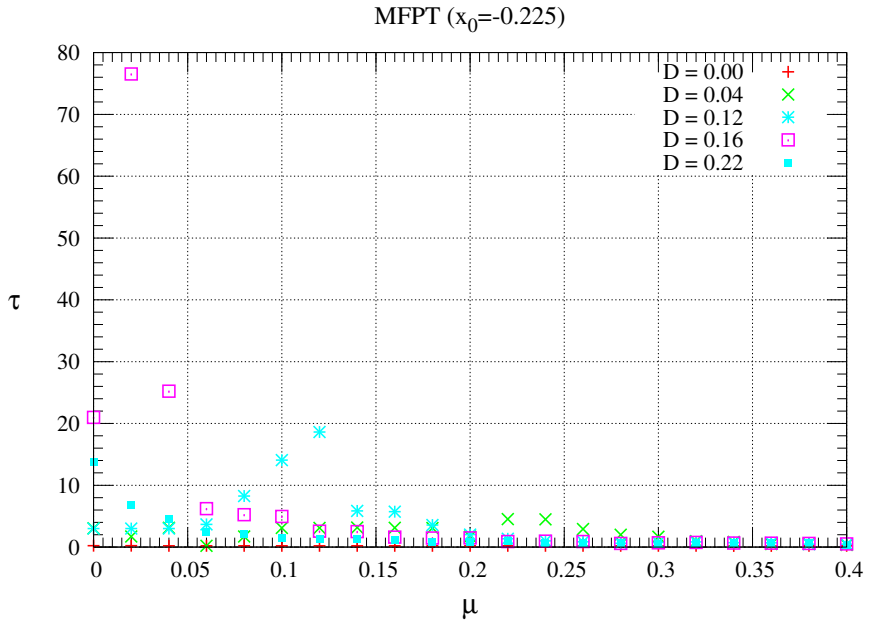

Figure 2.13: Plot of the behavior of the **MET** as function of μ for several values of the parameter D as shown in the legend. The initial condition is $x_0 = -0.225$

However the lowering of the maxima values has to be pointed out. The greater value of the maxima for the D-plots is near 120 for $x_0 = -0.25$ while for $x_0 = -0.225$ its value is near 50 and it is present for very small values of μ for both cases.

In order to study how the initial condition affects the behavior of the lifetime of the metastable state seen as function of μ we have to compare the Fig.2.6 with Fig.2.13. In Fig.2.6 we can observe that have two strong maxima of a similar intensity ($\tau \sim 100$) for the values $D = 0.16$ and $D = 0.12$. In the graph in Fig.2.13 ($x_0 = -0.225$) the maximum of the curve plotted for $D = 0.16$ has the value of 80 while the maximum for $D = 0.12$ has the value of 20. The nonmonotonic behavior of the average lifetime is still present with these initial conditions and as shown in calculations non here reported the **NES** island disappers.

By chosing as initial condition $x_0 = 0.1$, we obtain the graphs shown in Fig.2.14 left panel (τ as function of D) and in Fig.2.14 right panel (τ as function of μ).

2.6 Ising model

In Section 2.4 it is pointed out that a physical example of a system which can is affected by the presence of multiplicative noise is a ferromagnetic sample described by means of the Ising model (37, 111). Here we recall the main features of this model. In the Ising model of a m-dimensional material, a regular lattice arrangement of N^m molecules in space is considered. This model can be used for three kind of physical system (112):

1. magnets
2. mixtures of two kind of molecules
3. mixtures of molecules and holes

that can be oriented either up or down relative to the direction of an externally applied field

The Ising model can describe all those three kinds of materials if we suppose that to each node of the lattice is represented with a two-valued variable that can be oriented either up or down. The up and down value represents

1. up and down position of a molecule with a $\frac{1}{2}$ spin relative to the direction of an externally applied field
2. molecule species A or B
3. node occupied by a molecule or not (hole)

A configuration of the lattice is a particular set of all the values of the spins and this means that there will be 2^{N^m} different configurations. Another fundamental assumption is that the molecules exert short range forces on each other. Each molecule interacts only with its neighbours and then its interaction energy is

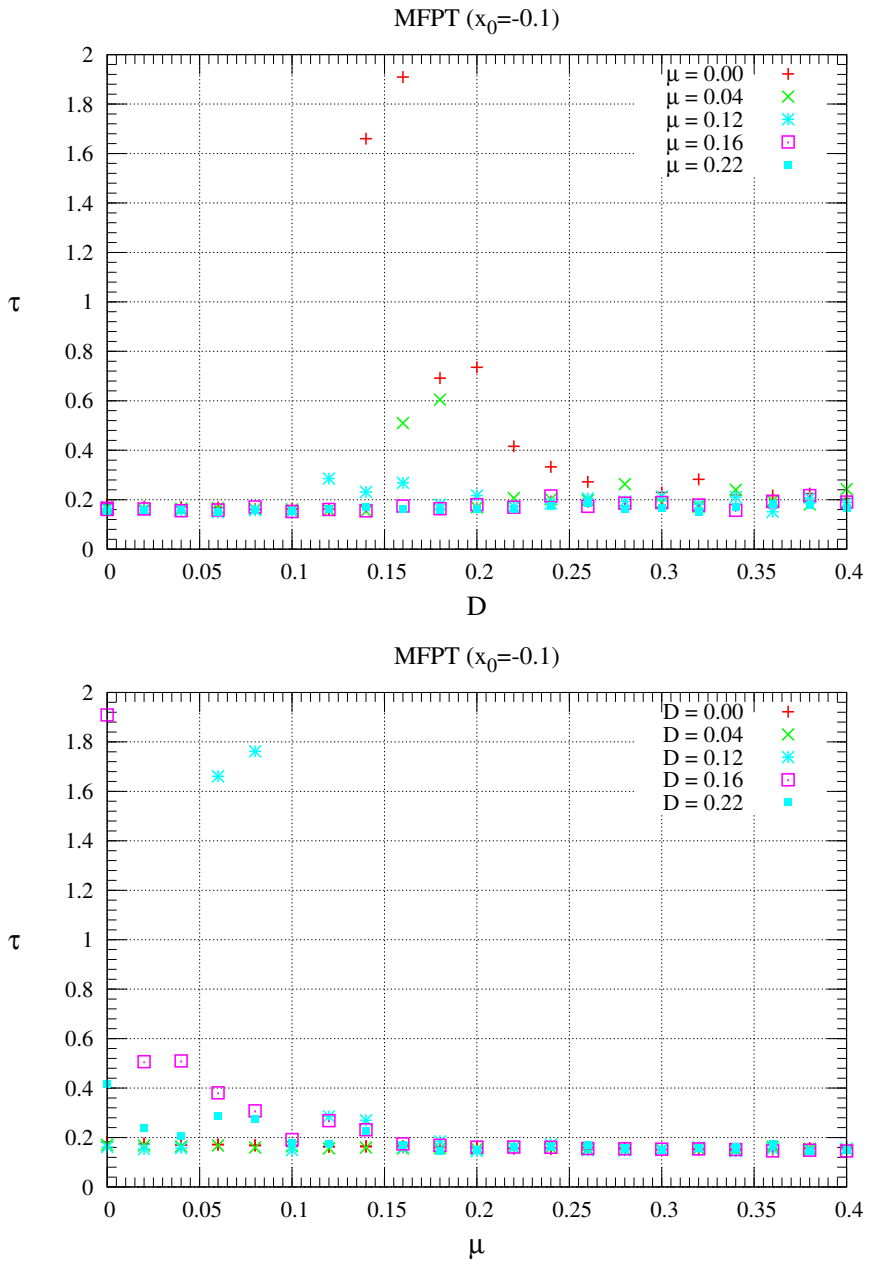

Figure 2.14: Plot of the behavior of the **MET** as function of D for several values of the parameter μ as shown in the legend (upper panel). Plot of the behavior of the **MET** as function of μ for several values of the parameter D as shown in the legend (lower panel). The initial condition is $x_0 = -0.1$

higher if the node has a characteristic value different from the one of the majority of its nearest neighbours. By minimizing the energy this model tends naturally to make neighboring spins have the same orientation.

This means that we can have

1. spontaneous magnetization
2. phase separation (molecules of the same kind gather)
3. condensation of molecules in a portion of space

For the physical system of the kind 1 the interaction energy is given by the term

$$E = -\vec{\mu} \cdot \vec{B}_{tot} \tag{2.72}$$

where $\dot{\mu}$ is the magnetic dipole moment and $\dot{B}_{tot}$ the magnetic field present in that node. The magnetic field that affects the dynamics of the spin in the i-th node is the sum of the external one and the ones generated by every spins in the lattice. Using the approximation of the nearest neighbors we take into account only the interaction with the spin that are far away in the lattice from the node considered just one step away in every direction.

The general Hamiltonian for a 3-dimensional lattice is then

$$H = -J \sum_{i,j} (S_{ix} S_{jx} + S_{iy} S_{jy} + \lambda S_{iz} S_{jz}) + D \sum_{i} S_{iz}^2 + B \sum_{i} S_{iz} \tag{2.73}$$

where J is the strength of the interaction between spins, λ accounts for an exchange anisotropy, D accounts a single ion anisotropy and B is the external magnetic field. The sum runs over the nearest neighbor pairs and this means that the spin in the (i, j) position interacts with all the spins which have at least an index that differ by an unity (i.e. $i \pm 1$ or $j \pm 1$ or both).

For a classical ferromagnet we have to set $\lambda = 1$ and $D = 0$ and $J > 0$ ($J < 0$ is for an antiferromagnet) and then the 2.73 becomes

$$H = -J \sum_{i,j} (S_{ix} S_{jx} + S_{iy} S_{jy} + S_{iz} S_{jz}) + B \sum_{i} S_{iz} \tag{2.74}$$

In 1925 Ising (113) started the study of this kind of model finding a solution for a 1-dimensional lattice and showing that for this case there is no spontaneous magnetization. In 1944 Onsanger (114) found an exact solution for the case of a 2-dimensional lattice showing that there is a phase transition. In the 1952 Yang (115) used the Onsanger solution as modified by Kaufman (116, 117) to calculate the spontaneous magnetization.

2.7 Metastability in Ising model

From the early times the Ising model, because of its complexity, is a system that can be studied through numerical simulation of its behavior also in order to check the approximations done in analytical investigations (118).

The main approach to the numerical simulations of the Ising model is the MonteCarlo method. In this protocol time evolution proceeds by a stochastic dynamics which consists of single spin flips. For each spin flip (at the i-th node) we have the transition rate given by

$$\omega(s \to s', i) = p + (1-p)F(\beta\Delta E) \tag{2.75}$$

where s and s' are the configurations before and after the spin flip, ΔE is the variation of the energy due to the change of the configuration and, as usual, $\beta = \frac{1}{k_B T}$. The parameter p is a transition rate which is indipendent from the temperature. This means that Eq.2.75 represents the transition rate of a single spin which is in contact with two thermal baths. One of this is at temperature $T = \frac{1}{\beta k_B}$ with a probability $1-p$ and the second one is at infinite temperature with probability p. This protocol is a way to block equilibrium. The bath at finite temperature captures the dynamics generated by the thermal processes which occurs at temperature T, the second bath (the one at infinite temperature) mimics any nonequilibrium process induced by, random impurities, rapidly diffusing local defects and quantum tunnelling (37, 119, 120)

In the Eq.2.75 the function $F(x)$ gives the probability of flipping. Useful choices are the so called Glauber rate

$$F_G(x) = \frac{1}{1 - e^{\beta\Delta E}} \tag{2.76}$$

or the so called Metropolis rate

$$F_M(x) = \min(1, e^{-\beta\Delta E}) \tag{2.77}$$

The different rates do not affect the results in most situations only for very high temperatures differences appear(121). In the case of very high temperatures the Metropolis algorithm gives a transition probability near to 1 for $\Delta E > 0$ (see 2.77) and then the spin will flip on every cycle and thus the system will oscillates between two states. The Glauber algorithm for $T \longrightarrow \infty$ gives a transition probability which approaches $\frac{1}{2}$. This means that for the above cited limiting case the Metropolis rate becomes non ergodic while Glauber algorithm is ever ergodic (121). However by using the Glauber rate the simulation times became longer. Because of the ergodicity property we choose the Glauber rate our simulations.

Moreover it has to be pointed out that if we don't want to deal with boundary effects it possible to wrap the n-dimensional lattice on a $(n+1)$-dimensional torus. These are called periodic boundary conditions and this means that the row (column) nearest neighbor of the spins which are in the last position of a row (of a column) is the first one of the row (column). This protocol eliminates boundary effects but the system is still characterized by the lattice size being the maximum value of the correlation length is half the size of the lattice.

2.7.1 Simulations for the Ising model

With the prescriptions stated above, simulations for a square lattice composed by $1000x1000$ two valued spins are carried out with different values of the non-equilibrium parameter p. This allows to show how the evolution of the sample depends on this parameter.

The sample is subjected to an external field $h = -0.1$ and each spin has a dipole moment $\mu = 0.6 \cdot 10^{-3}$ in the same units. The initial condition is an uniform magnetization with all the spins up. The lifetime of the metastable state "spin up" is defined as the time needed by the sample in order to reach a state with a global magnetization equal to 0.1.

Putting the absorbing barrier for the Brownian particle which corresponds to the order parameter 'state of the magnetization' at the value of 0.1 reflects the

arbitrary choice to consider the system in the metastable state "spin up" only when it has a strong magnetization. This is a similar choice to the one done in section 2.5 where the absorbing barrier is put at 99% of the well depth.

The temperature is measured in terms of the reduced temperature $\frac{k_B T}{J}$ where k_B is Boltzmann constant, T is the temperature and J is costant of coupling between the spins.

In fig.2.15 the lifetime of the metastable state as function of the temperature of the sample for a non equilibrium parameter $P = 0.001$ is shown. A nonmonotonic behavior vs. the temperature with the maximum at $T = 0.5$ is found.

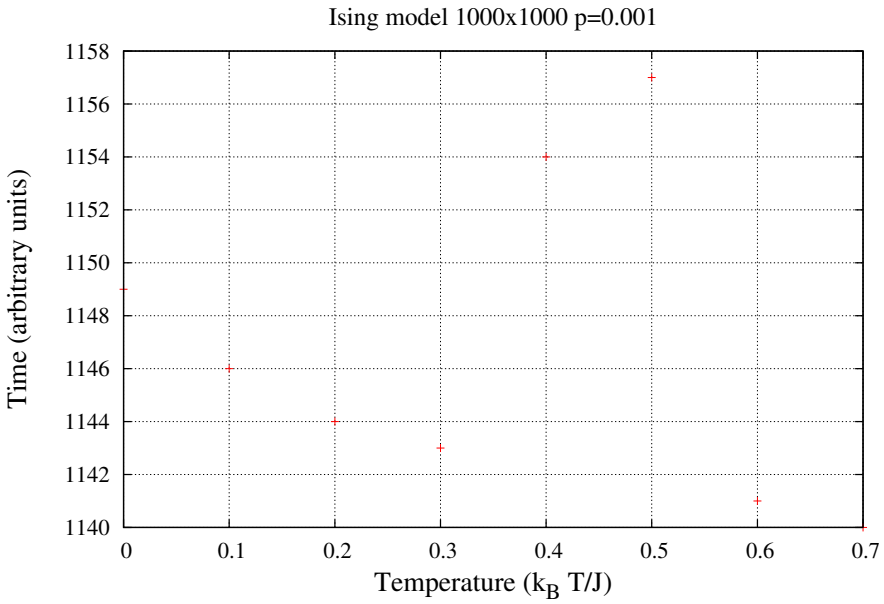

Figure 2.15: Behavior of the time needed to the sample to reach the level of magnetization of 0.1 starting from an uniform magnetization (all spins up) and for the nonequilibrium parameter value $p = 0.001$

In fig.2.16 the average lifetime of the metastable state as a function of the temperature of the sample for a lower value of the nonequilibrium parameter $P = 0.00001$ is shown. A nonmonotonic behavior with a maximum for $T = 0.3$ is found.

It is interesting to note that, as in the case of the simulations discussed in the section 2.5, we have a nonmonotonic behavior and the position of the maximum is depending on the value of the nonequilibrium parameter. The Fig.2.15 and Fig.2.16 has to be compared with the Fig.2.5 and Fig.2.12 which show a similar trend.

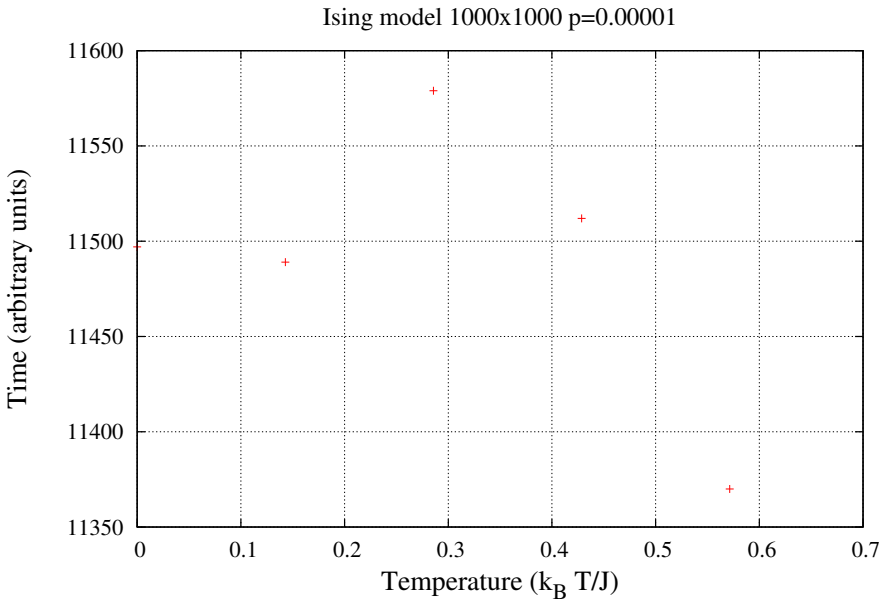

Figure 2.16: Behavior of the time needed to the sample to lose magnetization starting from an uniform magnetization for the nonequilibrium parameter value $p = 0.00001$

These results are in agreement with those theoretical results discussed in the previous sections of this chapter.

3

Open quantum systems

3.1 Introduction

In this chapter, in order to analyze the evolution of a quantum particle subjected to time-independent asymmetric bistable potential and affected by environmental noise, we use the Caldeira-Leggett model,(42) which allows to derive a quantum mechanical analogue of the generalized Langevin equation. The study is performed by using the approach of the Feynman-Vernon functional(56) in Discrete Variable Representation (**DVR**)(41, 57).

3.2 The Model

Our physical model consists of a quantum particle with mass M, interacting with a thermal bath which plays the role of environment. The dynamics of this quantum particle is investigated by using the Caldeira-Leggett model(42). In our analysis $\hat{q}$ and $\hat{p}$ are one-dimensional operators for position and momentum, respectively.

The unperturbed Hamiltonian of the system is

$$\hat{H}_0 = \frac{\hat{p}^2}{2M} + \hat{V}_0(\hat{q}) \tag{3.1}$$

where

$$\hat{V}_0(\hat{q}) = \frac{M^2\omega_0^4}{64\Delta U}\hat{q}^4 - \frac{M\omega_0^4}{4}\hat{q}^2 - \hat{q}\epsilon, \tag{3.2}$$

is the asymmetric bistable potential shown in Fig.3.1. Here, ϵ and ΔU are the asymmetry parameter and the barrier height, respectively, and ω_0 is the natural oscillation frequency. In our study we consider the lower eigenstates in order to study the dinamics of the system depending on the specific shape of the potential. This kind of potential is the same of the classical case studied in the previous chapter but in this case the dynamics of the system has another channel which may be used. This channel is the tunnel effect that is a typical behavior in the quantum world. The particle described with a wavefunction and whose position given by a probability density function extendend across the whole space has the possibility to pass through the potential barrier even when it has an energy lower than the potential barrier.

In Fig.3.1 these lower energy eigenvalues are shown on the vertical axis. In the same figure, on the horizontal axis the 8 position eigenvalues are displayed, obtained by using the **DVR**-state $|q_\mu\rangle$. The black circle marks the initial position of the particle, that is the system at $t = 0$ is in a state given by a proper linear combination of the 8 eigenstates $|q_\mu\rangle$ considered in this analysis. The curves shown in the figures are the eigenfunctions corresponding to the 8 energy eigenvalues.

In order to describe the dynamics of the particle interacting with environment, we consider the following Hamiltonian

$$\hat{H}(t) = \hat{H}_0(t) + \hat{H}_B, \tag{3.3}$$

where

$$\hat{H}_B = \sum_{j=1}^{\mathcal{N}} \frac{1}{2}\left[\frac{\hat{p}_j^2}{m_j} + m_j\omega_j^2\left(\hat{x}_j - \frac{c_j}{m_j\omega_j^2}\hat{q}\right)^2\right] \tag{3.4}$$

is the Hamiltonian which describes the thermal reservoir and its interaction with the particle. As usual in the Caldeira-Leggett model, the thermal bath is depicted by an ensemble of $\mathcal{N}$ harmonic oscillators with spatial coordinate $\hat{x}_j$, momentum $\hat{p}_j$, mass m_j, and frequency ω_j. The coefficients c_j are the coupling constant between system and thermal bath. We note that, as $\mathcal{N} \to \infty$, from Eq.(3.4)

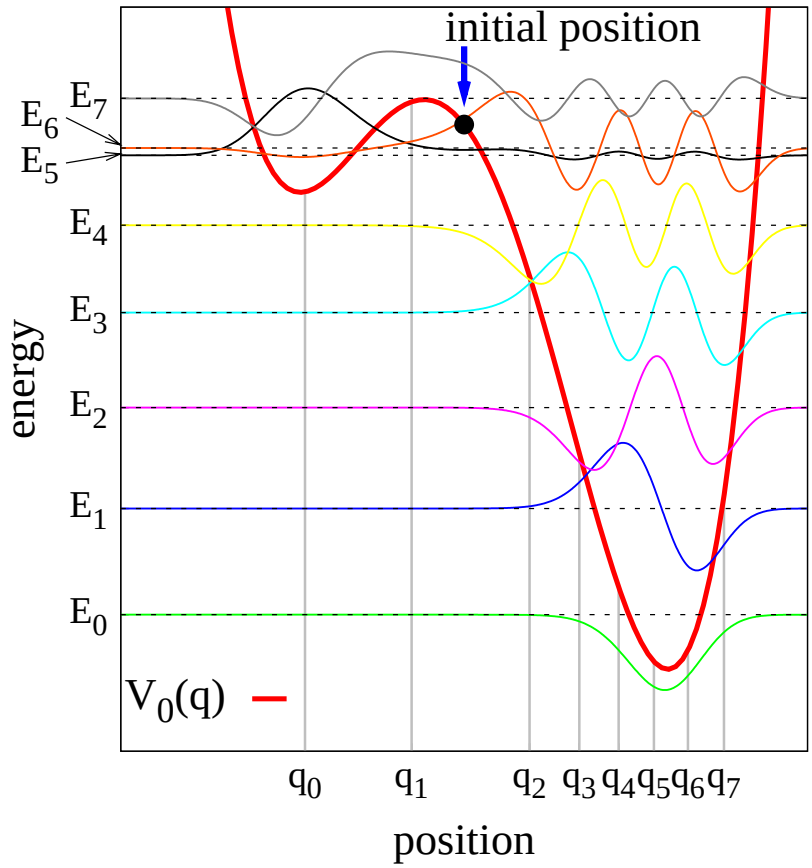

Figure 3.1: Potential profile $V_0(q)$ (see Eq.(3.2)) for $\Delta U = 3$ and $\epsilon = 0.5$. Energy levels and corresponding eigenstates considered in our analysis are indicated by horizontal lines and curves, respectively. The energy eigenvalues are $E_0 = -2.01$, $E_1 = -0.92$, $E_2 = 0.11$, $E_3 = 1.08$, $E_4 = 1.97$, $E_5 = 2.69$, $E_6 = 2.76$, $E_7 = 3.27$. By using the DVR-state $|q_\mu\rangle$, eigenvalues of the position operator are obtained and shown on the horizontal axis: $q_0 = -4.17$, $q_1 = -1.38$, $q_2 = 1.71$, $q_3 = 3.02$, $q_4 = 4.05$, $q_5 = 4.97$, $q_6 = 5.86$, $q_7 = 6.81$. The initial position is $q_{start} = 0$ (black circle).

a continuous spectral density is obtained. Being the reservoir described as an ensemble of harmonic oscillators the effects of the thermal bath on the system under study can be fully characterized by a spectral density(76).

An example of a physical case when the previous assumption cannot be made is discussed in chapter 4 and solved through the static path approximation (**SPA**).

For a reservoir made of harmonic oscillators we can write the spectral density in a very general way as follows

$$J(\omega) = \frac{\pi}{2}\sum_{j=1}^{N}\frac{c_j}{m_j\omega_j}\delta(\omega-\omega_j) \tag{3.5}$$

and for $N \longrightarrow \infty$ the spectral density might be considered as a function of ω.

Our starting point is the generalized Langevin equation for linear memory-friction force and additive noise (45)

$$M\ddot{q}(t) + \frac{\partial V(q)}{\partial q} + M\int_{-\infty}^{t} dt'\gamma(t-t')\dot{q}(t') = \xi(t). \tag{3.6}$$

In Eq.3.6 the random force $\xi(t)$ has the usual statistical properties

$$\langle\xi(t)\rangle_{\rho_R(0)} = 0 \tag{3.7}$$

$$\langle\xi(t)\xi(t')\rangle_{\rho_R(0)} = Mk_BT\gamma(t-t'), \tag{3.8}$$

where the function $\gamma(t-t')$ is the damping kernel and the average is taken with respect to the canonical classical equilibrium density operator of the unperturbed reservoir which reads

$$\rho_R(t_0) = \Big(tr\exp(-\beta\hat{H}_B(t=0))\Big)^{-1}\exp(-\beta\hat{H}_B(t=0) \tag{3.9}$$

where, as usual, $\beta = \frac{1}{k_BT}$. It might interesting to point out that the previous Eq.3.8 is the classical fluctuation-dissipation theorem.

In this context the connection between the damping kernel and the spectral density is established as follows (see (45))

$$\gamma(t) = \Theta(t)\frac{2}{\pi M}\int_0^{\infty} d\omega\frac{J(\omega)}{\omega}cos(\omega t) \tag{3.10}$$

which inverted gives

$$J(\omega) = M\omega \int_0^\infty dt\gamma(t)\cos(\omega t) \tag{3.11}$$

or, in term of the Laplace trasform

$$J(\omega) = \lim_{\epsilon\to 0^+} = M\omega\frac{[\gamma(\epsilon + i\omega) + \gamma(\epsilon - i\omega)]}{2} \tag{3.12}$$

From these results we have that in the Markovian limit, which corresponds to the dissipation in the Ohmic regime, where the damping is frequency indipendent (i.e. $\gamma(\omega) = \gamma$) the spectral density is given by (42)

$$J(\omega) = \eta\omega \tag{3.13}$$

A first generalization of this kind of dissipation law is the following

$$J(\omega) \propto \omega^s \tag{3.14}$$

If we choose $s < 1$ we say that we are dealing with a sub-ohmic case and for $s > 1$ we have a super-ohmic case.

In this study the spectral density used is the Ohmic one, whose functional law is Eq.3.13. The problem in using this kind of spectral density is given by its growth without limits for increasing ω. In order to avoid this 'ultraviolet catastrophe' in calculations, the spectral density used is characterized by an exponential cut-off with a cutting frequency ω_c as follows

$$J(\omega) = \eta\omega\exp\left(-\frac{\omega}{\omega_c}\right). \tag{3.15}$$

Here, as in the previous equations $\eta = M\gamma$ and γ is the strength of the coupling between system and thermal bath. It also to be noted that $\omega_c \gg \omega_0, \omega_j, \gamma$.

Because of the bilinear coupling between the coordinate $\hat{q}$ of the system and the coordinate $\hat{x}$ of the thermal bath, this model is the quantum analogue of a classical system affected by a constant random force(45). In the next two subsections the mathematical approach to this problem is outlined.

3.2.1 The Feynman-Vernon approach

In order to make our analysis independent by the internal degrees of freedom of the thermal bath, we have to trace out the degrees of freedom of the reservoir by using the reduced density operator

$$\rho(q_f, q'_f; t) = \int dq_0 \int dq'_0 K(q_f, q'_f, t; q_0, q'_0, t_0)\rho_S(q_0, q'_0, t_0), \tag{3.16}$$

where the propagator K is given by

$$K(q_f, q'_f, t; q_0, q'_0, t_0) = \int_{q(t_0)=q_0}^{q(t)=q_f} \mathcal{D}q \int_{q'(t_0)=q'_0}^{q'(t)=q'_f} \mathcal{D}q' \mathcal{A}[q]\mathcal{A}^*[q']\mathcal{F}_{FV}[q, q'] \tag{3.17}$$

and

$$\mathcal{A}[q] = \exp\left(i\frac{S_S[q]}{\hbar}\right) \tag{3.18}$$

with $S_S[q]$ being the classical action functional.

In Eq.(3.17), $\mathcal{F}_{FV}[q, q'] = \exp\left(-\frac{\phi_{FV}[q,q']}{\hbar}\right)$ is the Feynman-Vernon (**FV**) influence functional with the influence weight functional $\phi_{FV}[q, q']$ which is depending on the bath correlation function(45).

It is customary in this kind of calculation, in order to simplify the approach to the physical intuition, to trasform the influence functional in the framework of the relative coordinate

$$\xi_j(t) = q_j(t) - q'_j(t) \tag{3.19}$$

and of the center of mass

$$\chi_j(t) = q_j(t) + q'_j(t) \tag{3.20}$$

In this system of coordinates the Feynmann-Vernon influence weight functional reads

$$\phi_{FV} = \int_{t_0}^{t} dt' \int_{t_0}^{t'} dt''[\xi(t')S(t' - t'')\xi(t'') + i\xi(t')R(t' - t'')\chi(t'')]$$

$$
\begin{aligned}
&+ \quad \xi(t)\int_{t_0}^{t'} dt'[\xi(t')S(t-t') + i\chi(t')R(t-t')] + \\
&+ \quad \xi(t_0)\left[\xi(t)S(t-t_0) - \int_{t_0}^{t} dt'\xi(t')S(t'-t_0)\right] \\
&+ \quad i\chi(t_0)\left[\xi(t)R(t-t_0) - \int_{t_0}^{t} dt'\xi(t')R(t'-t_0)\right] \qquad (3.21)
\end{aligned}
$$

where $S(t)$ is the real part of the bath correlation function and $R(t)$ is the imaginary one.
The functional form of the bath correlation function is given by the relation

$$Q(t) = S(t) + iR(t) = \frac{1}{\pi}\int_0^\infty d\omega \frac{J(\omega)}{\omega^2}[\coth\frac{\hbar\omega\beta}{2}(1-\cos\omega t) + i\sin\omega t] \qquad (3.22)$$

This functional form is a general result of the fluctuation-dissipation theorem (45) and therefore is indipendent of the model (bath of harmonic oscillators or whatever) chosen to describe the reservoir.

3.2.2 Discrete Variable Representation

By solving the eigenvalue equation connected with the Hamiltonian $\hat{H}_0$ (see Eq.(3.1)), we get the energy eigenstates (see vertical axis in Fig.3.2). If we choose to change the base of the eigenstates going from the energy representation to the position one we put ourselves in the natural framework to discuss about the localization of the quantum particle. Because of this transformation it is possible to obtain the basis $\{|q_\mu\rangle\}$ of eigenstates of the position operator $\hat{q}$ and in horizontal axis in Fig.3.2 the eigenvalues of these eigenstates are shown.

Within the framework of the *discrete variable representation* (**DVR**)(41, 57) the dynamics in the **DVR** basis is described by a quantum mechanical path $q(t)$ which the system follows during its evolution in time. If we focus our attention to the N lower eigenstates, the integration over the double infinity of differentials in Eq.3.16 simplifies greatly becoming a sum of N terms.

The system starts at time $t = t_0$ in the state $q(t = t_0) = q_0$ and evolves via m jumps between the M discrete states into the final state $q(t = t_m) = q_m$. The full time interval splits into m short time intervals such that the jumps happen at times $t = t_j$. The intermediate states are labeled by q_j, where $j = 1, ..., N$ is

the quantum state index, and $j = 1, ..., m1$ denotes the time index, i.e. the time when the j-th jumps happens. The full path $q(t)$ becomes then a sequence of constant path segments which can be written as

$$q(t) = -q_{\mu_0}\Theta(t-t_1) + \sum_{j=1}^{m-1} q_{\mu_j}\left[\Theta(t-t_j) - \Theta(t-t_{j+1})\right] + q_{\mu_m}\Theta(t-t_m), \quad (3.23)$$

where $\Theta(t)$ is the Heaviside function. In the relative and center of mass coordinates the previous equation, written for the paths $q(t)$ and $q'(t)$, becomes

$$\xi(t) = -\xi_{\mu_0\nu_0}\Theta(t-t_1) + \sum_{j=1}^{N-1} \xi_{\mu_j,\nu_j}\left[\Theta(t-t_j) - \Theta(t-t_{j+1})\right] + \xi_{\mu_N\nu_N}\Theta(t-t_N) \quad (3.24)$$

and

$$\chi(t) = -\chi_{\mu_0\nu_0}\Theta(t-t_1) + \sum_{j=1}^{N-1} \chi_{\mu_j,\nu_j}\left[\Theta(t-t_j) - \Theta(t-t_{j+1})\right] + \chi_{\mu_N\nu_N}\Theta(t-t_N). \quad (3.25)$$

Thus the double path integral over the m-state paths $q(t)$ and $q'(t)$ in Eq. 3.16 is rewritten as an integral over a single path that jumps between the M^2 states of the reduced density matrix in the (q, q')-plane. The total number m of jumps is given by the sum of the number of jumps for the paths q and q' and then, as a result, using Eq.(3.17), the continuous real-time path integral given in Eq.(3.16) becomes a discrete path with m transitions at times $t_1, t_2, ...t_m$ which, using the definitions Eq. 3.19 and 3.20, becomes

$$\rho_{\mu_m\nu_m}(t) = \sum_{\mu_0\nu_0} \int_{\xi(t_0)=\xi_0}^{\xi(t)=\xi_m} \mathcal{D}\xi \int_{\chi(t_0)=\chi_0}^{\chi(t)=\chi_m} \mathcal{D}\chi\, \mathcal{C}[\xi,\chi]\, \mathcal{F}_{FV}[\xi,\chi]\, \rho_{\mu_0\nu_0} \quad (3.26)$$

where $\mathcal{C}[\xi,\chi] = \mathcal{A}[q]\mathcal{A}^*[q']$ and the influence weight functional of the FV functional is

$$\phi_{FV}[\xi,\chi] = -\sum_{l=1}^{m}\sum_{j=0}^{l-1}\xi_l S(t_l-t_j)\xi_j - i\sum_{l=1}^{m}\sum_{j=0}^{l-1}\xi_l R(t_l-t_j)\chi_j. \tag{3.27}$$

The path given in Eq.3.23 rewritten according to the definitions Eq.3.19 and Eq.3.20 can be split in the two kind of subpaths (see Eq. 3.24 and Eq. 3.24) as follows

$$q(t) = q(t) - q(t') + q(t') + q(t) = \xi(t) + \chi(t). \tag{3.28}$$

The system may be in a state where $\xi(t) = 0$ and $\chi(t) \neq 0$ or a state where $\xi(t) \neq 0$ and $\chi(t) \neq 0$. The first kind of states is called sojourn and the second kind of states is called blip. The chains of the consecutive blip states are called clusters. From the definition Eq. 3.19 it is clear that the sojourns are the diagonal states of the density matrix in the **DVR** representation while the blip are the off-diagonal states.

The main advantage in going in the **DVR** representation is that the functional integration over all the possible continuous paths turns into a discrete sum (with infinite terms) over all possible path configurations in the **DVR** basis and an integration over all intermediate times. If we are interested in the evolution of the populations, in Eq.(3.26) we have to consider the diagonal terms $\rho_{\mu_m\mu_m}(t)$.

A complete calculation of these elements in the **DVR** gives the following exact form which is calculated for a M-level system which follows a path with N transitions (41)

$$\begin{aligned}\rho_{\mu_N\mu_N}(t) &= \sum_{\mu_0,\nu_0=1}^{m}\sum_{N=1}^{\infty}\int_{t_0}^{t}\mathcal{D}\left[t_j\right]\sum_{\mu_j\nu_j}\exp\{i\sum_{j=0}^{N-1}\int_{t_j}^{t_{j+1}}dt' \\ &\times \left[E_{\mu_j}(t') - E_{\nu_j}(t')\right]\}\prod_{j=0}^{N-1}(-1)^{\delta_j}\left(\frac{i}{2}\right)^N\Delta_j \\ &\times \exp\{\sum_{l=1}^{N}\sum_{j=0}^{l-1}\xi_l S(t_l-t_j)\xi_j + i\sum_{l=1}^{N}\sum_{j=0}^{l-1}\xi_l R(t_l-t_j)\chi_j\}\end{aligned} \tag{3.29}$$

where the Kronecker symbol is 0 for a transition which allows the second index change while is 1 for a transition that changes the first index. In the previous

Eq.3.29 the probabilities of transitions towards/from the off-diagonal states are

$$\Delta_{\mu_{i+1}\mu_i} = \frac{2}{\hbar}\langle q_{\mu_{i+1}}|\mathbf{H}_0|q_{\mu_i}\rangle \tag{3.30}$$

and the energies of the diagonal states

$$E_{\mu_i}(t) = \frac{1}{\hbar}\langle q_{\mu_i}|\mathbf{H}_S|q_{\mu_i}\rangle \tag{3.31}$$

3.2.3 Approximations used

The 3.29 contains an infinite sum over all the (infinite) possible paths that the system might follow. In order to calculate the diagonal terms of the density matrix we have to reduce the number of the levels and of the paths taken into account to the relevant ones. For this reason it is necessary to state what kind of approximations we should use.

3.2.3.1 NIBA

The lower level of approximation, which is used in the spin-boson problem (so termed because only 2 levels are taken into account), is the *non-interacting blip approximation* (**NIBA**) (42). In this approximation are retained in a approximate calculation only the interactions between the sojourns and the neighboring blips neglecting all the interactions between the off-diagonal states (blips).

The **NIBA** can be used when the physical system is subjected to an Ohmic damping for high temperatures and large dissipation strenghts. Within these conditions the average blip length, that is the time the system spends in this state, is small compared to the average sojourn length. From the Eq.3.29 it is possible to see that the contribution of each step of the discrete paths increases with its length and so the contributions from blip-blip and and blip-sojourn can be not taken into account. The long blips are exponentially inhibited by the intrablip interactions.

3.2.3.2 IBCA

An improved approximation is the so called *interacting blip chain approximation* (**IBCA**) (122). In this improved approximation the interactions taken into account are those of all nearest neighbor pairs and the full interactions of the nearest

neighbor sojorn-blip pairs. It has the same range of validity of the **NIBA** but in an extended range of parameters.

3.2.3.3 NICA

If we look at Eq.3.28 it is possible to see that, in the time intervals when the system is following a subpath which is composed only by off-diagonal states (i.e. from a sojurn to another one), the sum of the weights are zero. For this reason these subpaths (which are called clusters) can be considered in the calculations as neutral objects (the ξ contribution for each cluster is zero) that don't interfere with each other. In the influence phase functional the contributions of the interactions between a blip from a cluster and a blip of another cluster is then neglected(123). This approximation is called *non interacting cluster approximation* (**NICA**).

3.2.3.4 gNICA

Following such way of thinking in Ref.(41) it is suggested a step further, that is to neglect all the intercluster interactions in the influence phase, by taking into account all the intracluster interactions and the interactions of a cluster with the preceding sojourn. Moreover, the interaction of any subpath, which a system that starts from a off-diagonal state follows before to reach the first sojourn, can be considered. This is called *generalized non interacting cluster approximation* (**gNICA**).

Again this approximation is valid if the system has an average sojourn length longer than the average cluster length. The interactions of the near cluster vanishes exponentially. For a number of levels $M > 2$ being non zero the off diagonal terms 3.30 the condition to fulfill becomes

$$\Delta_{max} = \max\{\Delta_1, \Delta_2, ...\} \lesssim \gamma \tag{3.32}$$

The previous condition means that the maximum energy gap between the level must be less than the intensity of the coupling constant.

3.2.4 Master Equation

Applying the generalized Non-Interacting Cluster Approximation described above we get the following master equation (**ME**)

$$\dot{\rho}_{\mu\mu}(t) = \sum_{\nu=1}^{N} \int_{t_0}^{t} dt' \mathcal{H}_{\mu\nu}(t-t')\rho_{\nu\nu}(t') + I_{\mu}(t-t_0), \quad \mu = 1, \ldots, N, \tag{3.33}$$

where N is the number of eigenstates. The kernel

$$\begin{aligned} \mathcal{H}_{\mu\nu}(t-t') &= \sum_{m=1}^{\infty} \int_{t_0}^{t} \mathcal{D}\left[t_j\right] \sum_{\mu_j\nu_j} \exp\{i \sum_{j=0}^{m-1} \int_{t_j}^{t_{j+1}} dt' \\ &\times \left[E_{\mu_j}(t') - E_{\nu_j}(t')\right]\} \prod_{j=0}^{m-1} (-1)^{\delta_j} \left(\frac{i}{2}\right)^m \Delta_j \\ &\times \exp\{\sum_{l=1}^{m} \sum_{j=0}^{l-1} \xi_l S(t_l - t_j)\xi_j + i \sum_{l=1}^{m} \sum_{j=0}^{l-1} \xi_l R(t_l - t_j)\chi_j\}, \end{aligned} \tag{3.34}$$

gives the contribution of the *cluster matrix* and takes into account of all possible transitions in the **DVR** paths (41). The term

$$\begin{aligned} I_{\mu}(t-t_0) &= \sum_{\mu_0,\nu_0=1\mu_0\neq\nu_0}^{m} \rho_{\mu_0\nu_0} \sum_{N=1}^{\infty} \int_{t_0}^{t} \mathcal{D}\left[t_j\right] \sum_{(\mu_j\nu_j)\mu_j\neq\nu_j} \exp\{i \sum_{j=0}^{N-1} \int_{t_j}^{t_{j+1}} dt' \\ &\times \left[E_{\mu_j}(t') - E_{\nu_j}(t')\right]\} \prod_{j=0}^{N-1} (-1)^{\delta_j} \left(\frac{i}{2}\right)^N \Delta_j \\ &\times \exp\{\sum_{l=1}^{N} \sum_{j=0}^{l-1} \xi_l S(t_l - t_j)\xi_j + i \sum_{l=1}^{N} \sum_{j=0}^{l-1} \xi_l R(t_l - t_j)\chi_j\} \end{aligned} \tag{3.35}$$

where $\rho_{\mu_0\nu_0}$ are the initial off diagonal term of the density matrix, takes into account the contribution of the first semicluster. For a off-diagonal starting condition this contribution is non zero only for long time, otherwise if the system for $t = t_0$ is in a diagonal condition the $\rho_{\mu_0\nu_0}$ are identically zero and then $I_{\mu}(t-t_0) = 0$.

According to the path integral technique based on the Feynman-Vernon theory, using **ME** corresponds to take into account only the paths connecting diagonal elements of the reduced density matrix of the position operator $\hat{q}$(41).

Within **gNICA** we neglect all intercluster interactions. Moreover, it is assumed that the characteristic memory time τ_{mem} of the matrix elements of $\mathcal{H}$ in Eq.(3.33) is the smallest time scale of the problem (*Markovian limit*. By this assumption we obtain the following *Markovian approximated master equation*

$$\dot{\rho}_{\mu\mu}(t) = \sum_{\nu=1}^{N} \Gamma_{\mu\nu}(t)\rho_{\nu\nu}(t) \tag{3.36}$$

with the time-dependent rate coefficients

$$\Gamma_{\mu\nu}(t) = \int_0^\infty d\tau \mathcal{H}_{\mu\nu}(t, t-\tau). \tag{3.37}$$

Since the diagonal elements $\rho_{\mu\mu}(t)$ obey Eq.(3.36), the long-time dynamics is ruled by a single exponential decay. Thus, Eq.(3.36) is a set of coupled ordinary first-order differential equations, which can be decoupled via a diagonalization procedure. The diagonalized rate matrix reads

$$\sum_{\kappa_1,\kappa_2=1}^{N} (S^{-1})_{\mu\kappa_1}\Gamma_{\kappa_1\kappa_2}S_{\kappa_2\nu} = \Lambda_\mu \delta_{\mu\nu}, \tag{3.38}$$

where $S_{\mu\nu}$ denotes the element of the transformation matrix and Λ_μ the eigenvalues of the rate matrix. The general solution of the Markov approximated **ME** is

$$\rho_{\mu\mu}(t) = \sum_{\nu,\kappa=1}^{N} S_{\mu\nu}(S^{-1})_{\mu\kappa}e^{\Lambda_\nu(t-t_0)}\rho_{\kappa\kappa}(t_0). \tag{3.39}$$

Because of the conservation probability, for the diagonal matrix elements holds the condition

$$\Gamma_{\nu\nu}(t) = -\sum_{\kappa\neq\nu} \Gamma_{\kappa\nu}(t). \tag{3.40}$$

This condition implies that one eigenvalue equals zero, i.e. $\Lambda_1 = 0$. Therefore,

$$\rho_{\mu\mu}(t) = \rho^\infty_{\mu\mu} + \sum_{\nu=2}^{N}\sum_{\kappa=1}^{N} S_{\mu\nu}(S^{-1})_{\mu\kappa}e^{\Lambda_\nu(t-t_0)}\rho_{\kappa\kappa}(t_0), \tag{3.41}$$

with

$$\rho^\infty_{\mu\mu} = \sum_{\kappa=1}^{N} S_{\mu,1}(S^{-1})_{1,\kappa}\rho_{\kappa\kappa}(t_0) \tag{3.42}$$

being the asymptotic population of the **DVR**-state $|q_\mu\rangle$. The rate which determines the dynamics over the largest time-scale is *the quantum relaxation rate*

$$\Gamma \equiv \min\left\{|\Re\left(\Lambda_\nu\right)|; \nu = 2, \ldots, N\right\}, \tag{3.43}$$

where Λ_ν are the eigenvalues of the rate matrix and $|\Re\left(\Lambda_\nu\right)|$ are the non-zero absolute values of the real part of Λ_ν.

In the section 3.4 the analysis is focused on the medium-short time behavior of the system, using the largest Λ_ν^{-1} as timescale to analyze the non-equilibrium dynamics of the quantum particle in the presence of thermal fluctuations.

In Fig.3.2 it is shown the first four global states $< q \mid \psi_1 >, \ldots, < q \mid \psi_4 >$ a for barrier height $E_B = \Delta U/\hbar\omega_0 = 1.4$ and asymmetry parameter $\varepsilon = 0.23$. The corresponding potential profile has a metastable state on the left well.

The quantum relaxation rate Γ as a function of the asymmetry parameter is reported in Fig.3.3 for different temperatures. There are many overlapping regions where is visible a nonmonotonic behavior of Γ as a function of the temperature. We can distinguish two different nonmonotonic behaviors: one with a maximum, reported in Fig.3.4, and the other one with a small minimum, this last one corresponds to the noise enhanced stability effect revealed in classical metastable systems.

3.3 Quantum Zeno effect

Before analyzing the results obtained by the method described applied to a dissipative quantum system subjected to a bistable potential it can be worthy to recall briefly an effect that can seem very strange but can result to be very useful. This effect may be used in controlling the evolution of the state of a quantum system. The problem we have to deal with in controlling quantum device is the fact that every system, which is in connection with a noisy environment, during its evolution loses its coherence. For this reason it becomes necessary designing a decoherence-free subspace of a Hilbert space which can be used to maintain, for the time needed, the state of quantum computing device 'frozen'(124).

This effect is named after the greek philosopher Zeno of Elea author of the famous arrow paradox and briefly it consists in a 'freezing' of a quantum state

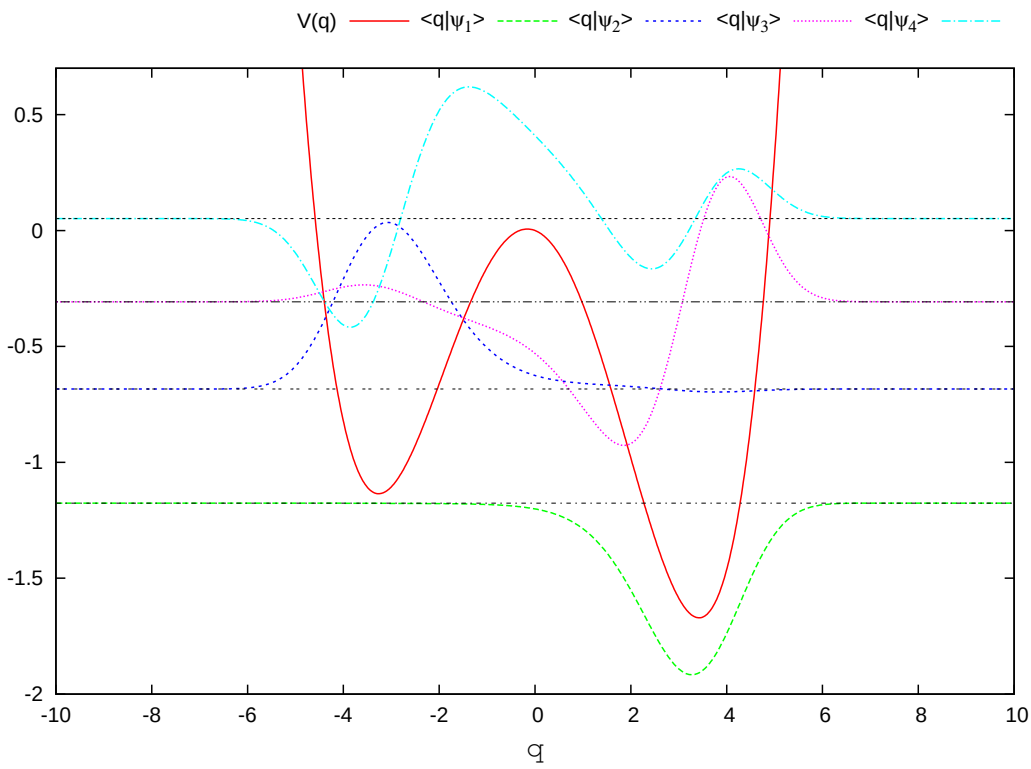

Figure 3.2: The first four global states $< q \mid \psi_1 >, \ldots, < q \mid \psi_4 >$ for barrier height $E_B = \Delta U/\hbar\omega_0 = 1.4$ and bias $\varepsilon = 0.23$.

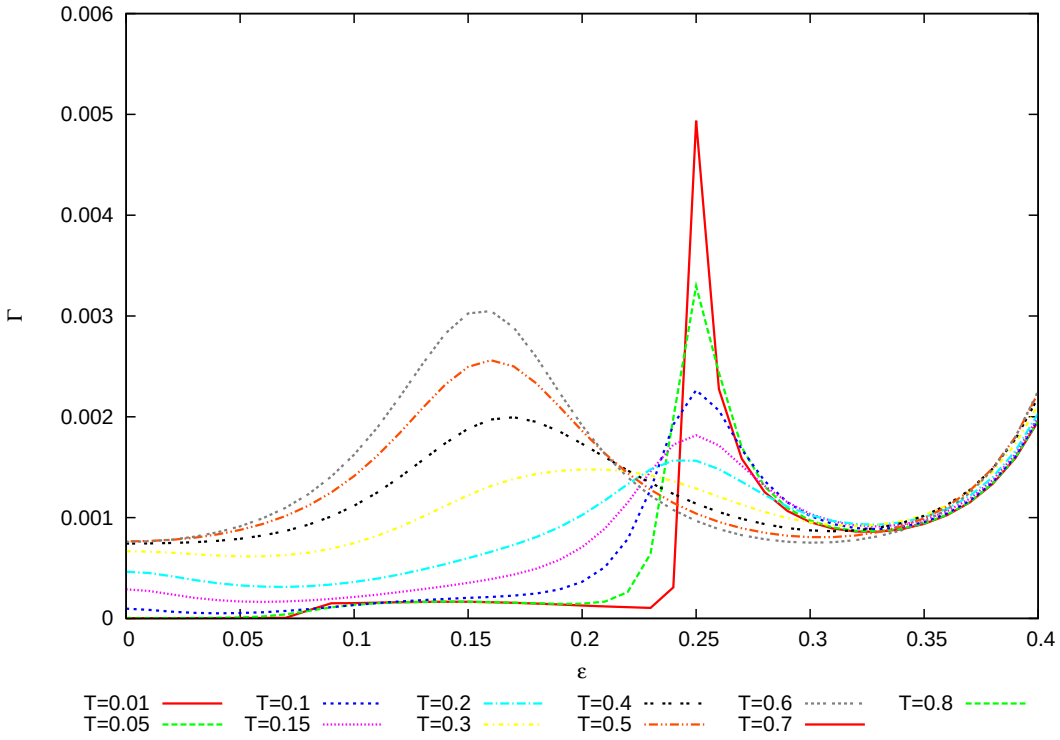

Figure 3.3: Quantum relaxation rate Γ as a function of the asymmetry parameter ε for different temperatures T. The barrier height is $E_B = 1.4$ and the number of energy levels is $M = 4$.The bath parameters are $\eta = 0.1$ and $\omega_c = 10.0$.

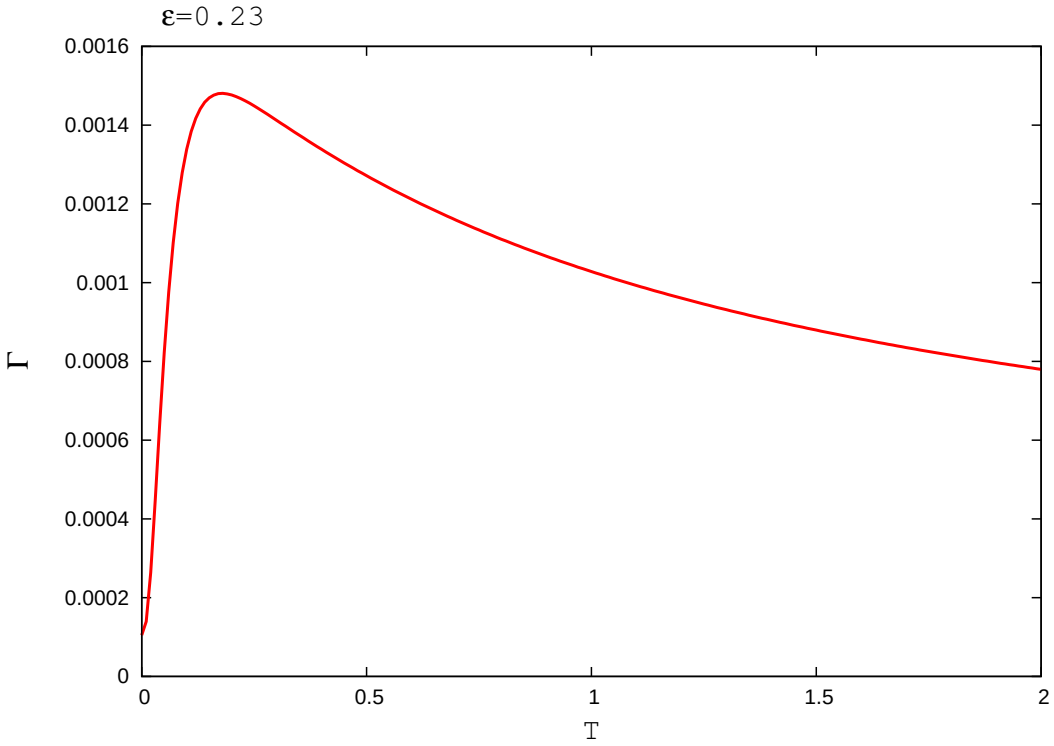

Figure 3.4: Quantum relaxation rate Γ as a function of the temperature T for fixed asymmetric parameter $\epsilon = 0.23$. The barrier height is $E_B = 1.4$ and the number of energy levels is $M = 4$.The bath parameters are $\eta = 0.1$ and $\omega_c = 10.0$.

when it interacts in certain ways (for example during a measurement process) with another (quantum or classical) system.

In Ref.(125) is shown a simple proof which gives an idea of this effect. Being the quantum system in a initial state $|\phi\rangle$ and its Hamiltonian is $\hat{H}$, the state at a time t is

$$\exp(\frac{-i\hat{H}t}{\hbar})|\phi\rangle \tag{3.44}$$

Then the probability $P(t)$ of finding the system in the initial state after a time t_0 is

$$P(t) = |\langle\phi| \exp(\frac{-i\hat{H}t_0}{\hbar})|\phi\rangle|^2 \cong 1 - \frac{(\Delta H)^2 t_0^2}{\hbar} \tag{3.45}$$

with

$$\Delta H = \langle\phi|\hat{H}^2|\phi\rangle - \Big(\langle\phi|\hat{H}^2|\phi\rangle\Big)^2 \tag{3.46}$$

If this probability is measured at $t = t_0/2$ we have

$$P(t_0/2) = 1 - \frac{(\Delta H)^2 (t_0/2)^2}{\hbar} \tag{3.47}$$

After a further period of $t_0/2$ we have

$$P(t_0) = \left[1 - \frac{(\Delta H)^2 (t_0/2)^2}{\hbar}\right]^2 = 1 - \frac{(\Delta H)^2 t_0}{\hbar} + \frac{(\Delta H)^4 (t_0/2)^4}{\hbar^2} \tag{3.48}$$

which, if is fulfilled the condition $t_0 << 1$, leads to the conclusion that the probability of decay $1 - P(t_0)$ in the case we do a measurement at $t_0/2$ is multiplied by a factor $\frac{1}{2}$. If the system is subjected to a number n equally spaced measurements the probability of decay is reduced by a factor n. Then letting $n \longrightarrow \infty$, the probability of decay goes to zero and the system freezes to its initial system.

In the above cited paper of Facchi et al. (124) the authors point out that this effect is not restricted to the measurement process but we can freeze a system in a state, or an interesting subspace of the state space of the system, through the right kind of interaction with another system. They show that this type of control can be achieved through three kinds of interaction:

- Quantum Zeno Control (frequent measurements)

- Quantum Dynamical Decoupling (the system is coupled with another system with a periodic Hamiltonian with a small period)
- Strong Continous Coupling (The system is continously coupled, i.e. we have a sort of infinitely quick detection)

The coupling with a noisy environment (thermal bath) can be seen as a particular case of the third case.

3.4 Results

In this section we study the time evolution of our quantum particle taking into account the 8 energy levels shown in Fig.3.1. The analysis is restricted to the 8 lowest levels of the system, because the study is oriented towards the dynamics of a particle that can not reach energy levels higher than the relative maximum of the potential. In particular, the attention is put on to the analysis of the time behavior of the populations for different values of the coupling strength, focusing on the time behavior of the state $|q_0\rangle$ (left side well of the potential). The approximation used in thius calculation is the **gNICA** (see section 3.2.3.4).

By using the **DVR**-state $|q_\mu\rangle$, as initial condition for the particle is chosen the non-equilibrium position $q_{start} = 0$. The corresponding state is given by

$$|q_{start}\rangle = c_1|q_1\rangle + c_2|q_2\rangle \tag{3.49}$$

with the coefficents $c_1 = 0.745$ and $c_2 = 0.667$ and all the other coefficients are zero.

By integrating Eq.(3.33) for different values of the parameter η, which represents the intensity of the environmental noise, for each eigenstate $|q_\mu\rangle$ the time behavior of the corresponding population $\rho_{q_\mu} \equiv \rho_{\mu\mu}$ (see Fig.3.5) is obtained. Moreover, by a simple change of basis, it is possible to calculate the time evolution of the populations also in the energy representation (see Fig.3.6).

It has to be noted that because of the method of calculation the order of approximation of the energy plots is lower than the order of approximation of the position plots. This is due to the fact that the trasformation is done by a

matrix product of the density matrix, with the trasformation matrix. Because the off-diagonal elements of the density matrix in position representation aren't calculated, the diagonal elements of the position density matrix are of zero order of approximation as well as the energy eigenvalues obtained.

Moreover it is necessary to note that the **gNICA** must satisfy the relation expressed in Eq.3.32 to furnish reliable results. For the bistable system under investigations the condition 3.32 becomes $\gamma \gtrsim \Delta_{max} = 1.09$. In these calculations, normalized constants are used and therefore the relation $\gamma = \eta$ (see Eq.3.15) holds. In the results presented, this condition is fulfilled for the panels **(b)** **(c)** and **(d)** of the Fig.3.5 and Fig.3.6. For the panel **(a)** of both figures it can be said that, as noted in (41), if the number of levels is moderately small ($M \leq 10$) the **gNICA** is still useful for numerical purposes.

As one can see from Eqs.(3.36),(3.38), for each value of η there are N relaxation times Λ_μ^{-1}. In order to set the time scale where to observe the behavior, it is convenient to consider the maximum of these relaxation times. A calculation shows that this time increases rapidly for larger values of η.

Therefore, to describe the time evolution of the system for different values of η, we choose as time scale τ the largest of the relaxation times obtained for $\eta = 0.01$ and calculate the evolution of the system for a maximum time $t = 600\,\tau$. This choice allows to follow the transient dynamics of the system for low and intermediate values of the coupling constant (see panels **(b)**, **(c)** and **(d)** in Figs.3.5,3.6). For higher values of η the system can not reach the regime condition, because of the presence of relaxation times longer than the maximum time chosen to calculate the numerical solution (see panel **(d)** in Figs.3.5,3.6). This delay in the system dynamics can be explained by the quantum Zeno effect, responsible for the suppression of the tunnel effect. Moreover, in Fig.3.5 a nonmonotonic behavior of the population ρ_{q_0} as a function of the time is detectable. Finally, as a consequence of the quantum Zeno effect, it is possible to say that the eigenstate $|q_0\rangle$ can be maximally populated at different times through the variation of the coupling strength and, therefore, the value of η. This could be an useful protocl in view of placing a quantum particle in a given position at a fixed time.

It would be interesting to compare these results with those obtained in the case of a harmonic oscillator coupled with a thermal bath without any cutoff,

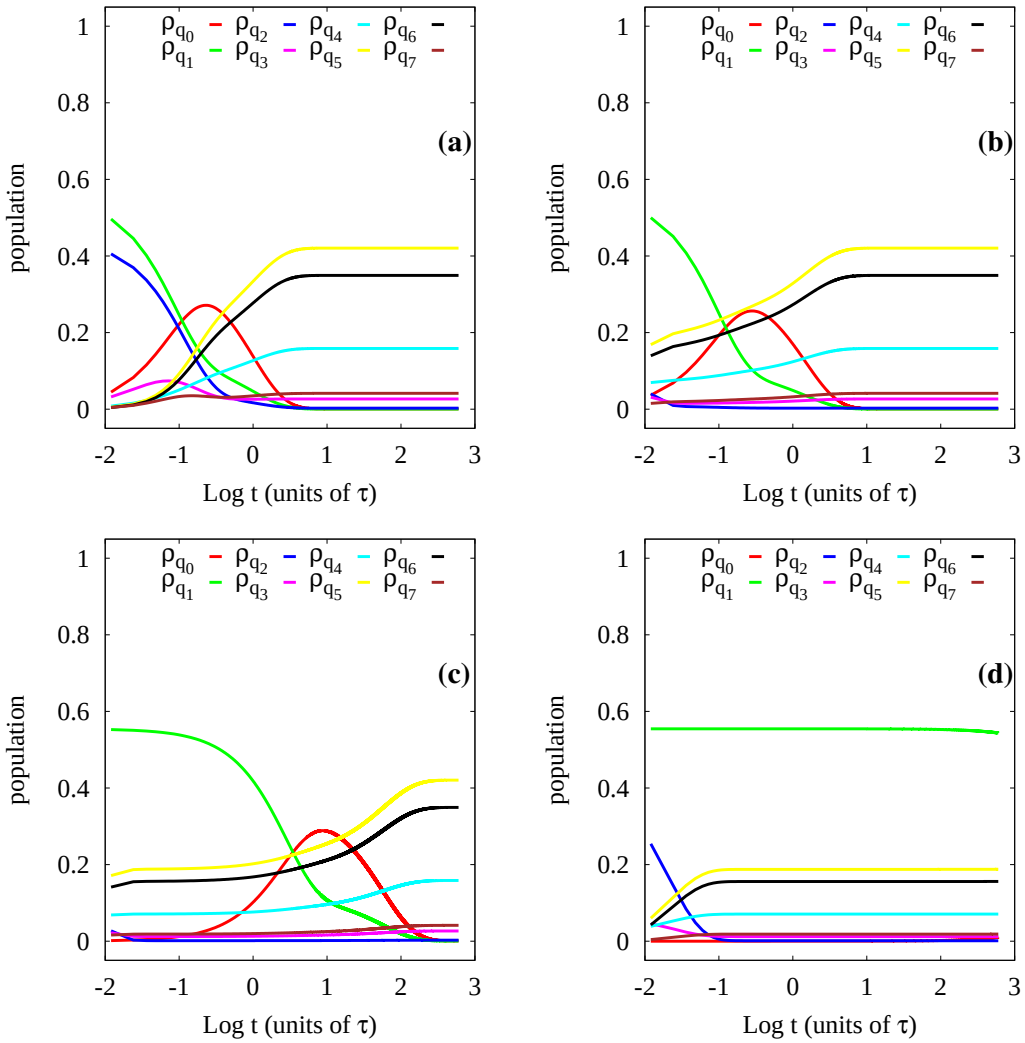

Figure 3.5: Time evolution of the diagonal elements, ρ_{q_μ} $(\mu = 0, 1, ..., 7)$, of the density matrix in q-representation. The matrix elements ρ_{q_μ} are the population distributions in the eight position eigenstates considered. The time evolution is obtained for different values of the coupling strength namely (a) $\eta = 0.01$, (b) $\eta = 0.4$, (c) $\eta = 1$ and (d) $\eta = 2.8$.

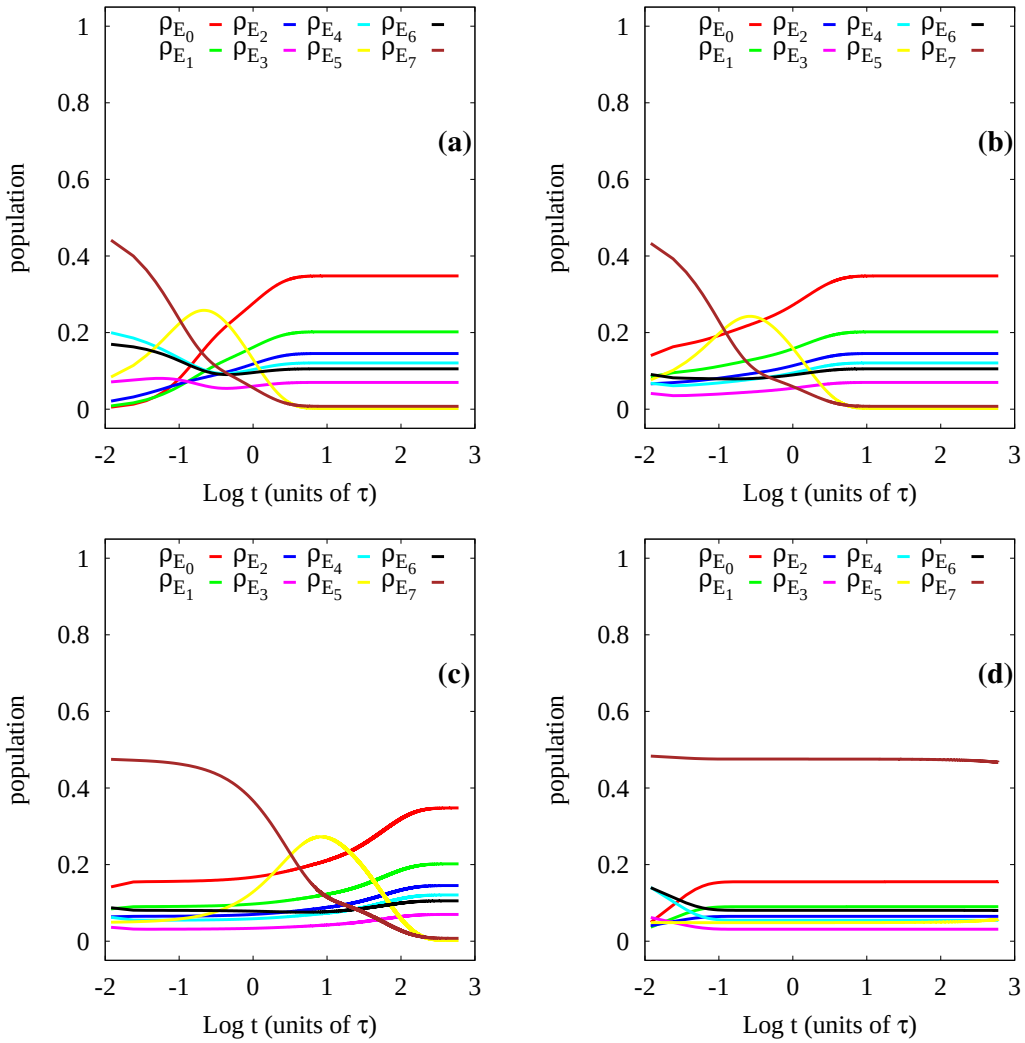

Figure 3.6: Time evolution of the diagonal elements, ρ_{E_μ} $(\mu = 0, 1, ..., 7)$, of the density matrix in energy representation. The matrix elements ρ_{E_μ} are the population distributions in the eight energy eigenstates considered. The time evolution is obtained for different values of the coupling strength, namely (a) $\eta = 0.01$, (b) $\eta = 0.4$, (c) $\eta = 1$ and (d) $\eta = 2.8$.

as studied in previous papers (126, 127, 128). On physical grounds it can be said that the time behavior of the purity of the system state might be strictly connected with the relaxation rates. In this analysis the relaxation rates have been used to determine the timescale in order to obtain the time evolution of the population distributions.

Moreover, by increasing the strength of the coupling, a freezing phenomenon of the state of the system due to the Zeno effect can be found (129).

3.5 Full density matrix

Finally, it has to be noted that the complete description of the dynamics of our initial state should be obtained by following the time evolution of all elements of the density matrix as expressed by Eq.(3.26) and this will be subject of future investigations.

The ρ_{ii} terms are the population of the i-th eigenstate while the ρ_{ij} (with $i \neq j$) terms are called the decoherences.

A possible starting point in order to obtain the full density matrix with all its elements (populations and decoherences) might be to consider that in the **gNICA** the evolution of the system may start from an off-diagonal state to ends in a diagonal state which is the final state. If we want to construct all the elements of the density matrix we have to follow the paths (the number of paths will be the order of approximation of the results) that end on the off diagonal term we seek for.

This procedure will make us able to discuss the purity of the system which is defined as the trace of the square of the density matrix ρ that is the main issue for the stability of a quantum device.

4

Noise in solid state device

4.1 Introduction

In this chapter the coherent population transfer is studied using the **STIRAP** protocol on three-level artificial atoms. In Sec.4.2 the **STIRAP** protocol is introduced, and also the sensitivity of the transfer efficiency to external parameters discussed. Then a specific implementation of three-level artificial atom based on the Quantronium design (79, 130) is considered and a model for low-frequency charge noise (Sec.4.3) is introduced. In Sec. 4.4, a way to characterize the effects of low-frequency noise, reducing the problem to that of the sensitivity of the transfer efficiency to fictitious correlated external parameters, is proposed.

4.2 Coherent population transfer in three-level atoms

In quantum optics the **STIRAP** technique is based on a Λ configuration (Fig.4.1) of two hyperfine ground states $|0\rangle$ and $|1\rangle$ and an excited state $|2\rangle$, with energies E_0, E_1 and E_2 respectively(85). The system is driven by two classical laser fields (85, 87), called the Stokes laser $\Omega_{12} = \Omega_s \cos \omega_s t$ and the Pump laser $\Omega_{02} = \Omega_p \cos \omega_p t$.

Each laser is nearly resonant with the corresponding transition. In the usual situations we can treat the driving laser fields in the rotating-wave approximation

(**RWA**). Moreover, one can introduce a phase transformation of the atomic basis and express the hamiltonian in a doubly rotating frame, with angular frequencies given by ω_i of the driving fields. The effective Hamiltonian reads as follows

$$\tilde{H} = \delta|1\rangle\langle 1| + \delta_p|2\rangle\langle 2| + \frac{1}{2}(\Omega_s|2\rangle\langle 1| + \Omega_p|2\rangle\langle 0| + \text{h.c.}) \tag{4.1}$$

where the single photon detunings are defined as follows

$$\delta_s = E_2 - E_1 - \omega_s \tag{4.2}$$

$$\delta_p = E_2 - E_0 - \omega_p \tag{4.3}$$

and the two-photon detuning is

$$\delta = \delta_p - \delta_s = E_2 - E_1 - (\omega_p - \omega_s) \tag{4.4}$$

At two-photon resonance, $\delta = 0$, the Hamiltonian (4.1) has an eigenstate which is a superposition of the two lowest atomic levels only

$$|D\rangle = \frac{1}{\sqrt{|\Omega_s|^2 + |\Omega_p|^2}} (\Omega_s|0\rangle - \Omega_p|1\rangle) \ . \tag{4.5}$$

It is usually referred as the dark state since, despite of the presence of the lasers, the atom cannot be excited to the state $|2\rangle$ and consequently decay by spontaneous emission (Fig.4.1). Instead, the laser fields interfere destructively and, as a result, the population is coherently trapped. A given dark state can be prepared by an appropriate choice of both the Rabi frequencies Ω_i and the relative phase of the ac fields.

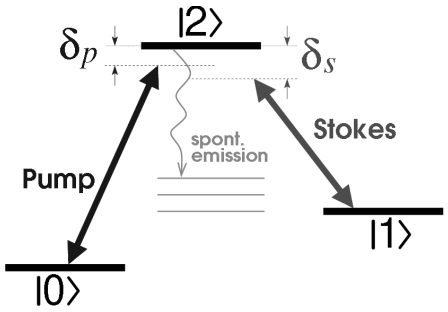

Figure 4.1: A three-level atom driven by two lasers tuned to two trasintions in the Λ scheme. The state $|2\rangle$ may have a large decay probability.

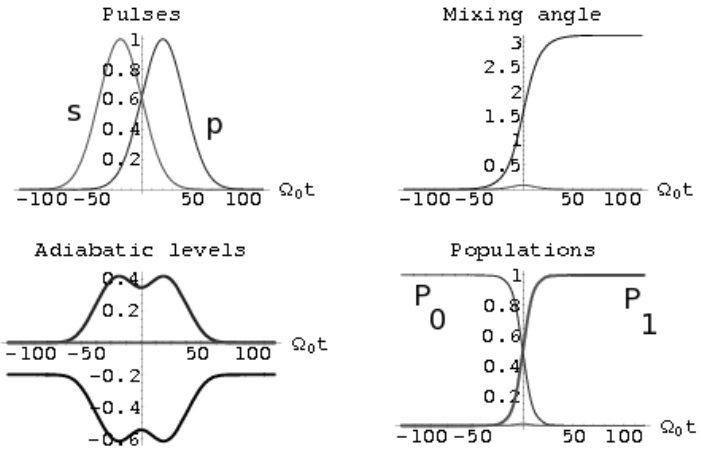

Figure 4.2: Ideal **STIRAP** at two-photon resonance $\delta = 0$, obtained by operating with two pulses in the counterintuitive sequence (top left panel). The system prepared in the state $|0\rangle$ follows the Hamiltonian along the zero-energy adiabatic level (left lower panel) yielding complete population tranfer (right lower panel, where $P_i = |\langle i|\psi(t)\rangle|^2$). In top right panel, the mixing angle of the dark state as a function of time for the adiabatic evolution. The pump laser is slightly detuned, $\delta_p = -0.2\Omega_0$.

4.2.1 The STIRAP protocol

From Eq.(4.5) it can be seen that by slowly varying the coupling strengths, $\Omega_s(t)$ and $\Omega_p(t)$, the dark state can be rotated in the two-dimensional subspace spanned by $|1\rangle$ and $|0\rangle$. Using adiabatic dynamics in the rotating frame, the **STIRAP** protocol implements coherent population transfer between the atomic states $|0\rangle \rightarrow |1\rangle$(87).

The system can be prepared in the state $|0\rangle$ by letting $\Omega_p = 0$ and switchig on $\Omega_s(t) \neq 0$. By slowly switching Ω_s off while $\Omega_p(t)$ is switched on, the population can be transferred from state $|0\rangle$ to state $|1\rangle$. Finally also Ω_p is switched off. The mixing angle of the dark state Eq.(4.5) is defined as $\theta(t) = 2\ \arctan[\Omega_p(t)/\Omega_s(t)]$, and evolves from $\theta = 0$ to $\theta = 2\pi$ (Fig.4.2, upper right panel).

This is the so-called counterintuitive scheme as opposed to the intuitive strategy where the pump pulse preceeds the Stokes pulse. In this case population transfer involves, as an intermediate step, population of the excited state $|2\rangle$, which can undergo spontaneous decay, strongly affecting the population transfer efficiency. One advantage of **STIRAP** is that, in the ideal procedure, the state $|2\rangle$ is never populated,(87, 88) therefore it is not sensitive to spontaneuos decay.

Moreover, provided adiabaticity is preserved, **STIRAP** is in principle insensitive to many details of the protocol, and in practice it turns out to be insensitive to the precise timing of the operations.

4.2.2 Sensitivity to parameters

Adiabaticity is critical to achieve high efficiency, therefore much effort has been devoted in the past to optimization of the pulse shapes (88). A necessary condition for adiabaticity is $|\dot{\Omega}_j/\Omega_j| \ll \omega_j$ $(j = s, p)$, which suggests that efficiency can be improved by using large enough Rabi peak frequencies. Formally, they determine a large (Autler-Townes) splitting of the instantaneous eigenstates in the rotating frame (87, 88). This splitting prevents unwanted transitions triggered by off diagonal parts (neglected in the adiabatic approximation) of the Hamiltonian in the instantaneous eigenbasis. These non-adiabatic terms are proportional to $\dot{\theta}(t)$ and tend to detrap the population, reducing the transfer efficiency.

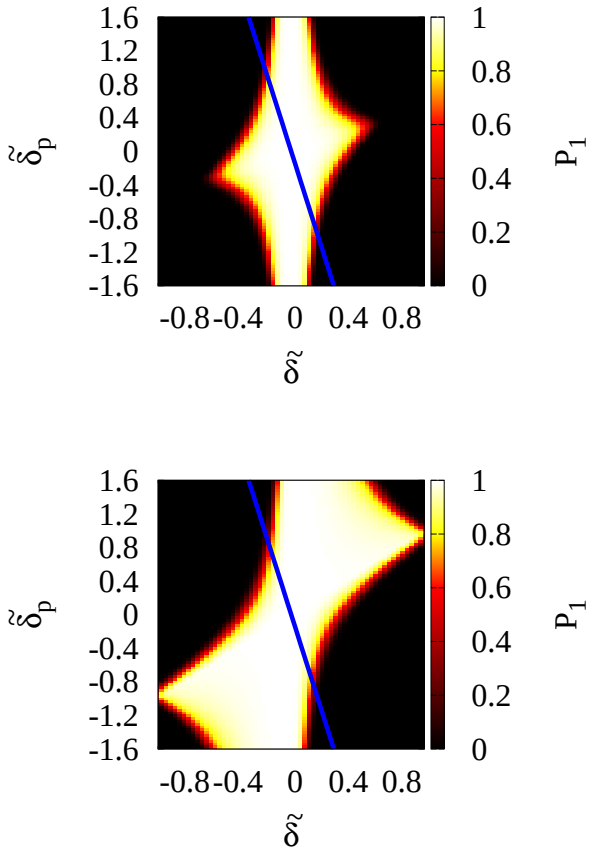

Figure 4.3: (left panel) Contour plot of the intensity of the transfer efficiency as a function of single-photon and two-photon detuning for equal peak Rabi frequencies $\kappa = \Omega_S/\Omega_P = 1$ (left panel) and $k = 2$ (right panel). In axes x, y we have $\tilde{\delta} = \delta/\Omega_0$ and $\tilde{\delta_p} = \delta_p/\Omega_0$, respectively. In both panels, the bright region corresponds to large efficiency of population transfer (more than 80%. A two-photon detuning $|\delta| \gtrsim \Omega_0/5$ determines a substantial decrease of the efficiency. The line corresponds to correlated detunings, which give an effective description of fluctuation in the Quantronium (Sec.4.4). Increasing the strength of the Stokes pulses enlarges asymmetrically the region of large transfer efficiency.

If we consider

$$\Omega_p(t) = \Omega_0 \, f[(t-\tau)/T] \tag{4.6}$$

$$\Omega_s(t) = \kappa\Omega_0 \, f[(t+\tau)/T], \tag{4.7}$$

a positive delay τ give rise to the counterintuitive sequence of **STIRAP**. For Gaussian pulses,

$$f(x) = \mathrm{e}^{-x^2} \tag{4.8}$$

optimal choices are $\Omega_0 T > 10$ and $\tau \approx T$ (88). Here a reduced pulse width $\Omega_0 T = 30$ and a delay $\tau = 0.7\,T$ are used.

4.2.2.1 Sensitivity to detunings

When the two frequencies ω_s and ω_p are not exactly resonant with the respective transitions, the presence of non-zero detunings δ_s and δ_p may strongly affect the efficiency. Actually, the two-photon detuning is the crucial parameter. As it is shown in Fig.4.3, small deviations of the two photon detuning δ lead to a substantial decrease of the efficiency, which is less sensitive to single-photon detunings at two-photon resonance $\delta = 0$. Actually, phenomena entering non-ideal **STIRAP** are qualitatively different according to δ vanishing or not, and their interplay leads to a rich physical picture.

Finite single photon detunings at $\delta = 0$ do not affect the formation of the dark state, because the mixing angle does not depend on it. Instead they increase the nonadiabatic terms(88). The efficiency is insensitive to small single-photon detunings ($\delta \lesssim \Omega_0$, see also Fig.4.2), while larger ones prevent the adiabatic follow on of the dark state.

The detuning from two-photon resonance is more detrimental for **STIRAP**, because it prevents the exclusive population of the trapped state, which is no longer an instantaneous eigenstate of the Hamiltonian. A more detailed analysis of the instantaneous eigenstates when $\delta \neq 0$ shows that there is no adiabatic transfer state providing an adiabatic connection from the initial to the target state, as does the dark state for $\delta = 0$. In this case, the evolution leads to complete population return of the system to its initial state. The only mechanism which leads to population transfer is by non-adiabatic transitions between the adiabatic

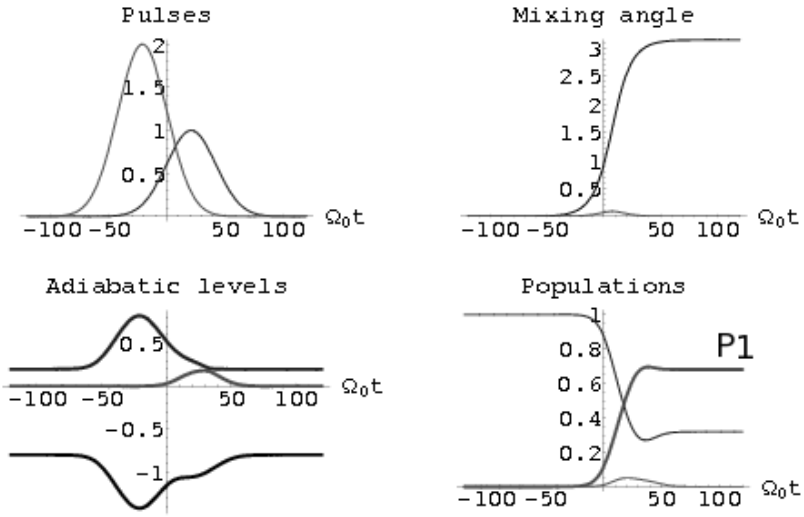

Figure 4.4: STIRAP with finite two-photon detuning $\delta = 0.2\,\Omega_0$, with the two pulses in sequence in top left panel. Population transfer occurs due to Zener transitions between crossing adiabatic levels (lower left panel), and the transfer efficiency is reduced (lower right panel). In top right panel, the mixing angle as a function of time. Here $\kappa = 2$ and $\delta_p = -4\delta$. This parametrization being appropriate for discussing effects of low-frequency noise in the Quantronium (Sec.4.4).

states. Actually for small values of δ, narrow avoided crossings between the instantaneous eigenvalues can occur and the population can be transferred by Landau-Zener tunneling(87, 88), as shown in Fig.4.4.

The above considerations lead to the conclusion that the correlations between the detunings δ_s and δ_p are very important. In fact, strongly correlated fluctuating detunings, nearly preserving two-photon resonance, still allow large transfer efficiency(131, 132). This issue becomes very important in the discussion of the effects of low-frequency noise in solid state nanodevices.

4.2.2.2 Sensitivity to Rabi frequencies

For ideal **STIRAP** it is better to have two nearly equal peak Rabi frequencies, i.e. $\kappa = \Omega_S/\Omega_P = 1$. Indeed if the two maximum Rabi frequencies are different, say $\kappa > 1$, while the pulse widths are about the same, the projection of the state vector onto the adiabatic transfer state is very good initially (because in our case the more intense pulse occurs first), but necessarily less good in the final stage. Consequently the transfer efficiency will be small(88).

The situation may be different if finite detuning is considered. In particular in the right panel of Fig.4.3 it is shown that the region of great transfer efficiency enlarges asymmetrically. This happens when the larger pulse occurs during the Zener process of imperfect **STIRAP** (the opposite situation is illustrated in Fig.4.4).

Of course, using large pulse areas, small deviations from the optimal conditions do not lead to significant drop in transfer efficiency, and in general increasing both the amplitudes is the convenient strategy to counteract the effect of imperfections. However, in solid state nanodevices there are restrictions on the amplitude and symmetry of the coupling to the microwave fields, playing the role of the lasers. Therefore, operating at $\kappa \neq 1$ may give room to further optimize the transfer efficiency.

4.3 STIRAP in the Quantronium

In this section the implementation of the Hamiltonian (4.1) in the Quantronium(79) is discussed. The basic unit of this device consists of a Cooper pair box, namely a superconducting loop interrupted by two adjacent tunnel junctions with Josephson energies $E_J/2$ (Fig.4.5).

The two small junctions define the superconducting island of the box, whose total capacitance is C and charging energy $E_C = (2e)^2/2C$. The electrostatic energy can be modulated by a gate voltage V_g connected to the island via a capacitance $C_g \ll C$ and the Hamiltonian reads

$$H_0(q_g) = \sum_q E_C[q - q_g]^2 |q\rangle\langle q| - \frac{E_J}{2}(|q\rangle\langle q+1| + h.c.), \tag{4.9}$$

where $\{|q\rangle\}$ are eigenstates of the number operator $\hat{q}$ of extra Cooper pairs in the island. It is useful to have defined the reduced gate charge $q_g = C_g V_g/(2e)$, which is the control parameter of the system. Eigenstates of the box are superpositions of charge eigenstates. The spectrum can be modified by tuning q_g (Fig.4.6) and the device is usually operated as a qubit close to the value $q_g = 1/2$. This is a symmetry point for the device Hamiltonian (4.9) and it turns out that it is an optimal working point where the system is well protected against external noise, allowing to obtain experimental dephasing times of several hundreds nanoseconds (79, 130).

Manipulation of the quantum state is performed by adding to the dc part of the gate voltage, ac microwave pulses with small amplitudes $q_g \rightarrow q_g + q_g^{ac}(t)$. The resulting Hamiltonian can be written as

$$H_{tot}(t) = H_0(q_g) + A(t)\,\hat{q}, \tag{4.10}$$

where $A(t) = -2E_C q_g^{ac}(t)$. The effective three-level artificial atom Hamiltonian, which reads

$$H(t) = \sum_i E_i |\phi_i\rangle\langle\phi_i| + A(t) \sum_{ij} q_{ij}\, |\phi_i\rangle\langle\phi_j| \tag{4.11}$$

is obtained by projecting $H_{tot}(t)$ onto the subspace spanned by the three lowest energy eigenvectors $|\phi_i\rangle$, $i = 0, 1, 2$ of $H_0(q_g)$. In Eq.4.11 we have, as usual,

$$q_{ij} = \langle\phi_i|\hat{q}|\phi_j\rangle \tag{4.12}$$

The **STIRAP** protocol can be carried out if we choose for the amplitude of the stimulating laser field

$$A(t) = A_s(t)\cos\omega_s t + A_p(t)\cos\omega_p t. \tag{4.13}$$

Moreover, it is useful to use the **RWA**. By retaining only quasi-resonant off-diagonal and co-rotating terms, The Hamiltonian simplifies to

$$A(t)\hat{q} \;\rightarrow\; H_{RWA}(t) = \frac{1}{2}\,q_{12}\,A_s(t)\,\mathrm{e}^{i\omega_s t}|\phi_1\rangle\langle\phi_2| + \frac{1}{2}\,q_{02}\,A_p(t)\,\mathrm{e}^{i\omega_p t}|\phi_0\rangle\langle\phi_2| \;+\; \text{h.c.} \tag{4.14}$$

In this approximation the truncated Hamiltonian (4.11) is transformed to the doubly rotated frame, at angular frequencies ω_s and ω_p. This yields an effective Hamiltonian $\tilde{H}(q_g)$ with the structure of Eq.(4.1), which therefore gives rise the Λ configuration. Notice that matrix elements $q_{ij} = \langle\phi_i|\hat{q}|\phi_j\rangle$ play the same role of the dipole matrix elements in defining the Rabi frequencies, $\Omega_s = q_{12}\,A_s$ and $\Omega_p = q_{02}\,A_p$.

The **RWA** of Eq.(4.14) is justified in the regime where peak Rabi frequencies are much smaller than the splittings, $\Omega_i \ll |E_i - E_j|$, which is the usual experimental regime. In this case the terms neglected are rapidly oscillating in the rotating frame, and only produce a small and fast modulation in the dynamics. The approximation is supported by simulations of the full Hamiltonian (4.10), using more than ten energy levels (93, 94, 133) for the usual operating region near $q_g = 1/2$.

It is worth stressing the dependence of the effective Hamiltonian $\tilde{H}(q_g)$ on the bias charge q_g. For instance in Eq.(4.1), the detunings depend on q_g via the energies E_i and peak Rabi frequencies via off diagonal matrix elements q_{ij} (see Fig.4.6). In particular at the symmetry point, $q_g = 1/2$, the matrix element q_{02} vanishes and selection rules hold, preventing transitions between energy states with the same parity of the label. The off-diagonal matrix elements q_{ij} shown in Fig.4.6 play the same role of the dipole matrix elements in atoms. The largest one is q_{01}, which provides the coupling for qubit operations. Fields in **STIRAP** are coupled via q_{12} and q_{02}. This latter vanishes due to a parity selection rule at the symmetry point $q_g = 1/2$.

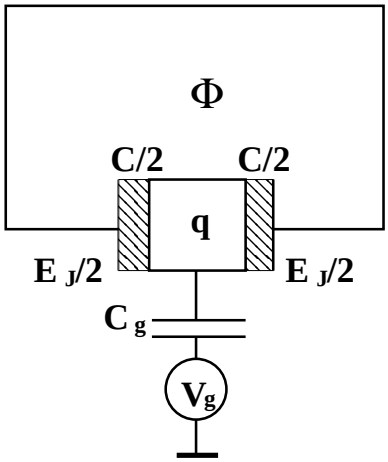

Figure 4.5: Equivalent circuit for the Quantronium. Here q and C are the charge and the capacitance of the superconducting island respectively; C_g and V_g are the capacitance and the voltage of the gate; E_g is the Josephson energy and Φ is the magnetic flux.

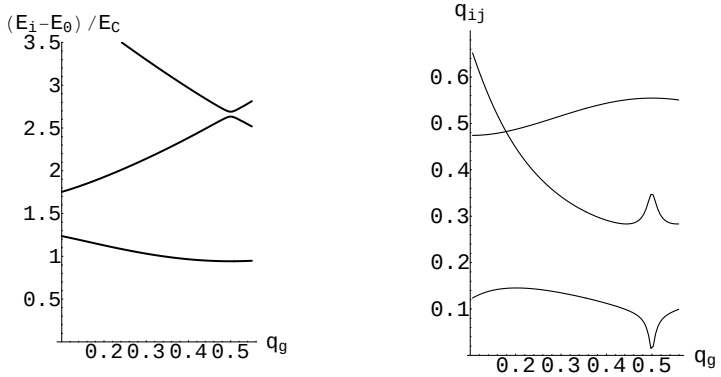

Figure 4.6: Left panel: energy spectrum of a Quantronium setup with $E_J = E_C$. The splitting $E_i - E_0$ in units of E_C is plotted as functions of q_g, The first splitting is given by $E_1(1/2) = 0.94$. Right panel: off-diagonal entries of the Cooper pair number operator, q_{01}, q_{12} and q_{02} from top to bottom.

4.3.1 Broadband noise

Since the nanocircuit is not isolated, the model has to be supplemented with noise terms. The structure of coupling to noise can be understood considering classical fluctuations of each of the parameters in the Hamiltonian of Eq.(4.9).

For instance fluctuations of the gate charge can be accounted for by adding a classical stochastic term $q_g \to q_g + \delta q_x(t)$. Physical processes described by these fluctuations are those leading to a stray electrical polarization of the island, and include effects of voltage fluctuations of the circuit and effects of switching impurities (77), located in the oxides and in the substrate close to the device. Since these latter are in practice the main source of decoherence (circuit fluctuations can be reduced by careful filtering) for the Quantronium, here only fluctuations of the gate charge will be considered, thus acting on the same gate used to drive the system. Thus we may write the resulting Hamiltonian as

$$H = H_0(q_g) + H_{RWA}(t) + \delta H \tag{4.15}$$

where $\delta H = -2E_C\,\delta q_x(t)\,\hat{q}$. In general, noise is due to the coupling of the device to an environment which is itself a quantum system, and the Hamiltonian is obtained by letting $\delta H = \hat{X}\,\hat{q} + H_{env}$, where H_{env} describes the environment and $\hat{X}$ is an environment operator. This model allows to treat high-frequency noise by a quantum optical master equation in the weak coupling regime. However the power spectrum of noise in the solid state has a large low-frequency component which invalidates the weak coupling approach.

A multistage approach has been proposed (76, 78) where high and low-frequency noise are separated, and the latter is treated as an adiabatic classical field. Formally $\hat{X} \to \hat{X}_f - 2E_C\,\delta q_x(t)$, where $\hat{X}_f$ describes fast environmental degrees of freedom and $\delta q_x(t)$ is now a classical slow stochastic process. In order to carry out the calculations it is useful to let $q_x(t) = q_g + \delta q_x(t)$ and write the Hamitonian as

$$H = H_0(q_x(t)) + H_{RWA}(t) + \hat{X}\,\hat{q} + H_{env}. \tag{4.16}$$

In many cases low-frequency noise with $1/f$ spectrum, which is the leading contribution of the slow dynamics of $q_x(t)$, is captured by a static-path approximation (**SPA**), that is approximating the stochastic process by a suitably distributed

random variable (76, 78, 130). In the case of many weakly coupled noise sources, the distribution of δq_x is characterized by an energy width $\sigma = 2E_C\,\sigma_x$.

Populations and coherences are obtained by averaging over this distribution the entries of the reduced density matrix of the system. This approach has quantitatively explained the power law decoherence observed in Quantronium (130) and in phase qubits (134), and has been recently studied for optimal tuning of multiqubit systems (102).

This point of view provides a simple argument explaining why the symmetry point $q_g = 1/2$ is well protected against external noise. Indeed, since the energy splitting $E_1 - E_0$ depends only quadratically on the fluctuations δq_x around this point, energy fluctuations are suppressed. As a consequence, superpositions of the two lowest energy levels keep coherent, yielding a power law suppression of the signal (76, 78, 130) and longer dephasing time.

4.3.2 Effective model for low-frequency noise in STIRAP

In order to study **STIRAP** we project the Hamiltonian (4.16) on the subspace spanned by the three lowest energy instantaneous eigenvectors of $H_0(q_x(t))$. In doing so the adiabaticity of the dynamics induced by $\delta q_x(t)$ is assumed, which allows to neglect effects of the time-dependence of the eigenvectors. Of course, if we start from the **SPA** version of the Hamiltonian (4.16), this condition is automatically verified. The focus is on the system plus drive Hamiltonian, $H_0(q_x(t)) + H_{RWA}(t)$, which has in the rotated frame the same structure of Eq.(4.1).

Parameters entering the Hamiltonian depend, of course, on the realization of the stochastic process. Fluctuations of the eigenenergies translate in fluctuations of the detunings (letting $E_0 = 0$)

$$\delta(q_x) = E_1(q_x) - \omega_p + \omega_s \quad \delta_p(q_x) = E_2(q_x) - \omega_p. \tag{4.17}$$

Also the effective drive fluctuates due to fluctuations of the charge matrix elements, for instance $\Omega_p = q_{02}(q_x)\,A_p$.

In the regime of validity of the **SPA**, this analysis shows that the effect of low-frequency noise in solid-state devices can be discussed in term of sensitivity of the transfer efficiency obtained by **STIRAP** to parameters characterizing an

equivalent drive. This allows to apply several results known from quantum optics to solid state devices.

For instance the large sensitivity to two-photon detuning, translates in the sensitivity to fluctuations of the lowest splitting, which is then the main characteristic to be minimized in order to achieve efficient population transfer in the solid state. Notice also that, the main steps of the analysis carried out for the Quantronium can also be applied to other solid state implementations devices, as long as decoherence in the dynamics of the two lowest energy levels is well characterized.

4.4 Effects of low-frequency noise in the Quantronium

In this section the above analysis will be applied to discuss the observability of **STIRAP** in the Quantronium, and it will be considered a device with $E_J = E_C$, whose spectral properties are given in Fig.4.6. An important point is that while dephasing is minimized by operating at the symmetry point $q_g = 1/2$, the selection rule $q_{02} = 0$ prevents to give rise **STIRAP**. Therefore, it has been proposed to operate slightly off the symmetry point.

In these conditions it has been shown that **STIRAP** allows a substantial coherent population transfer also in the presence of high-frequency noise. Notice that, while in quantum optical systems **STIRAP** connects two ground states, in solid state devices high-frequency noise leads to decay $1 \rightarrow 0$. These processes are well characterized experimentally (130).

In Ref.(93, 94) it has been shown that secular dephasing between the above two states does not produce relevant effects during population transfer. A careful analysis (133) has allowed to optimize parameters for **STIRAP** in the presence of high-frequency noise, showing that operating at $q_g = 0.47$ already provides sufficient coupling q_{02}.

On the other hand, it is known that the effect of low-frequency noise increases when the system is operated away from the symmetry point (130, 135). This opens the question of the trade-off between efficient coupling of the driving fields

and dephasing due to slow excitations in the solid-state. Here this issue is focuesd and the high-frequency noise is neglected.

Another consequence of the selection rule is that, in the vicinity of the symmetry point, coupling with the drives is asymmetric. At $q_g \approx 0.47$ we have $q_{02} \approx q_{12}/4$ (see Fig.4.6). Since in any case it is convenient to work with the largest pump pulse Rabi peak frequency Ω_0, this value is chosen.

It can be estimated by writing

$$\Omega_0 = (q_{02}/q_{01})\Omega_R \approx \Omega_R/6 \tag{4.18}$$

where Ω_R is the maximal angular frequency for Rabi oscillations between the lowest doublet. Frequencies of approximately $\nu_R = 750 - 900\,MHz$ can be achieved in the Quantronium, corresponding to a maximum field amplitude A_p yielding $\nu_p = 100 - 150\,MHz$. The peak Rabi frequency of the Stokes field could be chosen as $\nu_s = \kappa\nu_p$, with $\kappa \leq 4$, but it can be argued that $\kappa = 1$ is the optimal choice.

Fluctuations δq_x of the gate charge can be estimated from the dephasing time of the qubit at the symmetry point. This is due to energy fluctuations $\sigma/E_1(1/2) \sim 0.01$. Therefore fluctuations of gate charge, which are characteristic of the environment only, are estimated by $\sigma_x = \sigma/(2E_C) \approx 3 \cdot 10^{-3}$, where $E_C \sim 15\,GHz$ is used. Notice that these features may depend on details of the protocol as the total measurement time, but for $1/f$ noise the dependence is logarithmic and improving the procedure does not bring essential changes of σ_x.

Here choose to operate at single and two-photon resonance, $\delta = \delta_p = 0$ at $q_g = 0.47$. According to Eq.(4.17), fluctuations δq_x determine a distribution of the detuning. In the left panel of Fig.4.6, we can directly read off fluctuations of the splitting, which give the estimate

$$\Delta\delta = \Delta E_1(q_x) \approx (\partial E_1/\partial q_x)_{q_g}\,\delta q_x \tag{4.19}$$

$$\Delta\delta_p = \Delta E_2(q_x) \approx (\partial E_2/\partial q_x)_{q_g}\,\delta q_x \tag{4.20}$$

Therefore, fluctuations of the detunings are anticorrelated, $\Delta\delta_p = a\,\Delta\delta$, where the ratio of the two derivatives is given by $a \approx -5$. This corresponds to the lines

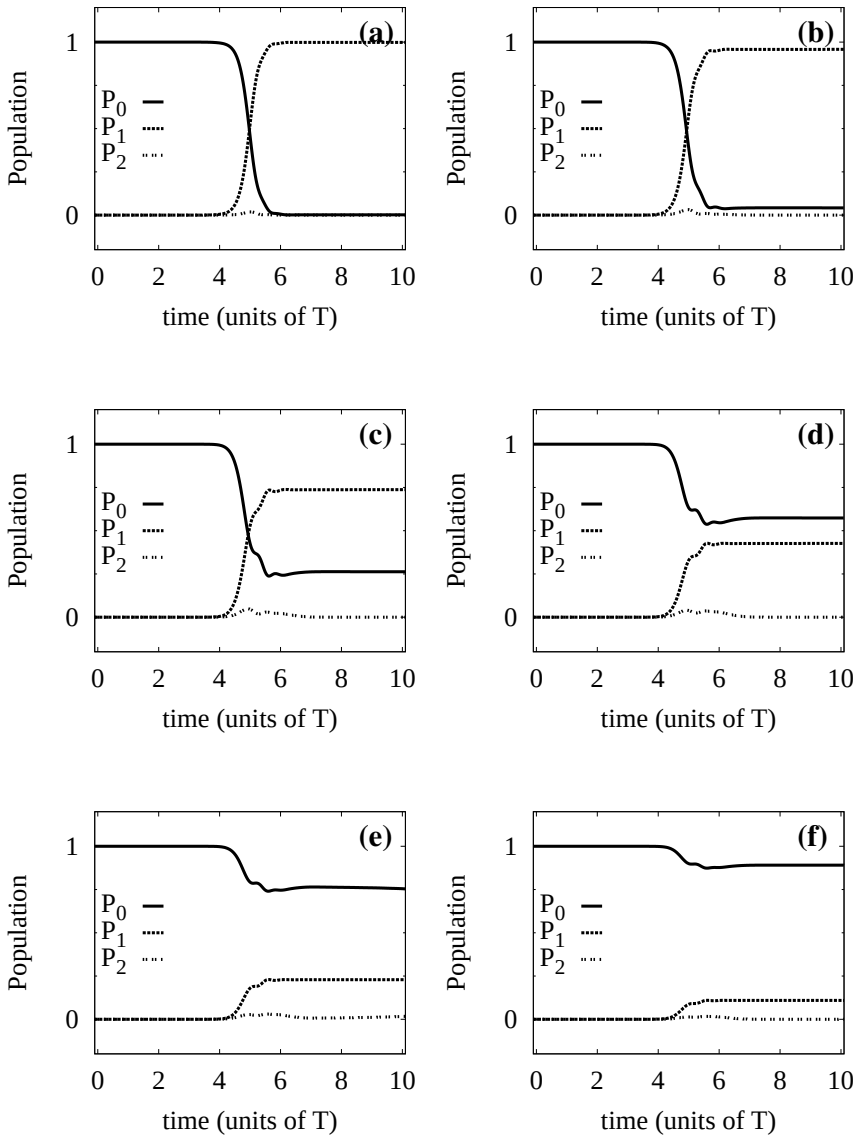

Figure 4.7: Averaged population histories for different values of the fluctuation intensity of the two-photon detuning, σ_δ. In panels (a)-(f), we have $\sigma_\delta = 0.05, 0.1, 0.2, 0.4, 0.8, 1.6$ in units of Ω_0, respectively. Here detunings are anticorrelated ($\delta_p = -5\delta$) and drives have been symmetrized ($\kappa = 1$) by using a lower amplitude A_s for the Stokes field. For $\Omega_0 = 2\pi \cdot 10^8\,\mathrm{rad/s}$ the relevant curve is $\sigma_\delta = 0.2$ and $T = 48\,ns$ yielding 60% of population transfer. Slightly increasing $\nu_p = 150MHz$ one obtains $\sigma_\delta = 0.125$ and $T = 30\,ns$.

drawn in the efficiency diagrams of Fig.4.3. Using $(\partial E_1/\partial q_x)_{q_g}\,\delta q_x \approx (E_J/4)$, the fluctuations of the two-photon detuning are estimated by

$$\sigma_\delta/\Omega_0 \approx E_J\sigma_x/(4\Omega_0) \approx \sigma/(8\Omega_0) \sim 0.1 - 0.2 \tag{4.21}$$

identifying the region of the efficiency diagrams explored by the system during the protocol. This estimate suggests that energy fluctuations in the Quantronium should still allow to observe coherent population transfer.

Fluctuations of the off-diagonal elements can be estimated by the plots in Fig. 4.6 (right panel), yielding figures of $\sim (1/4)\,\sigma_x\Omega_0 \sim 10^{-3}\Omega_0$, therefore they can be neglected. The transfer efficiency is then calculated by averaging the population histories over the distribution of correlated detunings. Results are shown in Fig. 4.7 for different values of the fluctuation intensity of the two-photon detuning σ_δ in units of Ω_0. Here detunings are anticorrelated ($\delta_p = -5\delta$) and drives have been symmetrized ($\kappa = 1$), by using a lower amplitude A_s for the Stokes field. It is seen that in standard experimental conditions the low-frequency noise allows from 60% to more than 90% population transfer in the Quantronium. Notice that even for $\sigma_\delta = 0.2\,\Omega_0$ the average population of the intermediate level is very small during the whole procedure.

Finally it is time to comment about the optimization of the laser amplitudes. In the above simulations it is used $\kappa = 1$, but it would be possible to use a larger Stokes pulse, up to $\kappa = 4$. However this does not improve the efficiency if fluctuations of the detunings are anticorrelated. As shown in Fig.4.8, in this case the region of large efficiency shrinks for increasing κ.

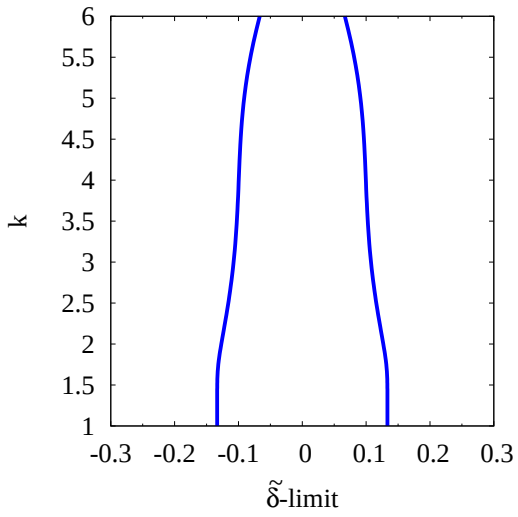

Figure 4.8: Ratio of the maximum drive amplitudes $k = \Omega_S/\Omega_P$ as a function of the two-photon detuning limits, $\tilde{\delta} = \delta/\Omega_0$, for anticorrelated noise, typical of Quantronium ($\delta_p = -5\delta$). The white zone is the region where we have more than 80% of transfer efficiency of **STIRAP**.

5

Conclusions

5.1 Classical systems

Each system which has an interaction with an external environment whose influence in not predictable is subjected to what we call ǹoise.

This kind of influence is represented by a stochastic force which can be dependent (multiplicative noise) or not (additive noise) by the state variable of the system. The dynamics of the system, interacting with a noisy environment, by a generalized Langevin equation.

In chapter 2 a functional approach is used in order to obtain from a Langevin equation the Fokker-Planck equation, whose solution is the probability density function (**PDF**) of the system under study.

In the same chapter 2 it is shown that in the case of multiplicative noise we can find a nonmonotonic behavior of the mean escape time from a metastable state as a function of the parameters that characterize the noise intensity. The results of the simulations pointed out (see Sec.2.5) that it is possible to find some ranges of parameters that makes the noise intensity capable to enhance the stability of the metastable state.

Also it is possible to find more than one maximum in the graph of the average lifetime of the metastable state, whose position depends on both the parameters. Moreover, the maxima are depending on both the parameters D and μ giving rise to **NES** islands.

In section 2.7 the Ising model is presented as a physical example for a nonequilibrium system. A series of simulations, which were carried out using the Montecarlo algorithm, are also discussed. Each spin in the Ising model has a probability of change its orientation which is depending on the temperature and on the magnetization of the nearest neighbors.

The rate used in these simulation is the one proposed by Glauber (121) which has the property of being ergodic also for $T \longrightarrow \infty$. In the simulations the metastable state chosen as initial condition is the state with all the spin up. Results for different values of the non equilibrium parameter p are reported.

The simulations show that the average lifetime of the metastable state is depending on both the parameter p (nonequilibrium parameter) and the parameter T (reduced Temperature). Moreover, the behavior of the average lifetime, seen as a function of T, is nonmonotonic and shows, for certain values of p, a maximum whose position depends on the value of the non equilibrium parameter. This result is in agreement with the model discussed in the previous sections of chapter 2.

5.2 Quantum systems

The dynamics of a quantum particle subject to an asymmetric bistable potential and interacting with a noisy environment has been analyzed (Chap. 3). The study is performed exploiting the approach of the Feynman-Vernon functional(56) within the framework of the discrete variable representation(41, 57). By using the Caldeira-Leggett model(42), the analysis of the transient dynamics of the system, for different values of the coupling strength between the particle and the noisy environment, modelled as a thermal bath, it is performed.

For a asymmetric bistable potential (reported in Fig. 3.2) it is found (see Sec. 3.2.4) that there are many overlapping regions where is visible a nonmonotonic behavior of Γ as a function of the temperature. It is possible to distinguish two different nonmonotonic behaviors: one with a maximum, reported in Fig.3.4, and the other one with a minimum.

Due to the quantum Zeno effect (see Sec.3.3), responsible for the slowering of the tunnel effect, a delayed dynamics of the system is observed for higher values of

the coupling strength. It is shown (Sec. 3.4) also that the metastable state inside the left side well of the potential can be populated at different times varying the value of the coupling strength.

In the chapter 4 the effect of low-frequency noise on the transfer efficiency of **STIRAP** is studied, proposing that low-frequency fluctuations of the spectrum can be analized in terms of fictitious correlated fluctuations of the detunings. For solid-state noise with large low-frequency component (e.g. for $1/f$ noise) the leading effect (**SPA** approximation) is equivalent to consider statistically distributed detunings and can be discussed by analizing the sensitivity to parameters of the protocol.

Then the theory has been applied to the Quantronium, showing that correlated fluctuations of the energy splittings have to be considered, and that transfer efficiency is mainly sensitive to decoherence in the subspace of the two-lowest levels, which is well characterized experimentally. Selection rules prevent to work at the symmetry point, where decoherence is minimal. Therefore, the observation of coherent population transfer requires optimization of the trade-off between increasing coupling and greater sensitivity to low-frequency noise. In chapter 4 it is shown that this is indeed possible, given the measured figures of low-frequency noise.

Notice that pulses of width $T = 48 - 30\,ns$ are used . Therefore, the total time of the protocol $\sim 200 - 350\,ns$ is longer than the dephasing time of the qubit, as determined solely by static inhomogeneities. This dephasing time is smaller off the symmetry point (in the experiment of Ref(130). the dephasing time for coherent oscillations dropped from $T_\phi \sim 600\,ns$ at the symmetry point to $T_\phi \sim 50\,ns$ at $q_g = 0.47$).

This shows that **STIRAP** is less sensitive than coherent oscillations technique to low-frequency noise. Actually, accounting for high frequency noise the process will be limited by the relaxation $T_1 \gtrsim 500\,\mathrm{ns}$.

This analysis applies as well to other superconducting nanodevices. In particular, it could allow to design correlations of fluctuations of the energy spectrum, which maximize the Zener channel of population transfer.

Appendix A

Publications

A.1 Paper on ISI journals

P. Caldara, A. La Cognata, D. Valenti, B. Spagnolo, M. Berritta, E. Paladino, G. Falci, *"Quantum Relaxation Time in Asymmetric Bistable Potential"*, International Journal of Quantum Information (in press) (2011)
A. La Cognata, P.Caldara, D. Valenti, B. Spagnolo, A. D'Arrigo, E. Paladino, G. Falci, *"Effect of broadband noise on adiabatic passage in superconducting nanocircuits"* International Journal of Quantum Information (in press) (2011)

A.2 Proceedings

B. Spagnolo, G. Augello, P. Caldara, A. Fiasconaro, A. La Cognata, N. Pizzolato, D. Valenti, A. A. Dubkov and A. L. Pankratov, *"Noise stabilization effects in models of interdisciplinary physics"*, J. Phys: Conf. Ser. **174** (2009) 012037
B. Spagnolo, A. Fiasconaro, N. Pizzolato, D. Valenti, D. Persano Adorno, P. Caldara, A. Ochab-Marcinek, and A.Gudowska-Nowak, *Cancer growth dynamics: stochastic models and noise induced effects*, American Institute of Physics Vol. **1129**, Melville, NY, USA, pp 539-544 (2009)

References

[1] G. Parisi. **Brownian motion**. *Nature 433*, page 221, 2005. 1

[2] O. A. Tretiakov, T. Gramespacher, and K. A. Matveev. **Lifetime of metastable states in resonant tunneling structures**. *Phys. Rev. B*, **67**(7):073303, Feb 2003. 1

[3] Hernán Larralde and Fran çois Leyvraz. **Metastability for Markov Processes with Detailed Balance**. *Phys. Rev. Lett.*, **94**(16):160201, Apr 2005. 1

[4] A. L. Pankratov and B. Spagnolo. **Suppression of Timing Errors in Short Overdamped Josephson Junctions**. *Phys. Rev. Lett.* ***93***, page 177001, 2004. 1

[5] R. Brown. **A brief account of microscopical observations made in the months of June, July, and August, 1827, on the particles contained in the pollen of plants; and on the general existence of active molecules in organic and inorganic bodies**. *Philos. Mag.(N.S.) 4*, pages 161–173, 1828. 2

[6] L. Bachelier. **Theorie de la spéculation [Ph.D. Thesis]**. *Annales scientifiques de l'ecole normale suérieure* ***III-17***, pages 21–86, 1900. 2

[7] A. Einstein. **Über die von der molekularkinetischen Theorie der Wärme geforderte Bewegung von in ruhenden Flüussigkeiten suspendierten Teilchen**. *Annalen der Physik* ***322*** *(8)*, page 549560, 2005. 2, 13

[8] M. von Smoluchowski. **Zur kinetischen Theorie der Brownschen Molekularbewegung und der Suspension**. *Ann. Phys.* ***21***, pages 756–780, 1906. 2

[9] P. Langevin. **Sur la théorie de movemente brownien**. *C. R. Acad. Sci.* ***146***, pages 530–533, 1908. 2

[10] C. W. Gardiner. *Handbook of stochastic Methods*. Springer Verlag, Berlin and Heidelberg, 1985. 2, 3, 5, 6, 16, 20

[11] F. Marchesoni and P. Hänggi. **100 years of Brownian motion**. *Chaos* ***15***, page 026101, 2005. 2

[12] E. Nelson. *Dynamical Theories of Brownian Motion*. Princeton University Press, 1967. 3

[13] P. Jung F. Marchesoni L. Gammaitoni, P. Hänggi. **Stochastic resonance**. *Rev. Mod. Phys.* ***70***, pages 223–287, 1998. 3

[14] P. Jung L. Gammaitoni, P. Hänggi and F. Marchesoni. **Stochastic Resonance: A remarkable idea that changed our perception of noise**. *Eur. Phys. J. B* ***69***, page 13, 2009. 3

[15] P. Jung F. Marchesoni L. Gammaitoni, P. Hänggi. **Stochastic Resonance**. *Rev. Mod. Phys.* ***70****(1), 223*, 1998. 3

[16] B. Spagnolo N. Mantegna. **Stochastic resonance in a tunnel diode**. *Phys. Rev. E* ***49*** *3*, pages R1792–1795, 1994. 3

[17] M. Trapanese R. N. Mantegna, B. Spagnolo. **Linear and nonlinear experimental regimes of stochastic resonance**. *Phys.Rev. E* ***63***, page 011101, 2001. 3

[18] D. Valenti N. V. Agudov, A. V. Krichigin and B. Spagnolo. **Stochastic resonance in a trapping overdamped monostable system**. *Phys. Rev. E* ***81***, page 051123, 2010. 3

[19] C. R. Doering and J. C. Gadoua. **Resonant activation over a fluctuating barrier**. *Phys. Rev. Lett.* ***69***, pages 2318–2321, 1992. 3

[20] Katja Lindenberg Marian Boguna, Josep M. Porra and Jaume Masoliver. **Properties of resonant activation phenomena**. *Phys. Rev. E* ***57*** *(4)*, page 3990, 1998. 3

[21] R.N. Mantegna and B. Spagnolo. **Experimental Investigation of Resonant Activation**. *Phys. Rev. Lett.* ***84*** *3025*, 2000. 3

[22] D. Persano Adorno B. Spagnolo N. Pizzolato, A. Fiasconaro. **Resonant activation in polymer translocation: new insights into the escape dynamics of molecules driven by an oscillating field**. *Phys. Biol.* ***7***, page 034001, 2010. 3

[23] A. L. Pankratov E. V. Pankratova A. Fiasconaro A. Ochab-Marcinek B. Spagnolo, A. A. Dubkov. **Lifetime of metastable states and suppression of noise in interdisciplinary physical models**. *Acta Physica Polonica B* ***38***, page 1925, 2007. 3

[24] N. Agudov and B. Spagnolo. **Noise-enhanced stability of periodically driven metastable states**. *Phys. Rev. E* ***64****, 035102(R)*, 2001. 3

[25] N. V. Agudov A. A. Dubkov and B. Spagnolo. **Noise enhanced stability in fluctuating metastable states**. *Phys. Rev. E* ***69****, 061103-1*, 2004. 3

[26] N. Mantegna and B. Spagnolo. **Noise enhanced stability in an unstable system**. *Phys. Rev. Lett.* ***76*** *4*, pages 563–566, 1996. 3

[27] A. Fiasconaro B. Spagnolo, D. Valenti. **Noise in ecosystems: a short review**. *Mathematical Biosciences and Engineering* ***64, 1*** *N.1*, 2004. 4

[28] Lefever R. Horsthemke W. *Noise-Induced Transitions*. Springer Verlag, 1984. 4, 16, 22, 25

[29] P.L. Garrido P. I. Hurtado, J. Marro. **Demagnetization via Nucleation of the Nonequilibrium Metastable Phase in a Model of Disorder**. *J. Stat. Phys.* ***133, 29***, 2008. 4, 23, 25

[30] W. Genovese and M. A. Mu noz. **Recent results on multiplicative noise**. *Phys. Rev. E60, 69*, 1999. 4

[31] F. Colaiori Miguel. M. Muñoz and C. Castellano. **Mean-field limit of systems with multiplicative noise**. *Phys. Rev. E72, 056102*, 2005. 4

[32] J. M. R. Parrondo C. Van den Broeck and R. Toral. **Noise-Induced Nonequilibrium Phase Transition**. *Phys. Rev. Lett.* ***73****, 3395*, 1994. 4

[33] R. Toral C. Van den Broeck, J. M. R. Parrondo and R. Kawai. **Nonequilibrium phase transitions induced by multiplicative noise**. *Phys. Rev. E* ***55****, 4084*, 1997. 4

[34] J. Garca-Ojalvo and J. M. Sancho. *Noise in Spatially Extended Systems*. Institute for Nonlinear Science (Springer, New York,), 1999. 4

[35] M.O.Hongler. **Exact time dependent probability density for a non-linear non-Markovian stochastic process**. *Helv. Phys. Acta* ***52****, 280*, 1979. 4

[36] M. San Miguel F. de Pasquale, J.M. Sancho. **Decay of an unstable state in the presence of multiplicative noise**. *Phys. Rev.* ***A*** *33, 4360*, 1986. 4

[37] J. Marro P. I. Hurtado and P L. Garrido. **Metastability, nucleation, and noise-enhanced stabilization out of equilibrium**. *Phys. Rev.E* ***74****, 050101(R)*, 2006. 4, 23, 37, 40

[38] H. A. Kramers. **Brownian motion in a field of force and the diffusion model of chemical reactions**. *Physica* ***7,4***, pages 284–304, 1940. 5, 6

[39] Yu. A. Pashkin & J. S. Tsai *et al.* Y. Nakamura. **Coherent control of macroscopic quantum states in a single-Cooper-pair box**. Nature ***398***, pages 786–788, 1999. 7, 10

[40] G. Strasser D. Rakoczy, R. Heer and J. Smoliner. **High energy ballistic transport in hetero- and nanostructures**. Physica E ***16***, pages 129–136, 2003. 7

[41] P. Hänggi M. Thorwart, M. Grifoni. **Strong coupling theory for tunneling and vibrational relaxation in driven bistable systems**. *Ann. Phys. 293*, pages 15–66, 2001. 7, 9, 45, 51, 53, 55, 56, 64, 88

[42] A. O. Caldeira and A. L. Leggett. **Influence of dissipation on quantum tunneling in macroscopic systems**. *Phys. Rev. Lett.* ***46***, pages 211–214, 1981. 7, 8, 45, 49, 54, 88

[43] A. T. Dorsey M. Fisher A.Garg A. J. Leggett, S. Chakravarty and W. Zwerger. **Dynamics of the dissipative two-state system**. *Rev. Mod. Phys.* ***59***, pages 1–85, 1987. 7

[44] M. Grifoni and P. Hänggi. **Driven quantum tunneling**. *Phys. Rep.,* ***304***, pages 229–354, 1998. 7

[45] U. Weiss. *Quantum Dissipative Systems.* World Scientific, Singapore, 1999. 7, 48, 49, 50, 51

[46] W. Chen S. K. Tolpygo & J. E. Lukens J. R. Friedman, V. Patel. **Quantum superposition of distinct macroscopic states**. *Nature* ***406***, pages 43–46, 2000. 7

[47] J. Aumentado C. Urbina *et al.* J. M. Martinis, S. Nam. **Rabi Oscillations in a Large Josephson-Junction Qubit**. *Phys. Rev. Lett.* ***89***, page 117901, 2002. 7

[48] P. Jung F. Grossmann, T. Dittrich and P.Hänggi. **Coherent destruction of tunneling**. *Phys. Rev. Lett.* ***67***, pages 516–519, 1991. 7

[49] R. Löfstedt and S. N. Coppersmith. **Quantum stochastic resonance**. *Phys. Rev. Lett.,* ***72***, pages 1947–1950, 1994. 7

[50] E. Knill L. Viola and S. Lloyd. **Dynamical Decoupling of Open Quantum Systems**. *Phys. Rev. Lett.* ***82***, pages 2417–2421, 1999. 7

[51] A. J. Leggett. **Quantum tunneling in the presence of an arbitrary linear dissipation mechanism**. *Phys. Rev. B* ***30***, pages 1208–1218, 1984. 8

[52] T. Yu C.-H. Chou and B. L. Hu. **Exact master equation and quantum decoherence of two coupled harmonic oscillators in a general environment**. *Phys. Rev E* ***77***, page 011112, 2008. 8

[53] S. M. Dutra M. Rosenau da Costa, A. O. Caldeira and H. Westfahl Jr. **Exact diagonalization of two quantum models for the damped harmonic oscillator**. *Phys Rev A* ***61***, page 022107, 2000. 8

[54] N. V. Prokofev and P. C. E. Stamp. **Theory of the spin bath**. *Rep. Prog. Phys.* ***63***, pages 669–726, 2000. 8

[55] F. Petruccione P. Breuer. *The Theory of Open Quantum Systems.* Claredon Press, Oxford, 2006. 8

[56] R. P. Feynman and F. L. Vernon Jr. **The theory of a general quantum system interacting with a linear dissipative system**. *Ann. Phys.,* ***24***, pages 118–173, 1963. 9, 45, 88

[57] G. G. Engerholm D. O. Harris and W. D. Gwinn. *J. Chem. Phys.,* ***43***, pages 1515–1517, 1965. 9, 45, 51, 88

[58] J. L. van Hemmen and A. Süt o. **Tunnelling of Quantum Spins**. *Europhys. Lett.****1***, page 481, 1986. 9

[59] J. L. van Hemmen and A. Süt o. **Tunnelling of Quantum Spins**. *Phys.* ***B 141***, page 37, 1986. 9

[60] S. Hill T. Hathaway J. A. A. J. Perenboom, J. S. Brooks and N. S. Dalal. **Relaxation of the magnetization of Mn_{12} acetate**. *Phys. Rev. Lett.* ***58***, page 330, 1998. 9

[61] R. Sessoli W. Wernsdorfer and D. Gatteschi. **Nuclear-spindriven resonant tunnelling of magnetisation in Mn_{12} acetate**. *Europhys. Lett.* ***42***, page 254, 1999. 9

[62] B. Barbara G. Bellessa, N. Vernier and D. Gatteschi. **Phonon-Assisted Tunneling in High-Spin Molecules: Experimental Evidence**. *Phys. Rev. Lett.* ***83***, page 416, 1999. 9

[63] W. Wernsdorfer and R. Sessoli. **Quantum Phase Interference and Parity Effects in Magnetic Molecular Clusters**. *Science* ***284***, pages 133–135, 1999. 9

[64] C. Sangregorio R. Sessoli D. Mailly W. Wernsdorfer, T. Ohm and C. Paulsen. **Observation of the Distribution of Molecular Spin States by Resonant Quantum Tunneling of the Magnetization**. *Phys. Rev. Lett.* ***82***, page 3903, 1999. 9

[65] R. Sessoli D. Gatteschi W. Wernsdorfer, I. Chiorescu and D. Mailly. **Quantum Phase Interference in Magnetic Molecular Clusters**. *Phys. B: Cond. Matt.* ***284288***, pages 1231–1232, 2000. 9

[66] A. Caneschi D. Gatteschi W. Wernsdorfer, R. Sessoli and A. Cornia. **Nonadiabatic Landau-Zener tunneling in Fe_8 molecular nanomagnets**. *Europhys. Lett.* ***50****(4)*, page 552, 2000. 9

[67] J. Lapointe S. Han and J. E. Lukens. **Observation of incoherent relaxation by tunneling in a macroscopic two-state system**. *Phys. Rev. Lett.* ***66***, page 810, 1991. 9, 10

[68] J. E. Lukens R. Rouse, S. Han. **Observation of Resonant Tunneling between Macroscopically Distinct Quantum Levels**. *Phys. Rev. Lett.* ***75***, page 1614, 1995. 9, 10

[69] R. Rouse S. Han and J. E. Lukens. **Generation of a Population Inversion between Quantum States of a Macroscopic Variable**. *Phys. Rev. Lett.* ***76***, page 3404, 1996. 9

[70] B. Ruggiero P. Silvestrini, V. G. Palmieri and M. Russo. **Observation of Energy Levels Quantization in Underdamped Josephson Junctions above the Classical-Quantum Regime Crossover Temperature**. *Phys. Rev. Lett.* ***79***, pages 3046–3049, 1997. 9

[71] R. Rouse S. Han and J. E. Lukens. **Observation of Cascaded Two-Photon-Induced Transitions between Fluxoid States of a SQUID**. *Phys. Rev. Lett.* ***84***, pages 1300–1303, 2000. 9

[72] W. Chen S. K. Tolpygo J. R. Friedmann, V. Patel and J. E. Lukens. **Quantum superposition of distinct macroscopic states**. *Nature* ***406***, pages 43–46, 2000. 9

[73] G. Blatter. **Schrödinger's cat is now fat**. *Nature* ***406***, page 25, 2000. 9

[74] L. Levitov L. Tian C. H. van der Wal J. E. Mooij, T. P. Orlando and S. Lloyd. **Josephson Persistent-Current Qubit**. *Science* ***285***, page 1036, 1999. 9

[75] F. K. Wilhelm R. N. Schouten-C. J. P. M. Harmans T. P. Orlando S. Lloyd C. H. van der Wal, A. C. ter Haar and J. E. Mooij. **Quantum Superposition of Macroscopic Persistent-Current States**. *Science* ***290***, pages 773–777, 2000. 9

[76] A. Mastellone G. Falci E. Paladino, A. D'Arrigo. *Phys. Scr. T137*, page 014017. 10, 11, 48, 80, 81

[77] G. Falci E. Paladino, L. Faoro and R. Fazio. **Decoherence and 1/f Noise in Josephson Qubits**. *Phys. Rev. Lett.* **88**, page 228304, 2002. 10, 11, 80

[78] A. Mastellone G. Falci, A. D'Arrigo and E. Paladino. **Initial Decoherence in Solid State Qubits**. *Phys. Rev. Lett.* **94**, page 167002, 2005. 10, 11, 80, 81

[79] A.Cottet P.Joyez H.Pothier C.Urbina D.Esteve D.Vion, A.Aassime and M.H.Devoret. **Manipulating the Quantum State of an Electrical Circuit**. *Science* **296**, page 886, 2002. 10, 69, 77

[80] C.J.P.M.Harmans I.Chiorescu, Y.Nakamura and J.E.Mooij. **Coherent Quantum Dynamics of a Superconducting Flux Qubit**. *Science* **299**, page 1869, 2003. 10

[81] O.Astafiev Y.Nakamura T.Yamamoto, Yu.A.Pashkin and J.S.Tsai. **Demonstration of conditional gate operation using superconducting charge qubits**. *Nature* **425**, page 941, 2003. 10

[82] A.C.J.ter Haar C.J.P.M.Harmans J.B.Majer, F.G.Paauw and J.E.Mooij. **Spectroscopy on Two Coupled Superconducting Flux Qubits**. *Phys.Rev.Lett.***94**, page 090501, 2005. 10

[83] A.Blais L.Frunzio R.S.Huang J.Majer S.Kumar S.M.Girvin A.Wallraff, D.I.Schuster and R.J.Schoelkopf. **Spectroscopy on Two Coupled Superconducting Flux Qubits**. *Nature* **431**, page 162, 2004. 10

[84] K. Semba Y. Nakamura C.J.P.M. Harmans I.Chiorescu, P. Bertet and J.E. Mooij. **Coherent dynamics of a flux qubit coupled to a harmonic oscillator**. *Nature* **431**, page 159, 2004. 10

[85] M.O. Scully and M.S. Zubairy. *Quantum Optics*. Cambridge Univ. Press, Cambridge, 1997. 10, 11, 69

[86] P. Caldara and E. Fiordilino. **High-order harmonic emission from a three-level atom in a laser field**. *J. Mod. Opt. **46** (5)*, pages 743–754, 1999. 10

[87] H. Theuer K. Bergmann and B.W. Shore. **Coherent population transfer among quantum states of atoms and molecules**. *Rev. Mod. Phys. **70***, pages 1003–1025, 1998. 11, 69, 72, 76

[88] B.W. Shore N.V. Vitanov, T. Halfmann and K. Bergmann. **Laser-induced population transfer by adiabatic passage techniques**. *Annu. Rev. Phys. Chem.* **52**, pages 763–809, 2001. 11, 72, 74, 76

[89] W.D. Oliver D.S. Crankshaw K. V. R. M. Murali, Z. Dutton and T. Orlando. **Probing Decoherence with Electromagnetically Induced Transparency in Superconductive Quantum Circuits**. *Phys. Rev. Lett.* **93**, page 087003, 2004. 11

[90] A.Yu. Smirnov M.H.S. Amin and A. Maassen v.d. Brink. *Phys. Rev. B* **67**, page 100508(R), 2003. 11

[91] J. Siewert and T. Brandes. **Application of adiabatic passage in solid-state devices**. *Adv. Solid State Phys.* **44**, page 181, 2004. 11

[92] L.F. Wei C.P. Sun Y.-X. Liu, J.Q. You and F. Nori. **Optical Selection Rules and Phase-Dependent Adiabatic State Control in a Superconducting Quantum Circuit**. *Phys. Rev. Lett.* **95**, page 087001, 2005. 11

[93] G. Falci J. Siewert, T. Brandes. **Adiabatic passage with superconducting nanocircuits**. *Opt. Comm.* **264**, page 435, 2006. 11, 78, 82

[94] G. Falci J. Siewert, T. Brandes. **Advanced control with a Cooper-pair box: Stimulated Raman adiabatic passage and Fock-state generation in a nanomechanical resonator Abstract**. *Phys. Rev.* **B 79**, page 024504, 2009. 11, 78, 82

[95] M.J. Storcz *et al.* M. Mariantoni. **On-chip microwave Fock States and quantum homodyne measurements**. *arXiv:cond-mat/0509737v2*, 2005. 11

[96] K. Cicak F. Altomare J.I. Park R.W. Simmonds G.S. Paraoanu P.J. Hakonen M.A. Sillanpää, J. Li. **Autler-Townes Effect in a Superconducting Three-Level System**. *Phys. Rev. Lett.* ***103***, page 193601, 2009. 11

[97] R. Bianchetti J.M. Fink M. Göppl L. Steffen P.J. Leek A. Blais A. Wallraff M. Baur, S. Filipp. **Measurement of Autler-Townes and Mollow Transitions in a Strongly Driven Superconducting Qubit**. *Phys. Rev. Lett.* ***102***, page 243602, 2009. 11

[98] J. Schlafer B. Mookerji T.A. Ohki J.S. Kline D.P. Pappas W.R. Kelly, Z. Dutton. **Direct Observation of Coherent Population Trapping in a Superconducting Artificial Atom**. *Phys. Rev. Lett.* ***104***, page 163601, 2010. 11

[99] A.A. Abdumalikov et al. **Electromagnetically induced transparency on a single artificial atom**. *arXiv 1004.2306v1* ***[quant-ph]***, 2010. 11

[100] M. Baur J. M. Fink C. Lang L. Steffen M. Boissonneault A. Blais A. Wallraff R.Bianchetti, S.Filipp. **Control and Tomography of a Three Level Superconducting Artificial Atom**. *arXiv:1004.5504v1*, 2010. 11

[101] G. Falci and D.L. Shepeliansky P. Zoller G. Benenti Eds. R. Fazio, in G. Casati. *Quantum Computer, Algorithms and Chaos p. 363-416.* IOS press, ISBN/ISSN: 1-58603-660-2. 11

[102] E. Paladino et al. **Optimal tuning of solid-state quantum gates: A universal two-qubit gate**. *Phys. Rev.* ***B 81***, page 052502, 2010. 11, 81

[103] V. I Klyatskin. *Stochastic equations through the eye of the Physicist.* Elsevier, 2005. 19

[104] R. L. Stratonovich. *Introduction to the theory of random noise.* Gordon and Breach (New York), 1963. 20

[105] I. F. Gihman and A. V. Skorokhod. *Stochastic differential equations.* Springer, Berlin, Heidelberg, 1972. 20

[106] L. Arnold. *Stochastic differential equations.* Wiley-Interscience, New York, 1974, 1974. 20

[107] S. Boccaletti A. Fiasconaro, B. Spagnolo. **Signatures of noise-enhanced stability in metastable states**. *Phys. Rev. E* ***72*** *061110*, 2005. 23

[108] B. Spagnolo A. Fiasconaro, D.Valenti. **Role of the initial conditions on the enhancement of the escape time in static and fluctuating potentials**. *Physica A* ***325****, 136*, 2003. 23

[109] B. Spagnolo A. Fiasconaro. **Stability measures in metastable states with Gaussian colored noise**. *Phys. Rev. E* ***80****, 041110*, 2009. 23

[110] N. V. Agudov A. A. Dubkov and B. Spagnolo. **Noise enhanced stability in fluctuating metastable states**. *Phys. Rev. E* ***69****, 061103*, 2004. 23

[111] A. Manor and N. M. Shnerb. **Multiplicative Noise and Second Order Phase Transitions**. *Phys. Rev. Lett.* ***103***, page 030601, 2009. 37

[112] S. G. Brush. **History of the Lenz-Ising Model**. *Rev. Mod. Phys.*, **39**(4):883–893, Oct 1967. 37

[113] **Beitrag zur Theorie des Ferromagnetismus**. 40

[114] L. Onsanger. **Crystal Statistics. I. A Two-Dimensional Model with an Order-Disorder Transition**. *Phys. Rev.* ***65***, page 117, 1944. 40

[115] C. N. Yang. **The Spontaneous Magnetization of a Two-Dimensional Ising Model**. *Phys. Rev.* ***85*** *5*, pages 808–816, 1952. 40

[116] B. Kaufman. **Crystal Statistics. II. Partition Function Evaluated by Spinor Analysis**. *Phys. Rev.* ***76***, pages 1232–1243, 1949. 40

[117] B. Kaufman and L. Onsanger. **Crystal Statistics. III. Short-Range Order in a Binary Ising Lattice**. *Phys. Rev.* ***76***, pages 1244–1252, 1949. 40

[118] F. Semeria C. Zannoni C. Chiccoli, P. Pasini. **An application of Cluster Monte Carlo method to the Heisenberg model**. *Int. Journ. Mod. Phys.* ***4*** *5*, pages 1041–1048, 1993. 40

[119] J. Marro and J.A. Vacas. **Demagnetization of spin systems at low temperature**. *Phys. Rev.* ***B 56***, pages 8863–8866, 1997. 40

[120] R. Dickman J. Marro. *Nonequilirium Phase Transitions in Lattice Models.* Cambridge University Press, Cambridge, 2005. 40

[121] K. Binder D. P. Landau. *A guide to Monte Carlo simulations in statistical physics.* Cambridge University Press, 2005. 41, 88

[122] M. Winterstetter and U. Weiss. **Dynamical Simulation of the Driven Spin-Boson System: the Influence of Interblip Correlations**. *Chem. Phys.* ***217***, page 155, 1997. 54

[123] C. H. Mak R. Egger and U. Weiss. **Rate concept and retarded master equations for dissipative tight-binding models**. *Phys. Rev. E* ***50***, page R655, 1994. 55

[124] P. Facchi, S. Tasaki, S. Pascazio, H. Nakazato, A. Tokuse, and D. A. Lidar. **Control of decoherence: Analysis and comparison of three different strategies**. *Phys. Rev. A*, **71**(2):022302, Feb 2005. 58, 62

[125] D. Home and M. A. B. Whitaker. **A Conceptual Analysis of Quantum Zeno; Paradox, Measurement, and Experiment**. *Ann. Phys.* ***258***, pages 237–285, 1997. 62

[126] A. Serafini M. G. A. Paris, F. Illuminati and S. De Siena. **Purity of Gaussian states: Measurement schemes and time evolution in noisy channels**. *Phys. Rev. A* ***68***, page 012314, 2003. 67

[127] M. G. A. Paris A. Serafini, F. Illuminati and S. De Siena. **Entanglement and purity of two-mode Gaussian states in noisy channels**. *Phys. Rev. A* ***69***, page 022318, 2004. 67

[128] F. Illuminati A. Serafini, M. G. A. Paris and S. De Siena. **Quantifying decoherence of continuous variable systems**. *J. Opt. B* ***7***, pages R19–R36, 2005. 67

[129] S. Pascazio H. Nakazato A. Tokuse P. Facchi, S. Tasaki and D. A. Lidar. **Control of decoherence: Analysis and comparison of three different strategies**. *Phys. Rev. A* ***71***, page 022302, 2005. 67

[130] P. Joyez P.J. Meeson D. Vion et al. G. Ithier, E. Collin. **Decoherence in a superconducting quantum bit circuit**. *Phys. Rev.* **B 72**, page 134519, 2005. 69, 77, 81, 82, 89

[131] B.W. Shore L.P. Yatsenko, V.I. Romanenko and K. Bergmann. **Stimulated Raman adiabatic passage with partially coherent laser fields**. *Phys. Rev.* **A 65**, page 043409, 2002. 76

[132] N.V. Vitanov P.A. Ivanov and K. Bergmann. **Effect of dephasing on stimulated Raman adiabatic passage**. *Phys. Rev.* **A 70**, page 063409, 2004. 76

[133] J. Siewert G. Mangano and G. Falci. **Sensitivity to parameters of STIRAP in a Cooper-Pair Box**. *Eur. Phys. Journ. ST* **160**, pages 259–268, 2008. 78, 82

[134] S. Poletto et al. **Coherent oscillations in a superconducting tunable flux qubit manipulated without microwaves**. *New Journ. Phys.* **11**, page 013009, 2009. 81

[135] A. D'Arrigo G. Falci, A. Mastellone and E. Paladino. **Low-Frequency Noise Characterization in Charge-Based Coherent Nanodevice**. *Open Sys. & Inf. Dyn.* **13**, page 323, 2006. 82